DFT Study of the Complexation of NOTA Chelator with Alkali Metal and Radiometal ions for Radiopharmaceutical Applications

FATIMA YETUNDE ADEOWO

213569756

UNIVERSITY OF
KWAZULU-NATAL

INYUVESI
YAKWAZULU-NATALI

Submitted in fulfilment of the requirements for the degree of Masters of Medical Sciences in the School of Health Science, University of KwaZulu-Natal

December 2016.

DFT STUDY OF THE COMPLEXATION OF NOTA CHELATOR WITH ALKALI METAL AND RADIOMETALS IONS FOR RADIOPHARMACEUTICAL APPLICATIONS

FATIMA YETUNDE ADEOWO

213569756

2016

A thesis submitted to the School of Health Sciences, Faculty of Health Science, University of KwaZulu-Natal, Westville, for the degree of Master of Pharmaceutical Chemistry.

This is a thesis in which the chapters are written as a set of discrete research papers, with an overall introduction and final discussion in which one of the chapters was published in internationally recognized, peer-reviewed journals and another one in preparation. Typically these chapters will have been published in internationally recognized, peer-reviewed journals.

This is to certify that the contents of this thesis are the original research work of Miss Fatima, Yetunde Adeowo.

Supervisor: Signed: **----------------------**Name: **Dr. Adam Skelton** Date: …………

Co-Supervisor: Signed: ------------------Name: **Dr. Bahareh Honarparvar** Date: ………….

DECLARATION

I, Miss Fatima, Yetunde Adeowo, declare as follows:

1. The research reported in this thesis, except where otherwise indicated is my original research.

2. This thesis has not been submitted for any degree or examination at any other university

3. This thesis does not contain other persons' data, pictures, graphs or other information, unless specifically acknowledged as being sourced from other persons.

4. This thesis does not contain other persons' writing, unless specifically acknowledged as being sourced from other researchers. Where other written sources have been quoted, then:
   a. Their words have been re-written but the general information attributed to them has been referenced.
   b. Where their exact words have been used, then their writing has been placed in italics and inside quotation marks, and referenced.

5. This thesis does not contain text, graphics or tables copied and pasted from the Internet, unless specifically acknowledged, and the source being detailed in the thesis and in the References sections.

6. A detail contribution to publications that form part and/or include research presented in this thesis is stated (include publications submitted, accepted, and published).

Signed: …………………. Date: ……………………..

DEDICATION

I dedicate this work to my lovely family, my husband; Chris Ifeacho and my children; Nkiru-Araoluwa and Chukwuma Ifeacho.

ACKNOWLEDGEMENT

LIST OF PUBLICATIONS AND CONFERENCE ATTENDED

Publications in peer review journals included in this thesis

Fatima Y Adeowo, Bahareh Honarparvar, Adam A. Skelton. The Interaction of NOTA as a Bifunctional Chelator with Competitive Alkali Metal ions: A DFT Study. *RSC Advances* **6** (**2016**): 79485-79496.

Contributions:

F.Y. Adeowo ran the project, carried out all calculations and wrote the paper as the main author.

A. A. Skelton and B. Honarparvar – Supervisors

Fatima Y Adeowo, Bahareh Honarparvar, Adam A. Skelton. DFT study on the complexation of NOTA as a bifunctional chelator with radiometal ions

Contributions:

F.Y. Adeowo ran the project, carried out all calculations and wrote the paper as the main author.

A. A. Skelton and B. Honarparvar – Supervisors

Conference: Centre for High Performing Computing (CHPC) National Conference 2015.

Poster topic presentation: "Evaluation of the interaction of NOTA chelator with alkali metal ions; DFT study

TABLE OF CONTENTS

LIST OF FIGURES

Chapter one

Chapter two

Chapter three

LIST OF TABLES

Chapter two

Chapter three;

LIST OF ACRONYMS

Ac	Actinium
As	Arsenic
B3LYP	Becke 3 Lee-Yang- Parr
BFC	Bifunctional Chelator
BSSE	Basis Sets Superimposition Error
Cal/mol	Calories per mole
COOH	Carboxylic acid
Cu	Copper
DFO	Desferrioxamine
DOTA	1, 4, 7, 10 –tetraazacyclododecane-tetraacetic acid
DOTA-BA	1, 4,7,10 –tetraazacyclododecane-tetraacetic acid – Barium
DOTA-D-phe-NH$_2$	1, 4, 7, 10 –tetraazacyclododecane-tetraacetic acid- D- Phenylalanine amide
DTPA	Diethylenetriaminepentaacetic acid
DOTATOC	Edotreotide
DFT	Density Functional Theory
EDTA	Ethylenediamine
EA	Electron Affinity
E$_a$	Anionic energy
E$_{ca}$	Cationic energy
Ga	Gallium
HEEDTA	Hydroxyethyl ethylenediamine acid

H$_2$dedpa (N$_4$O$_2$)	(1, 2-bis {[[6-(carboxyl) pyridine-2-yl] methyl] amino}-Ethane
H$_4$octapa	N, N'-bis(6-carboxy-2-pyridylmethyl)-ethylenediamine-N,N'-diacetic acid
HOMO	Highest Occupied Molecular Orbitals
HPLC	High Performance Liquid Chromatography
IEF	Integral Equation Formalism
In	Indium
IP	Ionization Potential
K	potassium
Kcal/mol	Kilocalories per mole
Li	Lithium
LUMO	Lowest Occupied Molecular Orbital
Na	Sodium
NAC	Natural Atomic Charges
NBO	Natural Bond Orbital
NETA	({4[2(Bis-carboxymethyl- amino)-ethyl]- 7-carboxymethyl) -1-[1, 4, 7] triazonan-1-yl} acetic acid)
NMR	Nuclear Magnetic resonance
NODAGA	1, 4, 7 –triazacyclononane-1-glutaric acid-4,7 diacetic acid.
NOPA	Triazacyclononane phosphinate
NOPO	(1, 4, 7-triazacyclononane- 1, 4,- bis [methylene(hydroxymethyl)phosphinic acid] -7- [methylene(2-carboxyethyl)phosphinic acid])
NODASA	1, 4, 7- Triazacyclononane-1-Succinic acid- 4, 7, diacetic acid

NOTA	1, 4, 7 –triazacyclononane-, 1, 4, 7-triacetic acid
NOTA-NCS	p-isothiocyanto benzyl- 1, 4, 7-triazacyclononane-1, 4, 7-triacetic acid
Pb	Lead
PCM	Polarizable Continuum Mode
p- SCN-Bn-NOTA	2-S- (4-Isothiocyanatobenzyl)-1, 4, 7, - triazacyclononane, - 1, 4, 7-triacetic acid
PET	Positron Emission Tomography
SPECT	Single Photon Emission Computed Tomography
Rb	Rubidium
Re	Rhenium
Sc	Scandium
SPE	Single Point Energy
Sr	Strontium
Tb	Terbium
TACN-TM	1, 4, 7 –tris (2-mercaptoethyl)-1, 4, 7-triazacyclononane
TC	Technetium
TCMC	1, 4,7,10, -tetrakia (carbomoylmethyl) -1, 4, 7, 10 – tetraazacyclododecane
TETA	Triethylenetetraamine
Ti	Titanium
TLC	Thin Layer Chromatography
TRAP	Triazacyclononane-phosphinic acid
Y	Yttrium

ABSTRACT

The application of chelators is an ongoing interest in diagnostic and therapeutic radiopharmaceuticals. Bifunctional chelators labelled with radiometal ions are covalently bonded with a lead compound to form complexes with targeted biomolecules. The binding affinity of a ligand is thus an exclusively essential feature of an ideal radiopharmaceutical ligand. 1,4,7 triazacyclononane-1,4,7 triacetic acid (NOTA) a key radiolabelling chelator in radiopharmaceuticals, which is studied in this project, has been identified as one of the popularly investigated chelators. NOTA is known with the ability to form a stable complex with radiometal ions.

A number of experimental investigations have been performed to study the structure and the radiolabelling efficiency of NOTA chelator while little attention has been paid to exploiting the structure and the binding features of the ligand at the molecular level. In this project, an investigation was made of the structure of NOTA and it complexation with alkali metal and radiometal ions, using density functional theory. In the first step, efforts were made to evaluate the complexation of NOTA with alkali metal ions (Na^+, Li^+, K^+ and Rb^+) with the intention of assessing the level of competition of alkali metal ions, found in the body. The complexation of NOTA with radiometal ions (Cu^{2+}, Ga^{3+}, In^{3+}, Sc^{3+}) was also investigated.

This study reveals that nitrogen and oxygen atoms in the NOTA molecule are important for complexation processes. Interaction and relaxation energies, Gibbs free energies and entropies show that the stability of NOTA— alkali metal ion complexes decreases down the group of the periodic table. In the case of NOTA—radiometal ions complexes, NOTA—Ga^{3+} is identified to be more stable than the remaining radiometal complexes, which is in good agreement with experimentally reported binding constants. For both alkali metal and radiometal ion complexes, implicit water solvation affects the NOTA—ion complexation, causing a decrease in the stability of the system. NBO analysis performed through the natural population charges and second order perturbation theory reveals the charge transfer between NOTA and both alkali metal and radiometal ions. The theoretical ^1H NMR chemical shifts of NOTA complexes, in vacuum and water, are in good agreement with experiment; these values are influenced by the presence of the ions, which have a deshielding effect on the protons of NOTA. A noteworthy conclusion from the investigation is that the interaction of NOTA with radiometal ions is stronger than the interaction of NOTA with alkali metal ions. Thus, confirming that the presence of alkali metal in human body may not interfere with the

binding of radiometal to NOTA chelator. This study serves as a guide to researchers in the field of organometallic chelators, particularly, radio-pharmaceuticals in finding the efficient optimal match between chelators and different metal ions.

CHAPTER ONE

INTRODUCTION

1.1.   Chelation

The word chelation is derived from the Greek word "chelos" which means claw.[1] It involves the combination of a mineral ion or cation into a complex ring structure by an organic molecule, referred to as chelating agent.[2] Most often, electron-donor atoms on the chelating molecule include sulphur, nitrogen, and/or oxygen. Chelant, metal ion and chelate are components of chelation process.[3] Basically, the chelant is made up of two or more electron donor atoms that are capable of holding the central metal ion (the acceptor) in a tight coordination complex. A detailed review on the historical background of chelating has been given by Dwyer.[4] It is known that, ethylenediamine and oxalic acid were the first chelating agents identified and have been extensively utilized in studying the structure of metal complexes.[5-10]
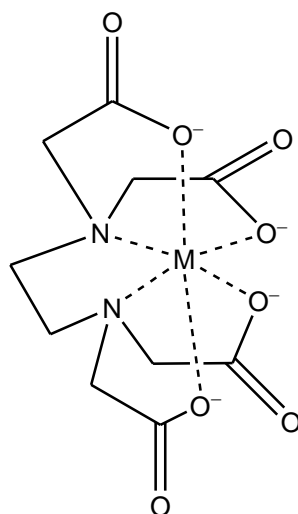
Figure 1: An ethylenediamine (EDTA) molecule binding to a generic central metal

The importance of the chelation process in science is enormous and cannot be ignored. Research has revealed that the technological applications of chelators and the chelation process have been widely embraced in our industries. Detoxification liquid waste from industries for domestic usage has been possible using chelation process. [11] Metal chelators are used as antioxidants for food preservation.[12] In the production of textile, EDTA has been used as chelating agent. The textile industry has exploited the use ETDA as a chelating agent to enhance enzyme reaction in cotton pre-treatment.[13, 14] and decolourization and detoxification

of textile industry waste water has be attained through chelation processes.[15, 16] In agricultural plant production, application of EDTA and Hydroxyethyl ethylenediamine acid (HEEDTA) as chelating agents allow easy uptake of phosphorous-based fertilizer in acidic soil, which was initially not possible as a result of the bonds of Phosphorous with iron and aluminium.[17] Examples of biochemical processes involving chelates are photosynthesis[18], oxygen transporting blood[19], certain enzymes reaction[20], and muscle contraction.[21]

1.1.1 The use of Radiometals-chelator complexes in radiopharmaceutical

The process of using chelating and radionuclide approach to study human disease is called nuclear medicine.[22] This branch of medicine has gained popularity over the years. Nuclear medicine techniques have taken an important position in molecular imaging, through its unique ability to translate findings in molecular biology, genetics, pharmacology and many other disciplines into imaging diseases for clarity on ailments and also to administer appropriate treatments .[23] Welch[22] pointed that there are two vital processes involved in nuclear medicine; these are, a suitable radiation detection apparatus which ascertain quality and sensitiveness of the procedure and a radiopharmaceutical which establish the usefulness and or anatomical information of the images produced. Thus radiopharmaceuticals are the mainstay of nuclear medicine.[24] A recent development in nuclear medicine is the use of radiometal- chelator complex as radiopharmaceuticals.[25] Generally, radiopharmaceuticals (unsealed radioactive elements) are dispensed intravenously for either diagnostic or therapeutic purposes.

1.1.2 Types of radiopharmaceutical

Radiopharmaceuticals are drugs containing radiometals that produce valuable emission properties for therapeutic and diagnostic use. The application of radiopharmaceutical in medical medicine cannot be over emphasized. New drug discovery[26] and direct target of treatment on tumor[27-31] has become much easier. It basically allows medical practitioners to detect a patient's ailments, recommend treatment, and observe the productiveness of the treatment with the use of imaging modalities such as Positron Emission Tomography (PET) and Single Photon Emission Computed Tomography (SPECT).[32, 33] Radiopharmaceuticals can be classified into two groups based on medical application; diagnostic and therapeutic radiopharmaceuticals. Diagnostic radiopharmaceuticals are substances labelled with gamma-emitting radiometal aimed at providing a detailed account of the structure of organ or tissue that allow studying the physiological feature through external monitoring device (SPECT,

PET, etc.). In contrast, therapeutic radiopharmaceuticals treat diseased cells by delivering cytotoxic radiation dose from the radiometal through a targeting vector or biomolecule to the diseased site.[24, 25] Radiopharmaceuticals can also be classified based on their bio distribution characteristic; target specific radiopharmaceuticals are the ones whose distributions are regulated solely by the receptor binding site or interaction with biological molecules. Non-target specific radiopharmaceuticals are the ones whose bio distribution is determined only by their physical and chemical properties.
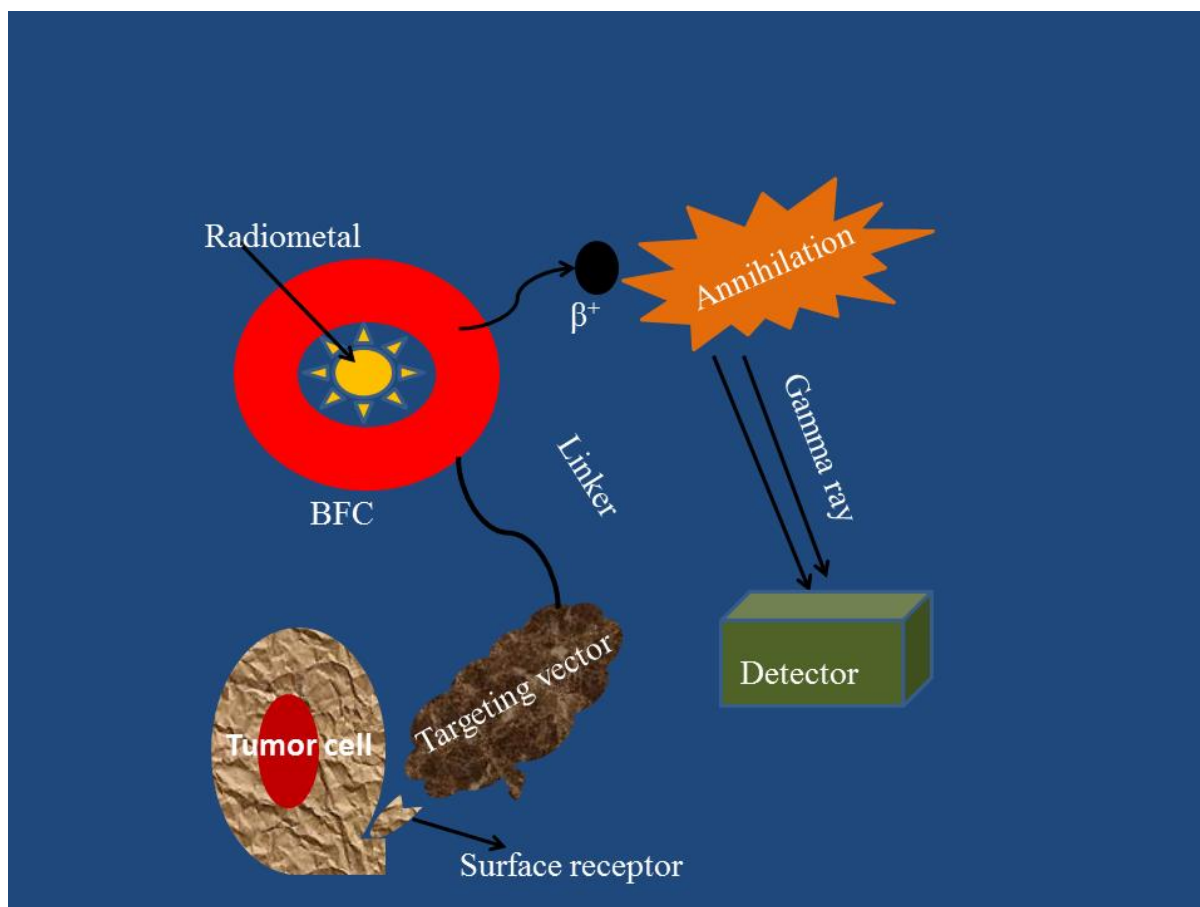
Figure 2: A cartoon illustration of the process involved in radiopharmaceuticals

1.2. Chelators or chelating agents

A chelator or chelating agent is used to bind metal ion in chelating process. Chelating agents are organic or inorganic compounds capable of binding metal ions to form complex ring-like structure called 'chelates'.[34] A useful application of a chelator for any biological use requires that a chelator or ligand is used to sequester the free radio isotopes form aqueous solution. Essentially, the chelator binds firmly to the radiometal so that when infused into the body , there will not be a loss of radiometal from the radiopharmaceutical.[35] For optimal effective

3

chelation, a chelator must fulfil the criteria that enable it to: (1) move across physiological obstacles into sections of the biological system where a toxic metal ion is concentrated or the target organ, (2) form a stable complex with the metal ion (3) form a chelate possessing non-toxic properties and can be easily excreted, from the site it was deposited and from the body.[36] Thus, an ideal chelator for any biological use must possess the following characteristic; highly soluble in water, resistance to modification, maintain chelating ability at the PH of the body fluid, be kinetically stable with radiometals, bind the radiometal ion and effectively radiolabel in high yields under a mild room-temperature and in a short reaction time.[36-39]

1.2.1. Types of chelators

Chelators can be classified into groups based on the arrangement of atoms that make up the chelate compound or the number of electrons coordinated to the centre metal ion.

1.2.1.1. Acyclic and macrocyclic chelators

The prevalent chelators that are commonly employed in radiopharmaceuticals can be grouped into two; acyclic (open chain) and macrocyclic (closed chain).[40-43] Basic physical modification is required during metal ion binding with macrocyclic chelators because their geometries are inherently constrained prior to ion binding. This feature of macrocyclic ligand helps to minimize entropic loss associated with ion coordination thus resulting in a greater thermodynamic stability of the complex , a phenomenon referred to as the macrocyclic effect.[44] Acyclic chelator on the other hand requires that it coordination and geometry be altered in order for the donor atom be properly positioned for complexation with ion. Thus they suffer major entropic loss which makes them less thermodynamically unfavourable compared to macrocyclic chelator. Even though the thermodynamic of these chelator types are commensurable, acyclic chelators are known to be less kinetically stable than macrocyclic analogues.[32]

1.2.1.2. Monodentate and polydentate chelators

Depending on the number of ligand donor atoms and the number of electrons through a ligand is coordinated to the central metal ion to form a chelate; a chelator could be monodentate, bidentate or multidentate.[36, 39, 45]
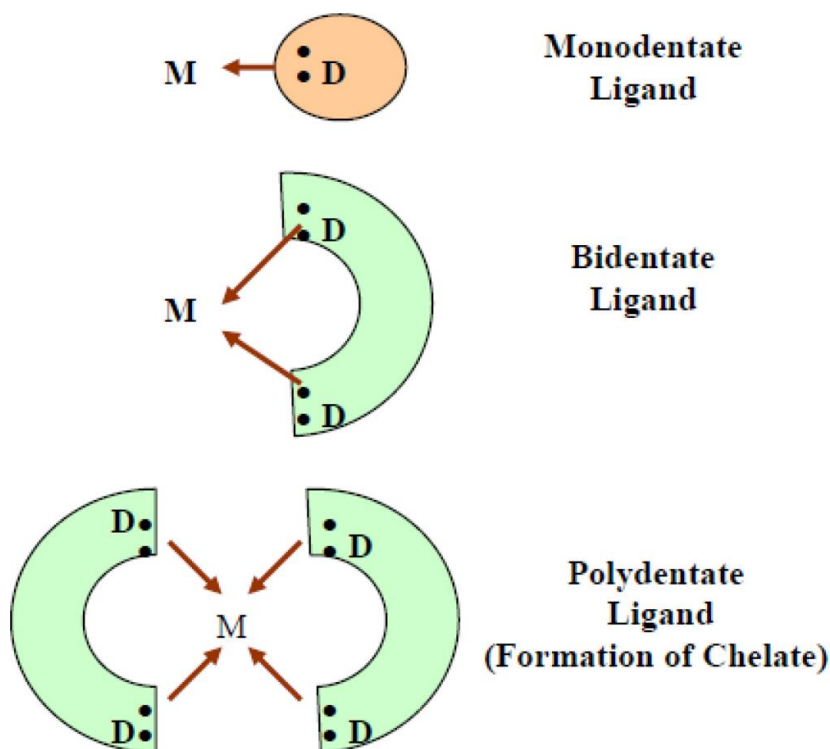
Figure 3: Mono, bi and polydentate ligand forming metal ligand complex. Mono ligand have only one donor atom and are coordinated through one pair of electrons. Polydentate ligands are ligands with two or more donor atoms and are coordinated more than one pair of electrons e.g. bidentate, tridentate. Reproduced from literature[34]

1.2.1.3 NOTA: Chelator Investigated

The present study focuses on the evaluation of the binding activity of 1,4,7-triazacyclononane-1, 4, 7-triacetic acid (NOTA). NOTA and it derivatives (NOPO, NETA, TACN-TM etc.), are popularly investigated chelators with amino carboxylic arms that can be utilized as a linker to form a peptide bond with a molecule. NOTA has the N_3O_3 coordination sphere geometry and consists of three carboxylic ($HCOO_2$) functional arms (**Figure 3**). NOTA is referred to as bifunctional because it is capable of binding metal ions (mostly radiometals) and can be covalently bonded to bio molecules such as monoclonal antibodies; thus they are able to deliver both diagnostic and therapeutic radiometals *in vivo* for radio-immunodiagnostic and radio - immunotherapy, respectively.[46]

NOTA is known to form a stable complex with gallium (III) isotopes, with favourable radiolabelling conditions and excellent *in vivo* stability[47, 48]; moreover, it has been approved for copper (II) isotopes where it forms hexadentate complexes with each[47, 49-51] Price et al[35] highlighted the experimental result of NOTA complexation with some selected radiometals.
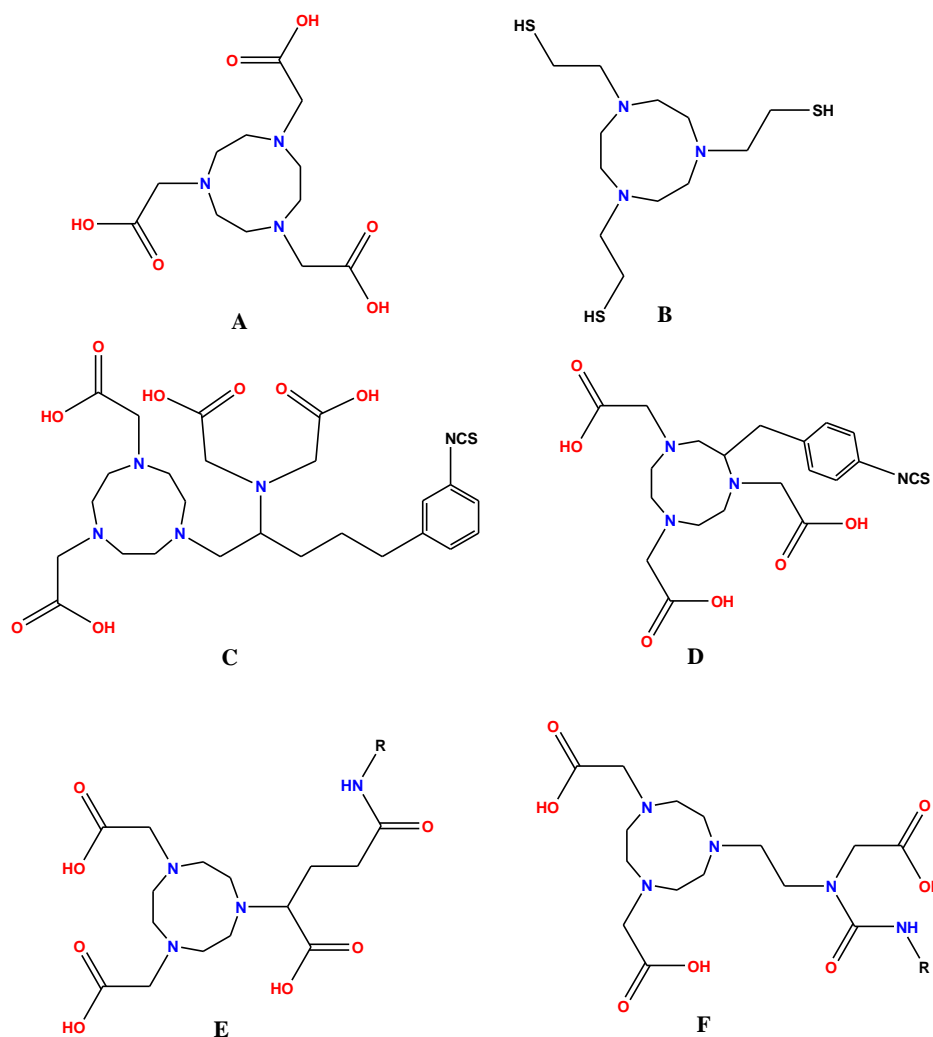
Figure 4: Structures of NOTA chelator and some of its derivatives.
A=NOTA, B=TACN-TM, C=3p-C-NETA, D= C-NOTA, E=NODAGA, F=NETAmonoamide

1.3. Radiometals

Radiometals emit radiation, which can be utilized for therapeutic and diagnosis purposes.[52] The use of radiometals in radiopharmaceuticals distinguishes it from the traditional therapeutic pharmaceuticals.[25] The availability of wide range of radio metals with differences in their features (half-lives, emissions types, energies and branching ratio) and different chemical demands (ligand donor atoms preference, hard or soft nature, aqueous chemistry, coordination number and coordination geometry) allow one to select the precise nuclear properties required for a specific application.[53] A deep knowledge of these features is required to help in selecting the appropriate chelator that will match with the radiometals of choice to create a complex that is stable and kinetically inert. In actual fact, before the synthesis of chelator for sequestering radio metal ions in aqueous solution or the reusing

chelators for a new radiometal ion, there is need for initial radiolabelling experiments to ensure the suitability of the radiometal with chelator or vice versa.[35]

1.4. Coordination chemistry of gallium, indium, copper, scandium and alkali metals

1.4.1. Gallium chemistry

Gallium is a member of elements found in the group three B (IIIB) of the periodic table, with a highly charged cation of ionic radius 47-62 pm and a prevalent oxidation state of +3 in aqueous solutions. Hard donor chelators like amine-N, carboxylate-O and phenolate-O atoms matches correctly with gallium owning to it high charge density. Gallium is able to attain *in vivo* stability with coordination number of six due to its small size[38, 54]; consequently, NOTA is able to sequester Ga(III) up to its maximum coordination number of 6 in a pseudo-octahedral geometry.[32] A detailed review on the coordination and radiopharmaceutical chemistry of gallium can be found in literature.[38, 54, 55] The challenges of the use of Ga^{3+} in radiopharmaceuticals is its strong affinity with transferrin (biological iron transporter), which could be detrimental to human system.[56, 57]

It is a well-known fact that NOTA (chelator investigated) is a gold standard chelator for gallium.[48, 58] An examination of the NOTA—Ga^{3+} complex structure affirmed a distorted octahedral encircling of the cation.[59] This effective envelopment of the gallium ion with an ionic radius 0.76Å within the macrocyclic cavity contributed to the exceptional stability[32]. *In vivo* stability and transchelation is provided by extra protection given by the carboxyl methyl pendant arm which prevent the Ga^{3+} ion from nucleophilic attack.

1.4.2. Indium chemistry

A common feature of 'In^{3+}' and 'Ga^{3+}' is that they are both members of the group three of the periodic table and, therefore, possess stable aqueous oxidation numbers of +3. The major difference between these two metals can be seen in their sizes and charge densities. Unlike Gallium, Indium is significantly large with an ionic radius of 62-92 and it able to attain a coordination of 7-8 in it complexes. This difference is generally seen in their different coordinating chemistry with DTPA and DOTA. For example, in Ga^{3+}—DOTA-D-phe-NH$_2$, Ga^{3+} has an ionic radius of 0.65Å[59] and a coordination number of 6[60] while In^{3+} has a coordination number of 8[61] and ionic radius of 0.92Å[59] in In^{3+}—DOTA-BA complex. A study of the complexation of Ga^{3+} and In^{3+} with DOTATOC confirms that the difference in the sizes of these two metal ions explain the reason while Ga—DOTATOC has a higher

tumor uptake and lower kidney uptake than In^{3+}—DOTATOC.[60] Although indium is a hard Lewis acid but when compared with gallium, it possesses a slightly enhanced affinity for soft donor chelators. It possesses a higher pKa of 4.0 and faster water exchange rate[32]. A study of In—Cl-NOTA complexation of NOTA confirms a near pentagonal bi-pyramidal geometry with protonation at one of it carboxylate arms.[62, 63] Price et al[35] in their recent review, however, confirms a distorted octahedral geometry for the complexation of NOTA with In^{3+}.

1.4.3. Copper chemistry

Copper is a first row transition metal with a few radioisotopes such as ^{60}Cu, ^{61}Cu, ^{62}Cu, ^{64}Cu and ^{67}Cu. The study of Cu(II) complexes with cyclam and cyclen derivatives reveals the elasticity of Cu(II) coordination chemistry.[64] The rich coordination chemistry of Cu has paved way for the synthesis of numerous diagnostic and therapeutic radiopharmaceuticals from the combination of diverse nuclear properties of Cu radionuclide and suitable chelator.[65] Donnelly[66] in his recent review gave an in-depth explanation of the role of coordination chemistry of copper in the development radiopharmaceuticals. He pointed out that the long-life of ^{64}Cu (912.7h) allows PET imaging to be performed at the site far from the cyclotron facility used to generate the radionuclide. Furthermore, ^{64}Cu emits β radiation that is useful for certain therapeutic applications. Although the coordination number of copper ranges from 4-6, the *d9* Cu (II) coordination chemistry in aqueous solution is amendable and prevalently used .[32] Comprehensive review on the coordination chemistry and radiochemistry of copper was presented by blower and co-workers.[67] The possibility of Cu displaying six coordination mode is shown during complexation of Cu with NOTA ligand with a distorted trigonal prismatic geometry.[68]

1.4.4. Scandium chemistry

Scandium, element of the periodic table is a member of the rare earth elements[69], with electronic configuration $[Ar]3d^14s^2$; it is a member of group III of the periodic table whose ionic radius has been reported as 0.745 Å[70]. Scandium is generally referred to as a lanthanide element because it shares similar properties with the lanthanide elements with $(n-1)d^1ns^2$ outermost electron configuration. It possesses a large ionic radius with the coordination number ranging from 3-12.[71] The isotopes of Sc includes; ^{45}Sc, ^{46}Sc, ^{47}Sc, ^{48}Sc, ^{49}Sc. Scandium (III) ion , which is the most common can easily form complexes with both organic and inorganic ligands, owing to it small ionic radius[72]. The study of the geometry of NOTA-Sc from literature confirms a distorted octahedral geometry.[73]

1.5. Optimal match of a chelator with a radiometal ion for radiopharmaceutical applications

In the synthesis of radiopharmaceuticals there is a need to match the a suitable chelator or ligand[4] with the right radiometal. This can expedite the development of efficient imaging probe by improving targeting features and providing positive *in vivo* pharmacokinetics of radiolabelled probe.[74] A thorough insight on chelator, radiometals and complexes were given by Price and Orvig[35], cutler, et al[75], Park J. and Jim J.Y.[76], Subramanian, et al[52] and Okarvi, et al.[77] Several factors have to be taken into consideration before preparing the chelator and before matching chelators with metal ion.

1.5.1. Thermodynamic stability and kinetic inertness

In radiopharmaceutical design, it is important that the principal properties such as thermodynamic stability and kinetic inertness of complexation kinetic of the metal-ligand complex be analysed.[53] This includes the ability of the chelator to bind the metal and adequately radiolabel at high yield, ability to radiolabel at ambient temperature and lastly a fast reaction time which is very necessary for short half-life isotopes like Gallium (^{68}Ga). The metal-chelate complex should be thermodynamically stable and must take into consideration not only the thermodynamic stability for the reaction between the metal ion and the chelator but also the equilibria involving H^+ binding to ligands and OH^- binding to metal that normally take place in all aqueous solutions.[52 78]

1.5.2. Attaching BFC to the biomolecule

Another factor that should be considered is the linker-bioconjugation strategies. The placement and the method of the BFC is vital; it is imperative that the conjugation mode does not hinder the binding ability of the ligand to metal ions and that of biomolecule to it proposed site in vivo.[53] It is essential to employ a binding mode that occurs speedily at room temperature, putting in mind that targeting vectors are sensitive biomolecules liable to degradation under a high temperature. The four conjugation strategies that are mostly used in radiopharmaceutical construction are; peptide, thiourea, thioether and click chemistry triazole bonds. Forster et al[79] highlighted two possible sites for connecting NOTA biomolecules and also for regulation of the pharmacokinetic properties of the radiopharmaceuticals. They proposed that the introduction of NOTA through the thiol groups of cysteine residues could

have better in vivo distribution of the radiopharmaceutical.[79] Example of a chelator developed by the altering of the c-site is p-SCN-Bn-NOTA(C-NOTA), while example of chelator formed by altering N-cite is NODASA.
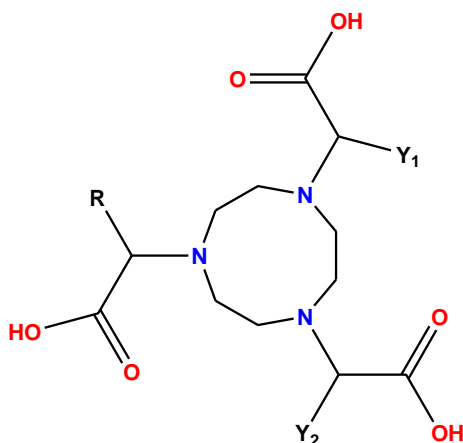
Figure 5: Possible sites in NOTA chelator for conjugation or modification to create more BFC. R, Y_1 and Y_2 indicate the methylene group of the acetic acid arm (N-site).

1.5.3. Flexibility

Flexibility should be incorporated in the synthesis of a chelator, such that one can incorporate different bioconjugation handles and also modify the denticity and other visible features by changing the polarity and charge of the chelate as this can influence the bio distribution of the radiopharmaceutical.[35]

1.5.4. Vector and biological targets

In the synthesis of radiopharmaceuticals for therapeutic treatment of a cancerous or diseased cell, the radiolabelled biomolecule or the targeting vector must be designed in such a way that enhances binding with high affinity and must be specific to the diseased tissue,[80, 81] ; this is because the concentration of the therapeutic doses of radiation at the tumor cell depends on the localization of radiolabelled biomolecule (receptor ligands) and how well it binds to the target cell.[25] Peptide, antibodies, antibody fragments, and nanoparticles are biomolecules that are frequently used to target surface receptor in a cancerous cell.[82 83]

The biological properties (half live, size) of the biomolecule must be considered and must match with the physical properties of the radiometals.[40] A higher percentage of the radiopharmaceutical must be accumulated at the site of the target tumor and the unbounded radiation dose must be excreted from the blood

1.5.5. Rate of dissociation

According to price et al[35], thermodynamic stability kinetic inertness and rate of dissociation should be given attention when assessing and making decisions on which chelator to match with a particular radiometal for radiopharmaceuticals. This is because, thermodynamic stability predicts *in vivo* stability effectively, while rate of dissociation governs the kinetic inertness of the radiometal complex to a great extent[84].

1.6. Displacement of radiometals from chelators by alkali metals.

There is possibility that radiometals are disassociated from chelators by other bio molecules because radiometals are used in minute quantities in an immensely dilute environment (human system); hence, the present of only a few nanomoles of impurity may actually be more than the radiometal ion concentration, which therefore, might compete for the binding site in a ligand.[85, 86] Furthermore, part of the factors that determine the dissociation of radiometals from the chelate includes, the amount of radiometal in the blood and the presence of active, native biological chelator competing ions (Na^+, K^+), which are usually present in higher concentration than the radiopharmaceuticals and are able to displace radio metals from radiopharmaceuticals. Hence experiments evaluating and measuring the comparative kinetic inertness of ligand- metal complex to acidic state have been performed, using techniques such as High Performance Liquid Chromatography (HPLC), Thin Layer Chromatography (TLC) and Nuclear Magnetic Resonance (NMR).

The present study, is employing computational techniques to study complexation of NOTA with competitive ions specifically alkali metal (Li^+, Na+ K^+ and Rb^+) to ascertain how well alkali metal ions bind with NOTA chelator which explains the level of competition of these ions with radiometals and the complexation of NOTA with the radiometals themselves(Cu^{2+}, Ga^{3+}, Sc^{3+} and In^{3+}).

1.7. Origin and applications of Computational Chemistry

Computational chemistry is a widely embraced measure by scientists to supplement or provide molecular insight to explain the observations from experimental studies. It is the use of computer to generate information that is supplementary to experimental data on structures, properties and reactions of substances.[87]

Mathematical science seems to be the relevant link between computational chemistry and theoretical chemistry. Mathematical science has provided the basic tools for creating and disseminating of conceptual framework at the atomic and molecular levels in computational chemistry. Mathematical science has also been used to construct and implement quantitative algorithms for organizing enormous quantity of data from laboratory to predicting the course and extend of chemical phenomena in situation that is strenuous or not possible to examine directly.[88] This thus accounts for the close similarity between computational and theoretical chemistry. In reality some scholars use the two interchangeably or concurrently.[89, 90] A school of thoughts believes that computational chemistry is a part of most general field of theoretical chemistry.[90, 91] To get a clear distinction between the two terms, David young pointed out that theoretical chemistry can defined as the mathematical description of chemistry while computational chemistry is used when an adequately developed mathematical method can be automatically implemented on a computer.[92]

Computational chemistry is a discipline consisting of several applications in most areas of chemistry, biochemistry and material science.[93] Using the software design for computational chemists, one is able to perform diverse studies on different systems few of which are; electronic structure determination[94-96], geometry optimization[97-101], definition of transition states[102 103-105], docking or protein calculations[106 107-109], electronic and charge distribution[110-113], calculation of potential energy surfaces[114-117] thermodynamic calculations.[118-121] The benefits of the use of computers in chemistry are worth underlining especially in the pharmaceutical industries where they employ the use for computers for drug discovery. Computational drug discovery is a well rooted discipline in the field of computational chemistry.[122-129] Computational chemistry can be utilized for the production of new drugs from the broad view of molecules[129, 130] and biological targets.[131, 132] For example, in the instance of an unknown unidentified drug target or non-existent target receptor, Quantitative Structural Activity Relationship (QSAR) can be created by comparing different ligands with changing biological actions.[133, 134] In other words, computational chemistry assists experts to make prediction before carrying out the real laboratory experiments to keep them readily prepared for making observation and also to save cost and time.[92]

1.7.1 Limitations of computational chemistry

Despite the progresses that have been made in the field of computational chemistry, there exist challenges as experienced in any other fields. The increase in the number of users

results from the availability of easy to use software accommodates users without knowledge of basic principles. For this reason, the work of many computational chemist is not explicitly explained which result to poor rating of the work. [91, 92] This apparently indicates that computational chemistry field lacks adequate professional experts. Jesen[91] pointed out that the bleak reputation of computational chemistry is as a result of absences of quality assessment, considering the fact that different computational methods give different results and computational chemists select the figures closet to experimental and therefore claim to provide results matching experimental data accurately.[91]

1.8. Tools used in computational chemistry

Computational Chemistry has some collections of methods to provide answers to questions on molecular geometry, energies of molecules, transition states of reaction, chemical reactivity etc. The main group available belong to five broad classes,[135] which consist the following:

1.8.1. Molecular mechanics (MM)

Molecular mechanic methods model the behaviour of very big molecules by setting up a simple algebraic expression of the total energy of the compound without necessarily computing the wave function or total electron density.[136] It is a method that characterizes the interaction between atoms using a set of parameters and simple potential energy function known as force field.[137] Out of all the different methods used to study structures of molecules, molecular mechanics has been identified as an approach that is cost effective and with a high level of accuracy. [138 135] Huge success has been recorded by applying molecular mechanic to many classes of isolated, gas-phase organic compounds.[139] Many computational bio-chemists uses MM because of its ability to analyse very large system (up to 10^6 atoms) with simple energy expression.[140] A Plethora of studies on free energies calculation, modelling of large systems, evaluation of several biological components and activities has been performed using MM.[141-146] MM is limited to employing force fields which majorly make use of information embodied in the input geometry, namely bond length, valence angle and dihedral angle,[147] thus ignoring many chemical properties like the electron excited state.[136, 137, 140] However, chemist over the years have combined the use of MM and Quantum Mechanics (i.e. QM/MM approach) in an attempt to study both the electronic structure of molecules and the interaction between atoms in a larger system.[137 147-150]

1.8.2. *Ab initio* methods

Ab initio methods are based on the Schrödinger equation.[135, 140] They are employed to investigate how electrons in a molecule behave by solving the Schrödinger equation for a molecule. It can provide the energies and wave function, which can be used to calculate electron structure.[135, 140, 151] The limitations of *Ab initio* calculations include the fact that they expensive[152] and also comparably slow, thus the calculation of a fairly large molecule can take a long time.[135] Examples of ab initio methods includes; Hartree-Fock, multi-configuration Hartree-Fock, Moller-Plessets(MP), Configuration Interaction.[140, 153]

1.8.3. Semi- empirical methods

Semi- empirical methods abide by a simple strategy by starting off from an ab initio or first principles formalism and then offer a rather drastic assumption to accelerate the calculation process, mostly by ignoring many of the less important terms in the underlying equations.[152] It involves the incorporation of theory with experiment which makes the method semi-empirical.[135, 152, 154] Semi empirical methods amongst all other methods has capacity to manage system composed of several thousand of atoms and usually faster than DFT.[155] A conspicuous flaw of the use of this method is that, it is only of sufficient accuracy when utilized to model molecules of the same type as used as the reference data in the parameterization, otherwise it will end up into unusual and erroneous results.[154] In spite of the limitation of semi-empirical methods, several investigations on modelling of organic molecules have been performed using the semi empirical method. PM3, PM6, AM1, MNDO, INDO, are examples of semi empirical methods that are regularly used.[156-159]

1.8.4 Molecular dynamics (MD) methods

Molecular dynamics is a computational stimulation tool that gives a detailed account of the physical forces and movement of interacting tiny elements like atoms and molecules.[160] Molecular dynamics basically employs the law of motions to molecules.[135, 161] The major limitation is the slow simulation time, which is in the order of nanoseconds for large systems.[162] This means that there is limit in configurational sampling that can be achieved by molecular dynamics. A recent paper by Yeguas and co-workers[160] evaluates the ongoing limitations associated with voluminous data analysis related to MD process and highlighted possible solutions to overcome this shortcoming.

1.8.5. Density Functional Theory (DFT) Methods

DFT methods are based on Schrödinger equation but contrary to semi- empirical and *ab initio* methods, they use   evaluate the electron distribution directly without considering the conventional wave function.[135] The attempt by Hohenberg, Kohn and Sham in the mid-60s to verify that electron density can serve as a fundamental quantity to determine the ground state of theories, applicable to any systems composed of atoms and molecules of any atomic, molecular, or system in solid state gave birth to DFT.[163] Today, DFT methods have successfully been used as tools to understand and anticipate the processes of chemical reactions, catalytic activity, bioactivity, photo physics, electronic and nuclear-magnetic resonance spectroscopy and properties in coordination chemistry.[164] To describe non static condition in matters such as atoms, molecules, solid and nanostructures, time-dependent density functional theory is usually employed.[165] In spite of drawbacks which include; too many approximations, failure for strongly correlated system, the benefit of cost effective computational work coupled with advantageous accuracy has made DFT an accepted technique.[166]

Recent literature exploring reaction mechanisms, electronic states and structures have   had considered the application of DFT methods of particular interest to coordination chemistry.[167-172] The present work uses DFT methods to investigate the complexation of NOTA ligand with alkaline metals and radio metals. The B3LYP functional, which is the most extensively accepted functional in quantum chemistry, and has presented excellent performance in the computation of structures, energies and properties of molecules[164], will be utilized in our investigation.

1.9. Gaussian 09 Program

There exist differs types of computational chemistry software, however, Gaussian software was utilized in the present study. Gaussian is a computer program for computational chemistry that was originally created in 1970 by John Pople[173] and his group as Gaussian 70.[174] Update has been done continually on the Gaussian program since invention.[175] Gaussian 09 was used to perform relevant calculations as regards to this study. A concise essay on how and the use of the software (Gaussian 09) was written by Anna Tomberg.[176] With the aim of speeding up the calculation steps involved in our investigation and also avoiding delay resulting from bulky computational calculations requiring huge computer resources; this investigation on the complexation of NOTA with alkaline metals and

radiometal ions is carried out using the Gaussian 09 software installed on cluster provided by the Center for High Performance Computing in Cape Town. (www.chpc.ac.za).

1.10. Types of calculation

Below are the descriptions of the job types that are relevant to our study.

1.10.1. Geometry Optimization

Schlegel[177], described geometry optimization procedure as a crucial step of most chemical calculations, necessary to calculate the wave function and geometry of a lowest energy. This process is continually carried out until the lowest attainable energy on the potential energy surface (PES) of the geometry is established.[176] The data that can be obtained from performing this calculation includes; atomic coordinates of the optimized molecular structure, optimized parameters in terms of the atomic distances and angles, HOMO/LUMO eigenvalues etc.

1.10. 2. Population Analysis

Population analysis is an approach in computational chemistry that estimates the charges of the atoms and in the studied molecule[136], providing a clear understanding of electron distribution which cannot be achieved experimentally.[176] Furthermore, it is an effective tool in anticipating likely sites for nucleophilic and electrophilic attack and other aspects of molecular activities. Amongst the available population analysis, this study selected the Natural Bond Orbital analysis[178] (NBO) to investigate the nature of electron transfer and distributions in the complexation process of NOTA chelator with alkali metal and radio metal.

1.10.3. The effects of solvation

By default, all calculations on Gaussian 09 are performed in gas phase. However, if there is need to perform any calculation in solution; one can either add solvation effect explicitly or implicitly.[176] The present study investigates the effect of explicit solvation on some of the calculated parameters, using Polarizable Continuum Model (PCM) using integral equation-formalism polarizable continuum model (IEF-PCM).

1.10.4. Nuclear Magnetic Resonance spectroscopy (NMR)

The use of NMR spectroscopy in exploring the properties of organic molecules has become a significant tool to organic chemists. NMR provides information about the structural composition of the molecule of a sample by evaluating the variety of interactions between the nuclei and the electrons of a molecule and neighbouring molecules.[179]

1.10.5. Basis sets

Basis sets are sets of functions that illustrate the shape of atomic orbitals (AOs),[176] through the use of specified theoretical models.[180] The objective of a basis set is to present the best description of the orbitals or electron densities that are not known using the little computational cost possible.[181] The choice of basis sets in quantum chemical calculation can have a colossal effect on the accuracy of the result.[182] Most commercial computational chemistry software packages for ab initio or DFT calculations usually come with some defined basis sets, out of which the user can make choice.[183] To make choice of the basis set to use for a system, each atoms in the molecule is optimized using different basis set until a convergence is attained. It is best that the basis set of choice be flexible enough to produce a good result while accounting for all atoms in the molecular geometry and adequately small enough for easy computation of the operation.[172] It should be noted that, a large basis set run longer but gives a more accurate result. This study will be coupling the Becke 3-parameter, Lee Yang-Parr (B3LYP) with 6-31 +(2d, 2p)[184, 185], LANL2DZ[186, 187] and DGDZVP[188, 189] basis set, to make sure that all atoms are accounted for in the reaction. A number of researchers have investigated on basis sets. Ahlrichs and Taylor[190], Feller and Davidson[190], has written on the choice of basis sets for molecular calculation. Frank[181] and grant[182] recently published a broad update on basis sets ; compiled some of the assumptions for the construction and analysis of basis sets, with focus on contemporary ranked basis sets.

1.10.6. Basis Sets Superposition Error

The non-completeness of basis set as a result of the truncation of basis set function introduced by the Linear Combination of Atomic Orbital (LCAO) approximations, results into an effect called the basis set superposition error (BSSE). It is crucial that the correct basis set is used in our calculation; otherwise the BSSE can increase even with a large basis set.[191] A comprehensive detail on the procedure for BSSE calculation is presented by

Xantheas.[192] The present study will be using the BSSE of different basis set to make our choice of basis sets to use in the investigation.

1.11. Aims and objectives.

➤ To understand the structural composition of NOTA chelator.

➤ To analyse the complexation of NOTA chelators with non-radioactive competing ions; alkaline metal ions (Li^+, Na^+, K^+, Rb^+) with the purpose of estimating the impact these competing ions on the radiolabelling yields of NOTA.

➤ To analyse the complexation of NOTA chelator with radiometals (Cu^{2+}, Ga^{3+}, Sc^{3+}, In^{3+}).

The extensive use of Density Functional Theory methods will be employed to determine all possible conditions involved during this reaction. Computational models present an exclusive opportunity to augment our understanding on basic parameters like charge distribution, interaction energies, complex conformation, etc.

1.12. Thesis outline

The layout of the study is presented in the following format:

Chapter 1 presents a brief background on subject matter of the study.

Chapter 2 presents the DFT investigation of the integration of NOTA chelator with alkaline metal ions.

Chapter 3 defines the theoretical investigation of NOTA chelator with radiometal ions.

Chapter 4 gives the summary of the dissertation.

REFERENCES

1.   Erkey, C. (2011) *Supercritical fluids and organometallic compounds: from recovery of trace metals to synthesis of nanostructured materials*, Vol. 1, Elsevier.

2.   Sears, M. E. (2013) Chelation: harnessing and enhancing heavy metal detoxification—a review, *The Scientific World Journal 2013*.

3.   Howard, W. L., and Wilson, D. (2000) Chelating agents, *Kirk-Othmer Encyclopedia of Chemical Technology*.

4.   Dwyer, F. (2012) *Chelating agents and metal chelates*, Elsevier.

5.   Niu, L., Shen, Z., Luo, C., Deng, Y.-e., and Wang, C. (2012) Accumulation mechanisms and subcellular distribution of Cu in maize grown on soil treated with [S, S]-ethylenediamine disuccinic acid, *Plant and soil 351*, 237-247.

6.   Huang, C.-H., Liu, S.-J., Lee, S.-F., Hwang, W.-S., and Lin, C.-F. (2013) A Pt/C Catalysts Using Chelating Agent Assisted Microwave Synthesis and Its Preparation, *Science of Advanced Materials 5*, 1737-1742.

7.   Zhang, Y.-q., Xie, X.-f., Huang, S.-b., and Liang, H.-y. (2014) Effect of chelating agent on oxidation rate of aniline in ferrous ion activated persulfate system at neutral pH, *Journal of Central South University 21*, 1441-1447.

8.   Leonova, K., Klimov, O., Kochubey, D., Chesalov, Y. A., Gerasimov, E. Y., Prosvirin, I., and Noskov, A. (2014) Optimal pretreatment conditions for Co–Mo hydrotreatment catalysts prepared using ethylenediamine as a chelating agent, *Catalysis Today 220*, 327-336.

9.   Kong, J.-Z., Yang, X.-Y., Zhai, H.-F., Ren, C., Li, H., Li, J.-X., Tang, Z., and Zhou, F. (2013) Synthesis and electrochemical properties of Li-excess Li 1+ x [Ni 0.5 Co 0.2 Mn 0.3] O 2 cathode materials using ammonia-free chelating agent, *Journal of Alloys and Compounds 580*, 491-496.

10.   Ilhan, S., Kalpakli, A. O., Kahruman, C., and Yusufoglu, I. (2013) The Use of Oxalic Acid as a Chelating Agent in the Dissolution Reaction of Calcium Molybdate, *Metallurgical and Materials Transactions B 44*, 495-505.

11.   Ahmed, Z., Kazmi, S. A., Shahid, M., and Buksh, N. (2014) The Divine Solution to the Fate of Metal Pollution from Industries.

12.   Allen, K. (2015) Metal chelators as antioxidants for food preservation, *Handbook of Antioxidants for Food Preservation*, 79.

13. Csiszár, E. l., Losonczi, A., Szakács, G., Rusznák, I., Bezúr, L., and Reicher, J. (2001) Enzymes and chelating agent in cotton pretreatment, *Journal of Biotechnology 89*, 271-279.

14. Cortez, J., Bonner, P. L., and Griffin, M. (2004) Application of transglutaminases in the modification of wool textiles, *Enzyme and Microbial Technology 34*, 64-72.

15. Khlifi, R., Belbahri, L., Woodward, S., Ellouz, M., Dhouib, A., Sayadi, S., and Mechichi, T. (2010) Decolourization and detoxification of textile industry wastewater by the laccase-mediator system, *Journal of Hazardous Materials 175*, 802-808.

16. Norman, P. I., and Seddon, R. (1991) Pollution control in the textile industry—the chemical auxiliary manufacturer's role, *Journal of the Society of Dyers and Colourists 107*, 150-152.

17. Edwards, C., Maguire, R., Alley, M., Thomason, W., and Whitehurst, G. (2016) Plant Available Phosphorus after Application of Synthetic Chelating Agents, *Communications in Soil Science and Plant Analysis*.

18. Afshan, S., Ali, S., Bharwana, S. A., Rizwan, M., Farid, M., Abbas, F., Ibrahim, M., Mehmood, M. A., and Abbasi, G. H. (2015) Citric acid enhances the phytoextraction of chromium, plant growth, and photosynthesis by alleviating the oxidative damages in Brassica napus L, *Environmental Science and Pollution Research*, 1-11.

19. Geyer, R. P. (2013) The design of artificial blood substitutes, *Drug Design: Medicinal Chemistry: A Series of Monographs 7*.

20. Dugas, H., and Penney, C. (2013) *Bioorganic chemistry: a chemical approach to enzyme action*, Springer Science & Business Media.

21. Al-Qudah, M., Alkahtani, R., Akbarali, H., Murthy, K., and Grider, J. (2015) Stimulation of synthesis and release of brain-derived neurotropic factor from intestinal smooth muscle cells by substance P and pituitary adenylate cyclase-activating peptide, *Neurogastroenterology & Motility 27*, 1162-1174.

22. Welch, M. J. (2013) *Radiopharmaceuticals and other compounds labelled with short-lived radionuclides*, Elsevier.

23. Decristoforo, C., Penuelas, I., Elsinga, P., Ballinger, J., Winhorst, A., Verbruggen, A., Verzijlbergen, F., and Chiti, A. (2014) Radiopharmaceuticals are special, but is this recognized? The possible impact of the new Clinical Trials Regulation on the preparation of radiopharmaceuticals, *European journal of nuclear medicine and molecular imaging 41*, 2005-2007.

24.   Knapp, F. R., and Dash, A. (2016) Introduction: Radiopharmaceuticals Play an Important Role in Both Diagnostic and Therapeutic Nuclear Medicine, In *Radiopharmaceuticals for Therapy*, pp 3-23, Springer.

25.   Liu, S. (2004) The role of coordination chemistry in the development of target-specific radiopharmaceuticals, *Chemical Society Reviews 33*, 445-461.

26.   Guasch, L., V Zakharov, A., A Tarasova, O., V Poroikov, V., Liao, C., and C Nicklaus, M. (2016) Novel HIV-1 Integrase Inhibitor Development by Virtual Screening Based on QSAR Models, *Current topics in medicinal chemistry 16*, 441-448.

27.   Cai, Z., Li, B. T., Wong, E. H., Weisman, G. R., and Anderson, C. J. (2015) Cu (I)-assisted click chemistry strategy for conjugation of non-protected cross-bridged macrocyclic chelators to tumour-targeting peptides, *Dalton Transactions 44*, 3945-3948.

28.   Sun, J., Zhang, D., Zheng, Y., Zhao, Q., Zheng, M., Kovacevic, Z., and Richardson, D. R. (2013) Targeting the metastasis suppressor, NDRG1, using novel iron chelators: regulation of stress fiber-mediated tumor cell migration via modulation of the ROCK1/pMLC2 signaling pathway, *Molecular pharmacology 83*, 454-469.

29.   Pérez-Medina, C., Abdel-Atti, D., Zhang, Y., Longo, V. A., Irwin, C. P., Binderup, T., Ruiz-Cabello, J., Fayad, Z. A., Lewis, J. S., and Mulder, W. J. (2014) A modular labeling strategy for in vivo PET and near-infrared fluorescence imaging of nanoparticle tumor targeting, *Journal of Nuclear Medicine 55*, 1706-1711.

30.   Lim, C.-K., Singh, A., Heo, J., Kim, D., Lee, K. E., Jeon, H., Koh, J., Kwon, I.-C., and Kim, S. (2013) Gadolinium-coordinated elastic nanogels for in vivo tumor targeting and imaging, *Biomaterials 34*, 6846-6852.

31.   Moussa, R. S., Kovacevic, Z., and Richardson, D. R. (2015) Differential targeting of the cyclin-dependent kinase inhibitor, p21CIP1/WAF1, by chelators with anti-proliferative activity in a range of tumor cell-types, *Oncotarget 6*, 29694-29711.

32.   Wadas, T. J., Wong, E. H., Weisman, G. R., and Anderson, C. J. (2010) Coordinating radiometals of copper, gallium, indium, yttrium, and zirconium for PET and SPECT imaging of disease, *Chemical reviews 110*, 2858-2902.

33.   Hong, H., Yang, K., Zhang, Y., Engle, J. W., Feng, L., Yang, Y., Nayak, T. R., Goel, S., Bean, J., and Theuer, C. P. (2012) In vivo targeting and imaging of tumor vasculature with radiolabeled, antibody-conjugated nanographene, *ACS nano 6*, 2361-2370.

34.   Flora, S. J. S., and Pachauri, V. (2010) Chelation in Metal Intoxication, *International Journal of Environmental Research and Public Health 7*, 2745-2788.

35.   Price, E. W., and Orvig, C. (2014) Matching chelators to radiometals for radiopharmaceuticals, *Chemical Society Reviews 43*, 260-290.

36.   Jones, M. M. (1993) Design of new chelating agents for removal of intracellular toxic metals, *Coordination Chemistry, A Century of Progress*, 427-438.

37.   Boros, E., Ferreira, C. L., Cawthray, J. F., Price, E. W., Patrick, B. O., Wester, D. W., Adam, M. J., and Orvig, C. (2010) Acyclic chelate with ideal properties for 68Ga PET imaging agent elaboration, *Journal of the American Chemical Society 132*, 15726-15733.

38.   Anderson, C. J., and Welch, M. J. (1999) Radiometal-labeled agents (non-technetium) for diagnostic imaging, *Chemical reviews 99*, 2219-2234.

39.   Price, E. W., Cawthray, J. F., Bailey, G. A., Ferreira, C. L., Boros, E., Adam, M. J., and Orvig, C. (2012) H4octapa: an acyclic chelator for 111In radiopharmaceuticals, *Journal of the American Chemical Society 134*, 8670-8683.

40.   Ramogida, C. F., Cawthray, J. F., Boros, E., Ferreira, C. L., Patrick, B. O., Adam, M. J., and Orvig, C. (2015) H2 CHX dedpa and H4 CHX octapa▯ Chiral Acyclic Chelating Ligands for 67/68Ga and 111In Radiopharmaceuticals, *Inorganic chemistry 54*, 2017-2031.

41.   Silva, F., Campello, M. P. C., Gano, L., Fernandes, C., Santos, I. C., Santos, I., Ascenso, J. R., Ferreira, M. J., and Paulo, A. (2015) Chemical, radiochemical and biological studies of new gallium (III) complexes with hexadentate chelators, *Dalton Transactions 44*, 3342-3355.

42.   Varasteh, Z., Mitran, B., Rosenström, U., Velikyan, I., Rosestedt, M., Lindeberg, G., Sörensen, J., Larhed, M., Tolmachev, V., and Orlova, A. (2015) The effect of macrocyclic chelators on the targeting properties of the 68 Ga-labeled gastrin releasing peptide receptor antagonist PEG 2-RM26, *Nuclear medicine and biology 42*, 446-454.

43.   Albrecht, R., Fehse, S., Pant, K., Nowag, S., Stephan, H., Haag, R., and Tzschucke, C. C. (2015) Polyglycerol-Based Copper Chelators for the Transport and Release of Copper Ions in Biological Environments, *Macromolecular bioscience*.

44.   Hancock, R. (1992) The basis of selectivity for metal ions in open-chain ligands and macrocycles, *J. Chem. Educ 69*, 615-621.

45.   Andersen, O. (1999) Principles and Recent Developments in Chelation Treatment of Metal Intoxication, *Chemical Reviews 99*, 2683-2710.

46.   Gupta, S., Batra, S., and Jain, M. (2014) Antibody Labeling with Radioiodine and Radiometals, In *Drug Delivery System*, pp 147-157, Springer.

47.   Correia, J. D., Paulo, A., Raposinho, P. D., and Santos, I. (2011) Radiometallated peptides for molecular imaging and targeted therapy, *Dalton Trans. 40*, 6144-6167.

48.   Velikyan, I., Maecke, H., and Langstrom, B. (2008) Convenient preparation of 68Ga-based PET-radiopharmaceuticals at room temperature, *Bioconjugate chemistry 19*, 569-573.

49.   Shokeen, M., and J Wadas, T. (2011) The development of copper radiopharmaceuticals for imaging and therapy, *Medicinal Chemistry 7*, 413-429.

50.   Ait-Mohand, S., Fournier, P., Dumulon-Perreault, V., Kiefer, G. E., Jurek, P., Ferreira, C. L., Bénard, F. o., and Guérin, B. (2011) Evaluation of 64Cu-labeled bifunctional chelate–bombesin conjugates, *Bioconjugate chemistry 22*, 1729-1735.

51.   Chang, A. J., Sohn, R., Lu, Z. H., Arbeit, J. M., and Lapi, S. E. (2013) Detection of rapalog-mediated therapeutic response in renal cancer xenografts using 64Cu-bevacizumab immunoPET, *PloS one 8*, e58949.

52.   Subramanian, R., and Meares, C. F. (2012) 9. Bifunctional chelating agents for radiometal-labeled, *Cancer Imaging with Radiolabeled Antibodies 51*, 183.

53.   Ramogida, C. F., and Orvig, C. (2013) Tumour targeting with radiometals for diagnosis and therapy, *Chemical Communications 49*, 4720-4739.

54.   Reichert, D. E., Lewis, J. S., and Anderson, C. J. (1999) Metal complexes as diagnostic tools, *Coordination Chemistry Reviews 184*, 3-66.

55.   Bandoli, G., Dolmella, A., Tisato, F., Porchia, M., and Refosco, F. (2009) Mononuclear six-coordinated Ga (III) complexes: A comprehensive survey, *Coordination Chemistry Reviews 253*, 56-77.

56.   Harris, W. R., and Pecoraro, V. L. (1983) Thermodynamic binding constants for gallium transferrin, *Biochemistry 22*, 292-299.

57.   Harris, W. R., Chen, Y., and Wein, K. (1994) Equilibrium constants for the binding of indium (III) to human serum transferrin, *Inorganic Chemistry 33*, 4991-4998.

58.   Martell, A. E., Motekaitis, R. J., Clarke, E. T., Delgado, R., Sun, Y., and Ma, R. (1996) Stability constants of metal complexes of macrocyclic ligands with pendant donor groups, *Supramolecular Chemistry 6*, 353-363.

59.   Moore, D. A., Fanwick, P. E., and Welch, M. J. (1990) A novel hexachelating amino-thiol ligand and its complex with gallium (III), *Inorganic Chemistry 29*, 672-676.

60.   Heppeler, A., Froidevaux, S., Mäcke, H., Jermann, E., Béhé, M., Powell, P., and Hennig, M. (1999) Radiometal-Labelled Macrocyclic Chelator-Derivatised Somatostatin Analogue with Superb Tumour-Targeting Properties and Potential for Receptor-Mediated Internal Radiotherapy, *Chemistry–A European Journal 5*, 1974-1981.

61.   Maecke, H., Scherer, G., Heppeler, A., and Hennig, M. (2001) Is In-111 an ideal surrogate for Y-90? If not why?, In *EUROPEAN JOURNAL OF NUCLEAR MEDICINE*, pp 967-967, SPRINGER-VERLAG 175 FIFTH AVE, NEW YORK, NY 10010 USA.

62.   Clarke, E. T., and Martell, A. E. (1991) Stabilities of trivalent metal ion complexes of the tetraacetate derivatives of 12-, 13-and 14-membered tetraazamacrocycles, *Inorganica Chimica Acta 190*, 37-46.

63.   Craig, A. S., Helps, I. M., Parker, D., Adams, H., Bailey, N. A., Williams, M. G., Smith, J. M., and Ferguson, G. (1989) Crystal and molecular structure of a seven-coordinate chloroindium (III) complex of 1, 4, 7-triazacyclononanetriacetic acid, *Polyhedron 8*, 2481-2484.

64.   Bakaj, M., and Zimmer, M. (1999) Conformational analysis of copper (II) 1, 4, 8, 11-tetraazacyclotetradecane macrocyclic systems, *Journal of molecular structure 508*, 59-72.

65.   Wadas, T., Wong, E., Weisman, G., and Anderson, C. (2007) Copper chelation chemistry and its role in copper radiopharmaceuticals, *Current pharmaceutical design 13*, 3-16.

66.   Donnelly, P. S. (2011) The role of coordination chemistry in the development of copper and rhenium radiopharmaceuticals, *Dalton Transactions 40*, 999-1010.

67.   Blower, P. J., Lewis, J. S., and Zweit, J. (1996) Copper radionuclides and radiopharmaceuticals in nuclear medicine, *Nuclear medicine and biology 23*, 957-980.

68.   Wieghardt, K., Bossek, U., Chaudhuri, P., Herrmann, W., Menke, B. C., and Weiss, J. (1982) 1, 4, 7-Triazacyclononane-N, N', N''-triacetate (TCTA), a new hexadentate ligand for divalent and trivalent metal ions. Crystal structures of [CrIII (TCTA)],[FeIII (TCTA)], and Na [CuII (TCTA)]. bul. 2NaBr. bul. 8H2O, *Inorganic Chemistry 21*, 4308-4314.

69.   Horovitz, C. T. (2012) *Biochemistry of scandium and yttrium, Part 1: physical and chemical fundamentals*, Vol. 13, Springer Science & Business Media.

70.   TÜRKEL, N., AYDIN, R., and ÖZER, U. (1999) Stabilities of complexes of scandium (III) and yttrium (III) with catechol Derivatives, *Turkish Journal of Chemistry 23*, 139-152.

71.   Huang, C.-H. (2011) *Rare earth coordination chemistry: fundamentals and applications*, John Wiley & Sons.

72.   Horovitz, C. T. (2012) *Scandium Its Occurrence, Chemistry Physics, Metallurgy, Biology and Technology*, Elsevier.

73.　　Majkowska-Pilip, A., and Bilewicz, A. (2011) Macrocyclic complexes of scandium radionuclides as precursors for diagnostic and therapeutic radiopharmaceuticals, *Journal of inorganic biochemistry 105*, 313-320.

74.　　Deng, H., Wang, H., and Li, Z. (2015) Matching chelators to radiometals for positron emission tomography imaging-guided targeted drug delivery, *Current drug targets 16*, 610-624.

75.　　Cutler, C. S., Hennkens, H. M., Sisay, N., Huclier-Markai, S., and Jurisson, S. S. (2013) Radiometals for combined imaging and therapy, *Chem. Rev 113*, 858-883.

76.　　Park, J., and Kim, J. Y. (2013) Recent advances in radiopharmaceutical application of matched-pair radiometals, *Current topics in medicinal chemistry 13*, 458-469.

77.　　Okarvi, S. M., and Maecke, H. R. (2015) Radiometallo-Labeled Peptides in Tumor Diagnosis and Targeted Radionuclide Therapy, *Advances in Inorganic Chemistry*.

78.　　Martell, A. E., and Hancock, R. D. (2013) *Metal complexes in aqueous solutions*, Springer Science & Business Media.

79.　　Förster, C., Schubert, M., Pietzsch, H.-J., and Steinbach, J. (2011) Maleimido-Functionalized NOTA Derivatives as Bifunctional Chelators for Site-Specific Radiolabeling, *Molecules 16*, 5228-5240.

80.　　Deal, K. A., Davis, I. A., Mirzadeh, S., Kennel, S. J., and Brechbiel, M. W. (1999) Improved in vivo stability of actinium-225 macrocyclic complexes, *Journal of medicinal chemistry 42*, 2988-2992.

81.　　Boswell, C. A., and Brechbiel, M. W. (2007) Development of radioimmunotherapeutic and diagnostic antibodies: an inside-out view, *Nuclear medicine and biology 34*, 757-778.

82.　　Ciavarella, S., Milano, A., Dammacco, F., and Silvestris, F. (2010) Targeted therapies in cancer, *BioDrugs 24*, 77-88.

83.　　Hamoudeh, M., Kamleh, M. A., Diab, R., and Fessi, H. (2008) Radionuclides delivery systems for nuclear imaging and radiotherapy of cancer, *Advanced drug delivery reviews 60*, 1329-1346.

84.　　Martell, A. E., and Smith, R. M. (1977) *Other organic ligands*, Vol. 3, Springer.

85.　　Zeng, D., and Anderson, C. J. (2013) Rapid and sensitive LC-MS approach to quantify non-radioactive transition metal impurities in metal radionuclides, *Chemical Communications 49*, 2697-2699.

86.   Zeng, D., and Anderson, C. J. (2013) Production and Purification of Metal Radionuclides for PET Imaging of Disease, *Solvent Extraction and Ion Exchange 31*, 337-344.

87.   Lipkowitz, K. B. (1998) Applications of computational chemistry to the study of cyclodextrins, *Chemical reviews 98*, 1829-1874.

88.   Weidman, S. (1995) Mathematical Challenges From Theoretical/Computational Chemistry, DTIC Document.

89.   Csizmadia, I. G., and Daudel, R. (2012) *Computational theoretical organic chemistry: proceedings of the NATO Advanced Study Institute held at Menton, France, June 29-July 13, 1980*, Vol. 67, Springer Science & Business Media.

90.   Bort, J. A., and Rusca, J. B. (2007) *Theoretical and Computational Chemistry: Foundations, methods and techniques*, Universitat Jaume I.

91.   Jensen, F. (2013) *Introduction to computational chemistry*, John Wiley & Sons.

92.   Young, D. C. (1999) Computational Chemistry: A Practical Guide for Applying Techniques to Real World Problems. 2001.

93.   Karlström, G., Lindh, R., Malmqvist, P.-Å., Roos, B. O., Ryde, U., Veryazov, V., Widmark, P.-O., Cossi, M., Schimmelpfennig, B., Neogrady, P., and Seijo, L. (2003) MOLCAS: a program package for computational chemistry, *Computational Materials Science 28*, 222-239.

94.   Rowley, C. N., and Roux, B. t. (2012) The solvation structure of Na+ and K+ in liquid water determined from high level ab initio molecular dynamics simulations, *Journal of Chemical Theory and Computation 8*, 3526-3535.

95.   Shao, Y., Gan, Z., Epifanovsky, E., Gilbert, A. T., Wormit, M., Kussmann, J., Lange, A. W., Behn, A., Deng, J., and Feng, X. (2015) Advances in molecular quantum chemistry contained in the Q-Chem 4 program package, *Molecular Physics 113*, 184-215.

96.   Chrostowska, A., Xu, S., Lamm, A. N., Mazière, A., Weber, C. D., Dargelos, A., Baylère, P., Graciaa, A., and Liu, S.-Y. (2012) UV-Photoelectron spectroscopy of 1, 2-and 1, 3-azaborines: a combined experimental and computational electronic structure analysis, *Journal of the American Chemical Society 134*, 10279-10285.

97.   Minenkov, Y., Singstad, Å., Occhipinti, G., and Jensen, V. R. (2012) The accuracy of DFT-optimized geometries of functional transition metal compounds: a validation study of catalysts for olefin metathesis and other reactions in the homogeneous phase, *Dalton Transactions 41*, 5526-5541.

98.   Winter, N. O., Graf, N. K., Leutwyler, S., and Hättig, C. (2013) Benchmarks for 0–0 transitions of aromatic organic molecules: DFT/B3LYP, ADC (2), CC2, SOS-CC2 and SCS-CC2 compared to high-resolution gas-phase data, *Physical Chemistry Chemical Physics 15*, 6623-6630.

99.   Waller, M. P., Kruse, H., Mück-Lichtenfeld, C., and Grimme, S. (2012) Investigating inclusion complexes using quantum chemical methods, *Chemical Society Reviews 41*, 3119-3128.

100.   Chen, P.-Q., Tan, C.-x., Weng, J.-q., and Liu, X.-H. (2012) Synthesis, Structure and DFT calculation of chlorimuron-ethyl, *Asian Journal of Chemistry 24*, 2808.

101.   Wanbayor, R., and Ruangpornvisuti, V. (2012) A periodic DFT study on binding of Pd, Pt and Au on the anatase TiO 2 (001) surface and adsorption of CO on the TiO 2 surface-supported Pd, Pt and Au, *Applied Surface Science 258*, 3298-3301.

102.   Castro-Gómez, F., Salassa, G., Kleij, A. W., and Bo, C. (2013) A DFT study on the mechanism of the cycloaddition reaction of CO2 to epoxides catalyzed by Zn (Salphen) complexes, *Chemistry-A European Journal 19*, 6289-6298.

103.   Nikbin, N., Do, P. T., Caratzoulas, S., Lobo, R. F., Dauenhauer, P. J., and Vlachos, D. G. (2013) A DFT study of the acid-catalyzed conversion of 2, 5-dimethylfuran and ethylene to p-xylene, *Journal of Catalysis 297*, 35-43.

104.   Armstrong, A., Boto, R. A., Dingwall, P., Contreras-García, J., Harvey, M. J., Mason, N. J., and Rzepa, H. S. (2014) The Houk–List transition states for organocatalytic mechanisms revisited, *Chemical Science 5*, 2057-2071.

105.   González, L., Escudero, D., and Serrano-Andrés, L. (2012) Progress and challenges in the calculation of electronic excited states, *ChemPhysChem 13*, 28-51.

106.   Balakrishnan, C., Subha, L., Neelakantan, M., and Mariappan, S. (2015) Synthesis, spectroscopy, X-ray crystallography, DFT calculations, DNA binding and molecular docking of a propargyl arms containing Schiff base, *Spectrochimica Acta Part A: Molecular and Biomolecular Spectroscopy 150*, 671-681.

107.   Xu, W., Huang, J.-J., Shao, B.-H., Xu, X.-J., Jiang, R.-W., and Yuan, M. (2015) X-ray Crystallography, DFT Calculations and Molecular Docking of Indole-Arylpiperazine Derivatives as α1A-Adrenoceptor Antagonists, *Molecules 20*, 19674-19689.

108.   Carter, E. E. (2012) MP2 and DFT Calculations of Ligand Binding in Acetylcholine Binding Protein's Aromatic Box, Memphis, Tenn.: Rhodes College.

109.   Efremenko, I., and Fish, R. H. (2015) Quantum Chemical and Molecular Docking Studies of [(η6-Cp* Rh-Tyr1)-Leu-enkephalin] 2+ to G-Protein-Coupled μ-,∂-, and κ-Opioid

Receptors and Comparisons to the Neuropeptide [Tyr1]-Leu-enkephalin: Conformations, Noncovalent Amino Acid Binding Sites, Binding Energies, Electronic Factors, and Receptor Distortion Forces, *Organometallics 34*, 4117-4126.

110.   Joseph, T., Varghese, H. T., Panicker, C. Y., Thiemann, T., Viswanathan, K., Van Alsenoy, C., and Manojkumar, T. (2014) Spectroscopic (FT-IR, FT-Raman), first order hyperpolarizability, NBO analysis, HOMO and LUMO analysis of 2, 4-bis (2-methoxyphenyl)-1-phenylanthracene-9, 10-dione by ab initio HF and density functional methods, *Spectrochimica Acta Part A: Molecular and Biomolecular Spectroscopy 117*, 413-421.

111.   Nassar, M. Y., El-Shahat, M., Khalile, S., El-Desawy, M., and Mohamed, E. A. (2014) Structure investigation of mesalazine drug using thermal analyses, mass spectrometry, DFT calculations, and NBO analysis, *Journal of Thermal Analysis and Calorimetry 117*, 463-471.

112.   Sheela, N., Muthu, S., and Sampathkrishnan, S. (2014) Molecular orbital studies (hardness, chemical potential and electrophilicity), vibrational investigation and theoretical NBO analysis of 4-4′-(1H-1, 2, 4-triazol-1-yl methylene) dibenzonitrile based on abinitio and DFT methods, *Spectrochimica Acta Part A: Molecular and Biomolecular Spectroscopy 120*, 237-251.

113.   Alen, S., Sajan, D., Sundius, T., Chaitanya, K., and Blockhuys, F. (2015) Vibrational spectral analysis, electronic absorption and non-linear optical behavior of (E)-1-(2, 4, 6-trimethoxyphenyl) pent-1-en-3-one, *Vibrational Spectroscopy 79*, 1-10.

114.   Österman, T., and Persson, P. (2012) Excited state potential energy surfaces of bistridentate Ru II complexes–A TD-DFT study, *Chemical Physics 407*, 76-82.

115.   Xu, X., Gozem, S., Olivucci, M., and Truhlar, D. G. (2012) Combined Self-Consistent-Field and Spin-Flip Tamm–Dancoff Density Functional Approach to Potential Energy Surfaces for Photochemistry, *The Journal of Physical Chemistry Letters 4*, 253-258.

116.   Reguzzoni, M., Fasolino, A., Molinari, E., and Righi, M. (2012) Potential energy surface for graphene on graphene: Ab initio derivation, analytical description, and microscopic interpretation, *Physical Review B 86*, 245434.

117.   Shustova, N. B., Cozzolino, A. F., and Dincă, M. (2012) Conformational Locking by Design: Relating Strain Energy with Luminescence and Stability in Rigid Metal–Organic Frameworks, *Journal of the American Chemical Society 134*, 19596-19599.

118.   Karabacak, M., and Cinar, M. (2012) FT-IR, FT-Raman, UV spectra and DFT calculations on monomeric and dimeric structure of 2-amino-5-bromobenzoic acid, *Spectrochimica Acta Part A: Molecular and Biomolecular Spectroscopy 86*, 590-599.

119.   Grimme, S. (2012) Supramolecular binding thermodynamics by dispersion-corrected density functional theory, *Chemistry-A European Journal 18*, 9955-9964.

120.   Yi, T.-F., Xie, Y., Zhu, Y.-R., Zhu, R.-S., and Shen, H. (2013) Structural and thermodynamic stability of Li 4 Ti 5 O 12 anode material for lithium-ion battery, *Journal of Power Sources 222*, 448-454.

121.   Zheng, Y., Jiao, Y., Zhu, Y., Li, L. H., Han, Y., Chen, Y., Du, A., Jaroniec, M., and Qiao, S. Z. (2014) Hydrogen evolution by a metal-free electrocatalyst, *Nature communications 5*.

122.   Cosconati, S., Forli, S., Perryman, A. L., Harris, R., Goodsell, D. S., and Olson, A. J. (2010) Virtual screening with AutoDock: theory and practice, *Expert opinion on drug discovery 5*, 597-607.

123.   Konteatis, Z. D. (2010) In silico fragment-based drug design, *Expert opinion on drug discovery 5*, 1047-1065.

124.   Talele, T. T., Khedkar, S. A., and Rigby, A. C. (2010) Successful applications of computer aided drug discovery: moving drugs from concept to the clinic, *Current topics in medicinal chemistry 10*, 127-141.

125.   Bajorath, J. (2015) Computer-aided drug discovery, *F1000Research 4*.

126.   Durrant, J. D., and McCammon, J. A. (2010) Computer-aided drug-discovery techniques that account for receptor flexibility, *Current opinion in pharmacology 10*, 770-774.

127.   Lill, M. A., and Danielson, M. L. (2011) Computer-aided drug design platform using PyMOL, *Journal of computer-aided molecular design 25*, 13-19.

128.   Lindert, S., Li, M. X., Sykes, B. D., and McCammon, J. A. (2015) Computer-Aided Drug Discovery Approach Finds Calcium Sensitizer of Cardiac Troponin, *Chemical biology & drug design 85*, 99-106.

129.   Prachayasittikul, V., Worachartcheewan, A., Shoombuatong, W., Songtawee, N., Simeon, S., and Nantasenamat, C. (2015) Computer-Aided Drug Design of Bioactive Natural Products, *Current topics in medicinal chemistry*.

130.   Wallach, I. (2011) Pharmacophore inference and its application to computational drug discovery, *Drug Development Research 72*, 17-25.

131. Speck-Planche, A., Luan, F., and Cordeiro, M. (2012) Abelson tyrosine-protein kinase 1 as principal target for drug discovery against leukemias. Role of the current computer-aided drug design methodologies, *Current topics in medicinal chemistry 12*, 2745-2762.

132. Sliwoski, G., Kothiwale, S., Meiler, J., and Lowe, E. W. (2014) Computational methods in drug discovery, *Pharmacological reviews 66*, 334-395.

133. Liaw, A., and Svetnik, V. (2015) QSAR modeling: prediction of biological activity from chemical structure, *Statistical Methods for Evaluating Safety in Medical Product Development*, 66-83.

134. González-Díaz, H., Frías-Fraire, M. F., Aguirre-Crespo, A., Aguirre-Crespo, F. J., and Prado Prado, F. J. (2015) Multi Activity QSAR Models for Anti-Parasite Drugs Using Markov Entropy Indices, In *2nd International Electronic Conference on Entropy and Its Applications*, Multidisciplinary Digital Publishing Institute.

135. Lewars, E. G. (2010) *Computational chemistry: introduction to the theory and applications of molecular and quantum mechanics*, Springer Science & Business Media.

136. Ramachandran, K., Deepa, G., and Namboori, K. (2008) *Computational chemistry and molecular modeling: principles and applications*, Springer Science & Business Media.

137. van der Kamp, M. W., and Mulholland, A. J. (2013) Combined quantum mechanics/molecular mechanics (QM/MM) methods in computational enzymology, *Biochemistry 52*, 2708-2728.

138. Boeyens, J. C., and Comba, P. (2001) Molecular mechanics: theoretical basis, rules, scope and limits, *Coordination Chemistry Reviews 212*, 3-10.

139. Ren, P., and Ponder, J. W. (2003) Polarizable atomic multipole water model for molecular mechanics simulation, *The Journal of Physical Chemistry B 107*, 5933-5947.

140. van Leeuwen, P. W., Morokuma, K., and van Lenthe, J. H. (2012) *Theoretical aspects of homogeneous catalysis: applications of ab initio molecular orbital theory*, Vol. 18, Springer Science & Business Media.

141. Homeyer, N., and Gohlke, H. (2012) Free energy calculations by the molecular mechanics Poisson− Boltzmann surface area method, *Molecular Informatics 31*, 114-122.

142. Šponer, J., Šponer, J. E., Mládek, A., Jurečka, P., Banáš, P., and Otyepka, M. (2013) Nature and magnitude of aromatic base stacking in DNA and RNA: Quantum chemistry, molecular mechanics, and experiment, *Biopolymers 99*, 978-988.

143. Previs, M., Previs, S. B., Gulick, J., Robbins, J., and Warshaw, D. (2012) Molecular mechanics of cardiac myosin-binding protein C in native thick filaments, *Science 337*, 1215-1218.

144.   Corey, D. (2012) " Molecular Mechanics of Sensory Transduction in the Inner Ear, Max-Planck-Institute for Experimental Medicine.

145.   Fakhrabadi, M. M. S., Khani, N., and Pedrammehr, S. (2012) Vibrational analysis of single-walled carbon nanocones using molecular mechanics approach, *Physica E: Low-Dimensional Systems and Nanostructures 44*, 1162-1168.

146.   Ansari, R., Mirnezhad, M., and Rouhi, H. (2015) An efficient molecular mechanics model for the torsional buckling analysis of multi-walled silicon carbide nanotubes, *European Physical Journal Applied Physics 70*, 10401.

147.   Quesne, M. G., Borowski, T., and de Visser, S. P. (2015) Quantum Mechanics/Molecular Mechanics Modeling of Enzymatic Processes: Caveats and Breakthroughs, *Chemistry–A European Journal*.

148.   Lonsdale, R., Hoyle, S., Grey, D. T., Ridder, L., and Mulholland, A. J. (2012) Determinants of reactivity and selectivity in soluble epoxide hydrolase from quantum mechanics/molecular mechanics modeling, *Biochemistry 51*, 1774-1786.

149.   Rivail, J.-L., Monari, A., and Assfeld, X. (2015) The Non Empirical Local Self Consistent Field Method: Application to Quantum Mechanics/Molecular Mechanics (QM/MM) Modeling of Large Biomolecular Systems, In *Quantum Modeling of Complex Molecular Systems*, pp 343-365, Springer.

150.   Bayse, C. A., and Merz, K. M. (2014) Mechanistic Insights into Mg2+-Independent Prenylation by CloQ from Classical Molecular Mechanics and Hybrid Quantum Mechanics/Molecular Mechanics Molecular Dynamics Simulations, *Biochemistry 53*, 5034-5041.

151.   Ohno, K., Esfarjani, K., and Kawazoe, Y. (2012) *Computational materials science: from ab initio to Monte Carlo methods*, Vol. 129, Springer Science & Business Media.

152.   Thiel, W. (2014) Semiempirical quantum–chemical methods, *Wiley Interdisciplinary Reviews: Computational Molecular Science 4*, 145-157.

153.   Schaefer III, H. F. (2012) *Quantum chemistry: the development of ab initio methods in molecular electronic structure theory*, Courier Corporation.

154.   Stewart, J. J. (2013) Optimization of parameters for semiempirical methods VI: more modifications to the NDDO approximations and re-optimization of parameters, *Journal of molecular modeling 19*, 1-32.

155.   Voityuk, A. A. (2012) Semi-empirical methods: current status and future directions, *Drug Des Strateg Comput Tech Appl*, 107-119.

156. Segal, G. (2012) *Semiempirical Methods of Electronic Structure Calculation: Part B: Applications*, Vol. 8, Springer Science & Business Media.

157. Govender, K. K. (2014) The development of hybrid quantum classical computational methods for carbohydrate and hypervalent phosphoric systems, University of Cape Town.

158. Wang, S., MacKay, L., and Lamoureux, G. (2014) Development of semiempirical models for proton transfer reactions in water, *Journal of Chemical Theory and Computation 10*, 2881-2890.

159. Manoel Filho, A., Dutra, J. D. L., Rocha, G. B., Freire, R. O., and Simas, A. M. (2013) Sparkle/RM1 parameters for the semiempirical quantum chemical calculation of lanthanide complexes, *RSC Advances 3*, 16747-16755.

160. Yeguas, V., and Casado, R. (2014) Big Data issues in Computational Chemistry, In *Future Internet of Things and Cloud (FiCloud), 2014 International Conference on*, pp 389-392, IEEE.

161. Merz, K. M., and Roux, B. (2012) *Biological membranes: a molecular perspective from computation and experiment*, Springer Science & Business Media.

162. Deuflhard, P., Hermans, J., Leimkuhler, B., Mark, A. E., Reich, S., and Skeel, R. D. (2012) *Computational Molecular Dynamics: Challenges, Methods, Ideas: Proceeding of the 2nd International Symposium on Algorithms for Macromolecular Modelling, Berlin, May 21–24, 1997*, Vol. 4, Springer Science & Business Media.

163. Labanowski, J. K., and Andzelm, J. W. (2012) *Density functional methods in chemistry*, Springer Science & Business Media.

164. Tsipis, A. C. (2014) DFT flavor of coordination chemistry, *Coordination Chemistry Reviews 272*, 1-29.

165. Ullrich, C. A. (2014) Time-dependent density-functional theory: features and challenges, with a special view on matter under extreme conditions, In *Frontiers and Challenges in Warm Dense Matter*, pp 1-23, Springer.

166. Burke, K. (2012) Perspective on density functional theory, *The Journal of chemical physics 136*, 150901.

167. Autschbach, J., Nitsch-Velasquez, L., and Rudolph, M. (2011) Time-dependent density functional response theory for electronic chiroptical properties of chiral molecules, In *Electronic and Magnetic Properties of Chiral Molecules and Supramolecular Architectures*, pp 1-98, Springer.

168. Hedström, A., Lindstedt, E., and Norrby, P. O. (2013) On the oxidation state of iron in iron-mediated C-C couplings, *Journal of Organometallic Chemistry 748*, 51-55.

169. Yang, Z., Yu, H., and Fu, Y. (2013) Mechanistic study on ligand-controlled cobalt-catalyzed regioselectivity-switchable hydroarylation of styrenes, *Chemistry - A European Journal 19*, 12093-12103.

170. Tanaka, R., Yamashita, M., Chung, L. W., Morokuma, K., and Nozaki, K. (2011) Mechanistic studies on the reversible hydrogenation of carbon dioxide catalyzed by an Ir-PNP complex, *Organometallics 30*, 6742-6750.

171. García-Melchor, M., Gorelsky, S. I., and Woo, T. K. (2011) Mechanistic analysis of iridium(III) catalyzed direct C-H arylations: A DFT study, *Chemistry - A European Journal 17*, 13847-13853.

172. García-Melchor, M., Braga, A. A., Lledós, A., Ujaque, G., and Maseras, F. (2013) Computational perspective on Pd-catalyzed C–C cross-coupling reaction mechanisms, *Accounts of chemical research 46*, 2626-2634.

173. Pople, J. (2004) Sir John A. Pople, 1925–2004.

174. Hehre, W., Lathan, W., Ditchfield, R., Newton, M., and Pople, J. (1970) Gaussian 70, *Quantum Chemistry Program Exchange, Program*.

175. David, C. Y. (2001) Computational chemistry.

176. Tomberg, A. (2013) Gaussian 09W Tutorial, Retrieved January.

177. Schlegel, H. B. (2011) Geometry optimization, *Wiley Interdisciplinary Reviews: Computational Molecular Science 1*, 790-809.

178. Weinhold, F., and Carpenter, J. E. (1988) The natural bond orbital Lewis structure concept for molecules, radicals, and radical ions, In *The structure of small molecules and ions*, pp 227-236, Springer.

179. Derome, A. E. (2013) *Modern NMR techniques for chemistry research*, Elsevier.

180. Jursic, B. S. (1996) Density functional Gaussian-type orbital approach in theoretical study of S2F2 isomerization, *Journal of computational chemistry 17*, 835-840.

181. Jensen, F. (2013) Atomic orbital basis sets, *Wiley Interdisciplinary Reviews: Computational Molecular Science 3*, 273-295.

182. Hill, J. G. (2013) Gaussian basis sets for molecular applications, *International Journal of Quantum Chemistry 113*, 21-34.

183. de la Vega, J. G., and Miguel, B. Basis sets for computational chemistry, *Introduction to Advanced Topics of Computational Chemistry, edited by LA Montero, LA Dıaz, and R. Bader*, 41-80.

184. Rassolov, V. A., Ratner, M. A., Pople, J. A., Redfern, P. C., and Curtiss, L. A. (2001) 6-31G* basis set for third-row atoms, *Journal of Computational Chemistry 22*, 976-984.

185.   Rassolov, V. A., Pople, J. A., Ratner, M. A., and Windus, T. L. (1998) 6-31G* basis set for atoms K through Zn, *The Journal of chemical physics 109*, 1223-1229.

186.   Dunning, T. H., Hay, P. J., and Schaefer, H. (1977) Methods of electronic structure theory, In *Modern theoretical chemistry*, p 1, Plenum Press New York.

187.   Hay, P. J., and Wadt, W. R. (1985) Ab initio effective core potentials for molecular calculations. Potentials for the transition metal atoms Sc to Hg, *The Journal of Chemical Physics 82*, 270-283.

188.   Sosa, C., Andzelm, J., Elkin, B. C., Wimmer, E., Dobbs, K. D., and Dixon, D. A. (1992) A local density functional study of the structure and vibrational frequencies of molecular transition-metal compounds, *The Journal of Physical Chemistry 96*, 6630-6636.

189.   Godbout, N., Salahub, D. R., Andzelm, J., and Wimmer, E. (1992) Optimization of Gaussian-type basis sets for local spin density functional calculations. Part I. Boron through neon, optimization technique and validation, *Canadian Journal of Chemistry 70*, 560-571.

190.   Ahlrichs, R., and Taylor, P. (1981) The choice of gaussian-basis sets for molecular electronic-structure calculations, *Journal De Chimie Physique Et De Physico-Chimie Biologique 78*, 315-324.

191.   Tzeli, D., and Tsekouras, A. A. (2010) Mind the basis set superposition error, *Chemical Physics Letters 496*, 42-45.

192.   Xantheas, S. S. (1996) On the importance of the fragment relaxation energy terms in the estimation of the Basis Set Superposition Error correction to the intermolecular interaction energy, *Journal of Chemical Physics 104*, 8821-8824.

CHAPTER TWO

The Interaction of NOTA as a Bifunctional Chelator with Competitive Alkali Metal ions: A DFT Study

F. Y. Adeowo, B. Honarpavar*, A. A. Skelton*,

School of Health Sciences, Discipline of Pharmacy, University of KwaZulu-Natal, Durban 4001, South Africa.

Corresponding authors: Skelton@ukzn.ac.za (A.A Skelton); Honarparvar@ukzn.ac.za (B. Honarparvar), School of Pharmacy and Pharmacology, University of KwaZulu-Natal, Durban 4001, South Africa Tel.: +27 31 2608520, +27 31 26084.

Abstract

1, 4, 7 triazacyclononane-1, 4,7 triacetic acid (NOTA) is a key chelator for radiolabelling pharmaceuticals. The ability of alkali metals in the human body to complex with NOTA and compete with radiometals can influence the radiolabelling process. The focus of the present work is to evaluate the NOTA—alkali metal complexation with density functional theory (B3LYP functional) using 6-311+G(2d,2p) basis set for Li^+, Na^+ and K^+ and Def2-TZVPD for Rb^+.

Two NOTA—ion conformations are reported in the study: '**A**' where six NOTA hetero atoms (N, O) are in close proximity to the cation, and '**B**', where four NOTA hetero-atoms interact with the cation. Interaction and relaxation energies, Gibbs free energies and entropies show that the stability of NOTA—ion complexes decreases down the group of the periodic table. Implicit water solvation affects the NOTA—ion complexation, causing a decrease in the stability of the system. NBO analysis performed through the natural atomic charges (NAC) and second order perturbation analysis reveals charge transfer between NOTA and alkali metals. The theoretical ^{1}H NMR chemical shifts of NOTA, in vacuum and water media, are in good agreement with experiment, these values being influenced by the presence of the ions, which have a deshielding effect on the protons of NOTA. Global scalar properties, such as

HOMO/LUMO energies, $\Delta E_{\text{LUMO-HOMO}}$ gap, and chemical hardness and softness, show that the chemical stability of NOTA―alkali metal complexes decreases down the periodic table. This study sheds light on the impact of competing alkali metal ions to the radiolabelling efficiency of NOTA.

Keywords: Chelator―ion interaction, Density functional theory (DFT); Natural bond orbital (NBO).

2.1. Introduction

The distribution of drugs *in vivo* can be monitored by delivering radioisotopes within a chelator that is chemically bonded to a biological vector, such as antibodies and lead compounds, which are designed specifically for a tumor or infected site.[1] This is beneficial in imaging for pharmacological applications, as it provides precise dosing information. Successful delivery of radio-pharmaceuticals to a selective tumour target can be established when antibodies are attached to a bifunctional chelator (BFC). A BFC possesses two reactive functional groups that can covalently bind to targeting vectors, as well as a suitable metallic radioisotope.[2,3-5] The efficacy of the imaging or chelation therapy depends on the optimal match between a particular chelator with the appropriate radioisotope, and the relative stability of the chelator-ion complexes.[6-8] The factors that should influence the stability of metal complexes are the size of the chelate ring, the number of rings in the chelating molecule, the basic strength of the chelating molecule, the nature of donor or ligand atoms, the electron affinity/ionic radius of the metal [9] and the ligand to metal charge transfer.[10]

1, 4, 7-triazacyclononane-1, 4, 7-triacetic acid (NOTA) 1, 4, 7-triazacyclododecane-1, 4, 7, tetraacetic acid (DOTA), diethylene triaminepentaacetic acid (DTPA), 1, 4, 7-triazacyclononane phosphinic acid (TRAP), 1,2-[[6-carboxy-pyridin-2-yl]-methylamino]ethane (H2dedpa), and N,N'-bis(6-carboxy-2-pyridylmethyl)-ethylenediamine-N,N'-diacetic acid) (H4octapa) are examples of the most widely researched chelators for radiolabelling. The focus of the present article is to investigate NOTA and its complexation to alkali metals.

NOTA, a hexadentate chelator, is one of the most extensively investigated macrocyclic BFCs, and is utilized for the complexation of a large array of bi- and trivalent metal ions.[11] NOTA chelator has the geometry of the N_3O_3 coordination sphere and consists of three carboxylic (―COOH) functional arms (see **Figure 1** for the structure of NOTA).
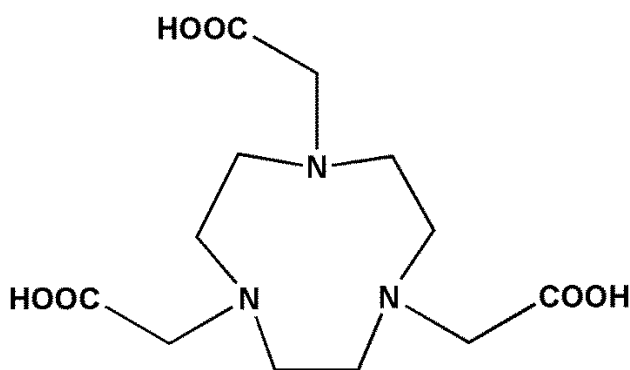
Figure 1: NOTA, 1, 4, 7-triazacyclononane-1, 4, 7- triacetic acid, CN = 6, N_3O_3

Several studies involving NOTA, its derivatives, and other chelators, such as DOTA, an analogue of NOTA with four nitrogen and four pendant arms, have been performed.[12-27] NOTA has been identified as a potential chelating agent for various radiopharmaceutical experiments and confirmed as a "gold standard" chelator for Ga^{3+} with a short radiolabelling time and outstanding *in vivo* stability[3]. Velikyan *et al*[28] reported that the ^{68}Ga—NOTA complex is stable in human plasma at 37^oC. Chakravarty[25] *et al.,* also reported that even in the presence of up to 10 ppm of other metal ion contaminations, such as Zn^+, Cu^+, Fe^+, Al^+, Sn^+ and Ti^+ ions, NOTA-based bifunctional chelators (NOTA—NCs) could be radiolabelled instantly with ^{68}Ga at room temperature. Jeong and co-workers[14] confirmed that NOTA is a better BFC than DOTA is for ^{68}Ga, exhibiting a high stability even when hindered by various metal ions.. Ferreira and co-authors[22] reported that at room temperature, a short reaction time is required when ^{68}Ga is radiolabelled with P-NO$_2$-Bn—NOTA, a NOTA derivative. Radiolabelling ^{64}Cu with NOTA has shown a better result than when ^{64}Cu is radiolabelled with common chelators, such as DOTA, EDTA, DTPA, and TETA.[19, 24] The results from these experiments show that NOTA is compatible with the heat sensitive, antibody vector due to its short radiolabelling time and ability to radiolabel at room temperature.[29] Geraldes *et al.*[30], reported that there is a weak complex species between NOTA and alkali ions in aqueous solution. Potentiometric measurements, multinuclear nuclear magnetic resonance spectrometry (NMR) and density functional theory calculations of the gallium complexes of NOTA derivatives revealed that phosphinic derivatives of NOTA (TRAP ligands) exhibit higher selectivity than NOTA for binding small metal ions.[31]

Our recent study showed the conformational behaviour and complexation between Na^+ cation and diazacrown[32] using density functional theory (DFT), Møller–Plesset (MP2) and molecular mechanics methods. It was shown that, upon complexation, there was charge transfer between the diazacrown and Na^+, causing a reduction in the +1 charge of the free ion.

Behjatmanesh- Ardakani *et al.*,[33] analyzed the host-guest interaction between alkali metals (Li^+, Na^+, and K^+) and some selected ligands using DFT-B3LYP level of theory. The same authors studied the interactions between aza, diaza, and triaza-12-crown-4 ligands as host molecules and Na^+ ion as a guest species using B3LYP/6-311G level of theory.[34]

To the best of our knowledge, little or no computational research has been performed on the complexations of alkali metals with NOTA chelator. In light of this, the aim of the present research is to perform electronic structure calculations to provide insight into the factors affecting the chelating ability of NOTA with alkali metals. This investigation will explore how NOTA interacts with alkali metal ions, Li^+, Na^+, K^+ and Rb^+? This can be expanded into exploiting the possible impacts of these competitive ions on the radiolabelling yield of NOTA, which is useful to predict how well NOTA will complex radio metals in the presence of other ions *in vivo*. To gain an in depth insight into the complexation of NOTA with alkali metals, the interaction energy values, relaxation energy of NOTA—alkali metal complexes and other thermodynamic properties, entropy, enthalpy, Gibbs free energy and interatomic distances of the optimized NOTA and ion complexes will be reported. NBO and NMR chemical shift analysis and DFT-based reactivity descriptors, the Electron affinity (EA), Ionization potential (IP), Softness (*S*) and Hardness (η) will also be reported.

2.2. Computational details

All calculations were performed with the Gaussian 09 program.[35] The Becke, 3-parameter, Lee-Yang-Parr (B3LYP)[36, 37] hybrid exchange correlation functional was used. The basis set, 6-311+G(2d,2p)[38-41], was applied for Li^+, Na^+ and K^+ complexes and for the Rb^+ complex, the 6-311+G(2d,2p) basis set was used for NOTA, while Def2-TZVPD[42] was employed for Rb^+ ion.

Two different NOTA—ion complex configurations were geometry optimized. The first configuration had six hetero atoms (three oxygen and three nitrogen atoms) in close proximity to the alkali metal cations (conformation '**A**'), while the second configuration had four hetero atoms (two oxygen and two nitrogen atoms) interacting with the cations (conformation '**B**') (**Figure 2**). The atoms in the complexes are classified based on the connectivity of the atoms involved in different functional groups.
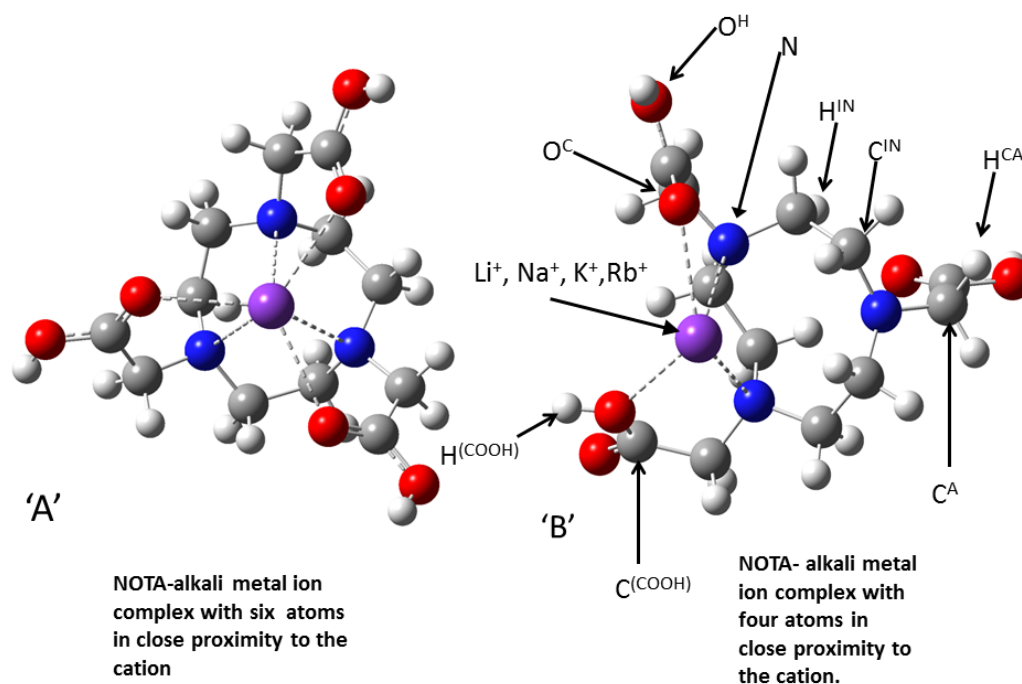
Figure 2: Conformations of complexes '**A**' and '**B**'. The dotted lines in the diagrams indicate intermolecular distances between alkali metal ion and hetero atoms that are in close proximity. Complex '**A**' has six hetero atoms close to the cation. Complex '**B**' has four hetero atoms interacting with the cation. H^{IN}, C^{IN}, N; hydrogen, carbon and nitrogen atoms in the ring. C^A, H^{CA}; carbon and hydrogen attached to the arm; $C^{(COOH)}$, $H^{(COOH)}$; carbon and hydrogen atoms in the functional group. O^H= hydroxyl oxygen, O^C= carbonyl oxygen.

Interaction energies (E_{int}), between NOTA and the different metal ions, were calculated using the following equation[32]:

$$E_{int} = E_{MOL1-MOL2} - E_{MOL2} - E_{MOL1} \ (1)$$

MOL1 and MOL2 are components of the complex. For instance, in the NOTA—Na^+ case, MOL1 represents a NOTA molecule and MOL2 represents Na^+. Relaxation energy was calculated by subtracting the complexation energy value (unrelaxed) from the interaction energy (relaxed). After the geometry optimization of the cations and NOTA, the cation was separated from the NOTA molecule and the two different situations were compared. First, the single point energy of the NOTA in that configuration was performed. Secondly, a further geometry optimization of the NOTA was carried out to allow the NOTA molecule to relax. The difference in energy between these two cases is the relaxation energy, which provides a measure of how the ion affects the conformation of the NOTA.[43-45]

The Polarizable Continuum Model (PCM), using the integral equation-formalism polarizable continuum model (IEF-PCM), was used to evaluate the solvent effect on the NOTA complexation with alkali metals. Thermodynamic properties (free energy, enthalpy, and entropy) were performed. Normal mode analysis was used in calculating the vibrational, translational and rotational contributions to entropy[46]. Electron donation between the filled donor and empty acceptor orbitals and their estimated energetic significance was assessed using second-order perturbation theory, with the NBO program implemented in Gaussian 09[47-49].

The calculated Basis Set Superposition Error (BSSE) with different basis sets provided rationale for selecting the basis set, 6-311+G(2d,2p), which showed the lowest BSSE value for the NOTA—Rb^+ complex, as well as reasonably low BSSE values for other ions compared with the more expensive 6-311G++(3d,3p) basis set (see **Table 1S** and **2S**).

The second-order Fock matrix was presented to evaluate the donor–acceptor interactions in the system.[50, 51] To provide a clear picture of electron delocalization between NOTA and the metals in the complexes, the donor and acceptor orbitals with the highest stabilization energy are presented in terms of E^2 from second-order theory[52, 53]. The second order perturbation energy E^2 of the occupied NBO (i) of an electron donor, which interacts with the unoccupied NBO (j) of electron acceptor, is estimated by the expression:

$$E^2 = \frac{q_i F(i,j)^2}{\varepsilon_j - \varepsilon_i} \ (\mathbf{2})$$

Where q_i is the donor orbital occupancy, ε_i and ε_j are diagonal Fock matrix elements and *F(i,j)* is the off diagonal NBO Fock matrix element.

The energy values of the highest occupied molecular orbital (E_{HOMO}) and the lowest unoccupied molecular orbital (E_{LUMO}) of all the complexes were calculated. Several other electronic properties, such as ionization potential (IP), electronic affinities (EA), hardness (η) and softness (*S*) were calculated. The ionisation potential (IP) is defined as the difference in ground state energy between the radical cationic (E_c) and the neutral species (E_n):

$$IP = \ E_C - E_n \ (\mathbf{3})$$

The electron affinity (EA) is defined as the difference in ground state energy between the radical anionic (E_a) and its corresponding neutral species (E_n):

$$EA = E_a - E_n \quad (\textbf{4})$$

The term "neutral" is the standard charge state, for instance, the ions have +1 charge and cationic and anionic species would have +2 and 0 charges, respectively.

Single point energies, at the geometry-optimized configurations of standard charge states, were performed for these calculations. The DFT-based structural features, chemical hardness, η, and softness, S, were obtained using the following equations [54, 55] :

$$\eta = \frac{IP - EA}{2} \quad (\textbf{5})$$

$$S = \frac{1}{2\eta} \quad (\textbf{6})$$

2.3. Results and discussions

For lucid data interpretation, the classification of atoms in the NOTA—ion complexes was made, based on the connectivity of the atoms with various functional groups, which dictates their different chemical environment (**Figure 2**).

2.4. Conformational analysis

To compare the two conformational possibilities in the NOTA—ion complexes, namely one conformation which includes the interaction between all three hydroxyl oxygen atoms (O^H) and the cation (**Figure 2S**) and the second conformation with the interactions between all three carbonyl oxygen atoms (O^C) and alkali metal ions (Complex '**A**' in **Figure 2**). The relative interaction energies ($\Delta E_{relative}$) for the two different NOTA— ion complexes are shown in **Table 1**.

Table 1: Relative interactions energies for different NOTA— ion complexes. All energies are in kcal/mol obtained by B3LYP/6-311G+(2d,2p) and LANL2DZ basis set for Rb^+.

Complexes	$\Delta E_{relative}$ O^C (kcal/mol)	$\Delta E_{relative}$ O^H (kcal/mol)
NOTA—Li^+	0	14.67
NOTA—Na^+	0	14.23
NOTA—K^+	0	13.23
NOTA—Rb^+	0	12.87

According to **Table 1**, the O^C—ion conformations were more stable than those of O^H—ion and this trend decreased down the alkali metal series. Consequently, it can be inferred that O^C—ion interactions have a more crucial contribution in the intermolecular ion chelation than O^H—ion.

2.5. Interaction and relaxation energies

The interaction energies of the NOTA—alkali metal ion complexes, basis set superposition error (BSSE) and relaxation energies for complexes in conformations '**A**' and '**B**' are discussed in this section to gain insight into its non-bonding interactions with the ions. The interaction energy values provide a measure of the specific interactions that are important for the complexation of NOTA with alkali metal ions. The interaction energies of the complexes in vacuum and solvent, BSSE energy values and relaxation energies of the complexes are reported in **Table 2**.

Table 2: Interaction energies of the complexes in vacuum and with solvent, BSSE energy values and relaxation energies of the complexes. All energies are in kcal/mol

Complex	E_{int}		E_{relax}		E_{BSSE}	
	complex '**A**'	complex '**B**'	complex '**A**'	complex '**B**'	Complex '**A**'	Complex '**B**'
NOTA—Li$^+$	-118.04 [-23.48]	-92.98 [-13.11]	12.36	6.70	1.38	1.08
NOTA—Na$^+$	-89.78 [-18.33]	-65.93 [-11.06]	8.04	5.00	1.80	1.42
NOTA—K$^+$	-64.01 [-14.08]	-44.28 [-9.10]	7.42	4.07	0.72	0.55
NOTA—Rb$^+$	-54.25 [-7.44]	-33.24 [-5.65]	6.35	3.72	0.43	0.28

Brackets indicate interaction energy values of the complexes in solvent, E_{int}: Interaction energy, E_{relax}; Relaxation energy, E_{BSSE}: Basis sets superposition error

For conformations '**A**' and '**B**', the interaction energies for NOTA complexation with alkali metal ion follow a decreasing order: NOTA—Li$^+$ > NOTA—Na$^+$ > NOTA—K$^+$> NOTA—Rb$^+$. The interaction energy values for complexes in conformation '**A**' are significantly more negative than that of the complexes in conformation '**B**', which signifies that there is greater intermolecular NOTA—ion interaction for complex '**A**', with six atoms in close proximity to the ions than for the complex '**B**', with four atoms interacting with the respective ion. Furthermore, complex '**A**' appears in the reported range for the coordination number of ions; that is, for Li$^+$ the coordination number is 4 or 6, Na$^+$ ranges between 4—8,

K^+ ranges between 5.6—8.3 while for Rb^+ varies between 6—8[56]. The interaction energy values in both cases, however, indicated that the stability of NOTA complexation with alkali metals decreases down the group of the periodic table, which agrees with the increased values of the distances between the hetero-atoms and the ions in the complexes, down the group (see Section 3.3). For all complexes, the calculated BSSE energy values were lower than 2 kcal/mol, which validates the reliability and effectiveness of the size of the applied basis set for the considered system.

The relaxation energy values decrease down the periodic table for conformations '**A**' and '**B**'. This implies that the larger the intermolecular interaction in NOTA—alkali metal complexes, the more the ion can induce a specific conformation that could be different from its preferred conformation. Conformation '**A**' complexes show greater relaxation energy values than conformation '**B**', this being due to the former having more hetero atoms in close proximity to the cations and the cations therefore having a greater effect on the conformation of the complexes than the latter.

To take into account the long-range and dispersion interactions, the geometry optimization of complex B was performed using the ωB97XD functional and the interaction energies are listed in **Table 7S**. Since less negative interactions energies were observed with the ωB97XD functional, it seems that dispersion is an important factor in binding of NOTA with alkali metal ions. It is notable that the interaction energies obtained with both B3LYP and ωB97XD functionals correlate as the observed decreasing trend within the alkali metal series was maintained; therefore, the results obtained with B3LYP are qualitatively valid.

2.6. Solvent effect

To gain an understanding of how NOTA—alkali metal complexes behave in bulk water, the IEFPCM solvation model was used to calculate the interaction energies of the complexes in implicit water (**Table 2**)**.** The results reveal that in the presence of water solvent, the interaction energy values of both '**A**' and '**B**' systems are significantly less negative than the in the absence of water, which this implies that the interaction of NOTA—alkali metals in bulk of water is less favourable and less stable. Indeed, the presence of water might compete with NOTA for interaction with the ion, and therefore reduce the stability of NOTA—ion complexes. The differences are greater for conformation '**A**' than '**B**', because each interaction of atom is affected by the presence of water. Complex '**A**', with six atoms in close proximity,

will therefore experience more disruption in the presence of water than complex '**B**', which has four atoms in close proximity.

2.7. Thermodynamic properties

Enthalpies, free energies, entropy and its individual contributions (translational, rotational, and vibrational) of the alkali metal, complexed with NOTA are listed in **Table 3**.

Table 3: The enthalpies, free energies, entropy and its individual contributions (Translational, Rotational, and Vibrational.) of the alkali metal complexed with NOTA

Complexes	ΔH (kcal mol^{-1})	ΔG (kcal mol^{-1})	ΔS (cal mol^{-1} K^{-1})	ΔS_{Rot} (cal mol^{-1} K^{-1})	ΔS_{Trans} (cal mol^{-1} K^{-1})	ΔS_{Vib} (cal mol^{-1} K^{-1})
NOTA—Li$^+$	-115.92 (-91.25)	-102.70 (-80.55)	-44.33 (-35.88)	-0.55 (-0.39)	-31.73 (-31.73)	-12.05 (-3.77)
NOTA—Na$^+$	-88.14 (-64.83)	-75.64 (-54.62)	-41.92 (-34.92)	-0.19 (-0.16)	-35.12 (-35.12)	-6.61 (1.03)
NOTA—K$^+$	-62.51 (-43.33)	-50.80 (-33.84)	-39.18 (-31.84)	0.12 (0.07)	-36.55 (-36.55)	-2.75 (4.64)
NOTA—Rb$^+$	-49.28 (-32.29)	-38.09 (-23.43)	-37.53 (-37.53)	0.42 (0.40)	-38.50 (-38.50)	0.56 (8.35)

Parentheses indicate thermodynamic values of the complexes '**B**'.

For complexes with conformations '**A**' and '**B**', ΔH values are slightly less negative than the interaction energy values (**Table 2**). The interaction energy value for the Li$^+$ complex is approximately 2 kcal mol^{-1} greater than the ΔH value, while for the other complexes, the interaction energy values are approximately 1 kcal mol^{-1} more than the ΔH values. The ΔH and ΔG values for the complexes in conformations '**A**' and '**B**' become less negative down the periodic table (**Table 3**). This emphasises the fact that the stability of the complexation of NOTA with alkali metals decreases down the group. While ΔS also becomes less negative down the group, it should be noted that a negative entropy value indicates a decrease in entropy of the system, which acts against the stability of the NOTA—alkali metal complexes $\Delta G = \Delta H - T\Delta S$.

The translational entropy contribution for all the complexes becomes more negative down the group, as the translation entropy for the free cations increases moves in this direction (**Table 3S**). Additionally, translational entropy contributions are of similar value for the two '**A**' and '**B**' conformations. The rotational and vibrational entropy contributions become more positive down the group.

Table 4: Thermodynamic properties for NOTA―ion complexes (conformation '**A**') in water obtained by B3LYP/6-311G+(2d,2p) and LANL2DZ basis set for Rb^+.

Complexes	ΔH (kcal mol^{-1})	ΔG (kcal mol^{-1})	ΔS (cal mol^{-1} K^{-1})	ΔS_{Rot} (cal mol^{-1} K^{-1})	ΔS_{Trans} (cal mol^{-1} K^{-1})	ΔS_{Vib} (cal mol^{-1} K^{-1})
NOTA―Li$^+$	-22.34	-12.05	-34.53	-0.46	-31.73	-2.34
NOTA―Na$^+$	-17.91	-9.29	-28.91	-0.11	-35.12	6.31
NOTA―K$^+$	-14.27	-6.40	-26.42	0.23	-36.55	9.89
NOTA―Rb$^+$	-7.85	-0.27	-25.41	0.51	-38.50	12.57

The effect of implicit solvation on the enthalpy, Gibbs free energy and entropy was considered. **Table 4** shows that the ΔH and ΔG values of the complexes are significantly less negative than the ΔH values of the complexes in vacuum (**Table 3**). Less negative ΔS values were observed in the water medium than the vacuum. The rotational and translational entropies decrease down the group, but are similar to the corresponding values in the vacuum. As for the contribution of solvent to the vibrational entropy, ΔS_{Vib} values have become more positive for all NOTA―ion complexes, although the trend remains the same. According to **Table 4S**, it can be inferred that the driving force behind the increase in ΔS_{Vib} is the decrease in vibrational entropy for free NOTA (-9.52 cal mol^{-1} K^{-1}) upon solvation. The reason for the drastic change in vibrational entropy could be attributed to the fact that in vacuum, there is great repulsion between the carboxylic pendant arms, which causes the distance between these arms to be greater than in the water medium, where the repulsion between the arms is reduced (**Figure 1S**). The larger distance between the carboxylic arms, in vacuum, compared to the shorter distances that appear in the water medium lead to an increase in the structural flexibility of the NOTA, and an increase in entropy. Overall, the values highlighted above indicate that the complexation of NOTA with alkali metal ions in water is less favourable and less stable. The formation of NOTA―Rb$^+$ complex appears to be significantly less favourable than other NOTA―ion complexes.

2.8. Interatomic distances

The average short-range interatomic distances between the metal ions and NOTA heteroatoms in each of the optimized complexes are reported in **Table 5**. This analysis was performed to assess the level of intermolecular interaction between NOTA and alkali metals. Heteroatom-ion distances lower than 3.0 Å were considered as binding interactions for Li$^+$,

Na$^+$ and K$^+$ complexes, while heteroatom-ion distances of less than 3.5 Å were considered to be binding interactions for the Rb$^+$ complex.

Table 5: The interatomic distances between alkali metals and NOTA's heteroatoms in the optimized structure at B3LYP/6-311+G(2d,2p) level of theory for Li$^+$, Na$^+$ and K$^+$. 6-311+G(2d,2p)/LANL2DZ basis sets were used for NOTA—Rb$^+$ complex.

Complex	Average O—ion distance (≤ 3 Å)	Average N—ion distance (≤ 3 Å)
NOTA—Li$^+$	2.06 {1.98}	2.26 {2.13}
NOTA—Na$^+$	2.34 {2.33}	2.58 {2.49}
NOTA—K$^+$	2.76 {2.71}	2.99 {2.96}
NOTA—Rb$^+$	2.90 {2.91}	3.22 {3.25}

Curly brackets indicate bond distances between heteroatoms and alkali metal ions in complexes in conformation '**B**'.

The distances between the ions and heteroatoms for both '**A**' and '**B**' complexes increased down the group. The heteroatom-oxygen distances for all complexes match closely to the results in the literature regarding alkali metals with different molecules: Li$^+$—O = 1.98[57, 58]; Na$^+$—O = 2.34[59, 60]; K$^+$—O = 2.76[60-62]; Rb$^+$—O = 2.95[63-65]. The ion-heteroatoms distances for complexes in conformation '**B**', however, are closer than those for complex '**A**', with the increased competition between the six heteroatoms in complex '**A**' resulting in a slight increase in the ion-heteroatom distances. The close proximity and high negative charge value of NOTA oxygen and nitrogen atoms, after geometry optimization, (see "Natural bond orbital (NBO) analysis" section, **Table 6**) signifies the importance of the contribution of these two atoms (N, O) for NOTA complexation with alkali metal ions.

To evaluate the dispersion effect on the geometric parameters, the interatomic distances using the ωB97XD functional are reported in **Table 8S**. It can be noticed Average N—ion distances are smaller with ωB97XD than with B3LYP; hence, it can be inferred that, with this functional the nitrogen in NOTA plays a more important role to interact with the ions in comparison to B3LYP where the carboxyl arms were in close proximity with the ions. The optimized geometry of free NOTA using the ωB97XD functional is also provided in **Figure 3S**.

2.9. Natural bond orbital (NBO) analysis

The charge transfer within the chelator-ion complexes is of importance, as it influences the interaction of alkali metals with NOTA. Charge transfer can be investigated using natural

bond orbital (NBO) analysis by monitoring the atom charges, change of atom charges upon complexation, and second order perturbation theory[66] .

2.9.1. Natural atomic charge analysis

Natural atomic charge (NAC) estimation plays a role in applying quantum mechanical calculations to molecular systems, as the atomic charge affects the electronic structure, dipole moment and other properties of the molecule[51]. Charge distribution, within the NOTA complexes and from NOTA to the alkali metals, is reported in **Table 6**. The atoms in all the complexes have been categorized into groups (**Figure 2**), and the average natural atomic charges have been reported.

The NBO analysis shows that there are considerable changes in the charges for the cations after complexation with alkali metals for all the complexes. For conformations '**A**' and '**B**', the alkali metals, with a charge of +1 before complexation, become less electron deficient after complexation, the atomic charge deficiency decreasing down the group, and implies that there was electron density transfer from NOTA to the alkali metal. The cations in complexes '**A**' are more electron deficient as more heteroatoms are involved in intermolecular NOTA-ion interactions. Furthermore, nitrogen and oxygen (O^C) atoms are more negatively charged in the complexed—NOTA compared to the free NOTA. This implies that charge transfer occurred to those atoms upon complexation (**Figure 3**). The charges for the NOTA oxygen and nitrogen atoms are more negatively charged than all other atoms in the complexes, which explains the greater electrostatic interaction, and the closer distances of the oxygen atoms and nitrogen atoms to the alkali metals.

Table 6: Averages of natural atomic charges (NAC) of atoms in specified groups of NOTA complex with alkali metals and NOTA before complexation at B3LYP/6-311+G(2d,2p) level of theory.

Atom groups	NOTA—Li$^+$	NOTA—Na$^+$	NOTA—K$^+$	NOTA—Rb$^+$	Free NOTA
Ion	0.48 [0.63]	0.69 [0.77]	0.77 [0.84]	0.79 [0.85]	Not applicable
N (3)	-0.59 [-0.60]	-0.59 [-0.60]	-0.58 [-0.59]	-0.58 [-0.59]	-0.57
O^H (3)	-0.66 [-0.68]	-0.66 [-0.70]	-0.66 [-0.70]	-0.66 [-0.70]	-0.71
O^C (3)	-0.60 [-0.60]	-0.63 [-0.61]	-0.63 [-0.61]	-0.63 [-0.61]	-0.61
C^{IN}(6)	-0.17 [-0.17]	-0.17 [-0.18]	-0.18 [-0.18]	-0.17 [-0.18]	-0.18
H^{IN} (12)	0.20 [0.21]	0.20 [0.20]	0.20 [0.20]	0.20 [0.20]	0.19
C^A (3)	-0.26 [-0.26]	-0.26 [-0.26]	-0.27 [-0.27]	-0.27 [-0.26]	-0.26
H$_C^A$(6)	0.23 [0.23]	0.23 [0.23]	0.22 [0.23]	0.22 [0.22]	0.22
C$^{(COOH)}$(3)	0.84 [0.84]	0.83 [0.82]	0.83 [0.82]	0.83 [0.82]	0.81
H$^{(COOH)}$(3)	0.50 [0.51]	0.50 [0.51]	0.50 [0.50]	0.50 [0.50]	0.49

Bracket indicates values for complex '**B**'. The numbers in () represent the number of atoms within the specific group shown in **Figure 2**.

2.9.2. Second perturbation stabilization energies

In this section, the possible charge transfer within NOTA and, between NOTA and alkali metals, using second order perturbation, is discussed. Second-order perturbation theory analysis for all the complexes is presented in the **Table 7,** which shows the average stabilization E^2 values. The larger the E^2 value, the greater the charge transfer between electron donors and electron acceptors.[67-69]

Table 7: The second-order perturbation energies, E^2 (kcal/mol), corresponding to the most important charge transfer interaction (donor → acceptor) within NOTA—alkali metal complexes obtained by B3LYP/6-311+G(d,p) level of theory.

Complexes	Donor	Acceptor	E^2(kcal/mol)
Within NOTA			
NOTA—Li$^+$	LP (O)	σ* (C-O)	45.47 [56.17]
NOTA—Na$^+$	LP (O)	σ* (C-O)	38.94 [54.40]
NOTA—K$^+$	LP (O)	σ* (C-O)	38.82 [53.57]
NOTA—Rb$^+$	LP(O)	σ* (C-O)	38.69 [53.28]
NOTA	LP(O)	σ* (C-O)	43.46 [45.62]
From NOTA to ions			
NOTA—Li$^+$	LP(O)	LP*(Li$^+$)	17.31 [23.33]
NOTA—Na$^+$	LP(O)	LP*(Na$^+$)	15.88 [12.28]
NOTA—K$^+$	LP(O)	LP*(K$^+$)	14.82 [9.45]
NOTA—Rb$^+$	LP(O)	LP*(Rb$^+$)	12.17 [7.42]

Brackets indicate values for complex '**B**'.

The highest stabilization energy values, due to the charge transfer within NOTA, are electron donations from the LP in O^H to the antibonding acceptor σ* (C-O^C). For conformations '**A**' and '**B**', the stabilization energy follows a decreasing order: NOTA—Li$^+$ > NOTA—Na$^+$ > NOTA—K$^+$ > NOTA—Rb$^+$. The stabilization energy values within complexes in conformation '**B**' are greater than those in conformation '**A**'. This signifies that the existence of a greater number of heteroatoms in close proximity to the cations in conformation '**A**', leads to competition for heteroatom-ion interactions; this results in a reduced charge transfer per heteroatom.

For complexes '**A**' and '**B**', the stabilization energy values for electron transfer from a lone pair of O^C of NOTA to a lone pair* of alkali metals, decreases down the group. There is a charge transfer from the nitrogen atom lone pair to the lone pair* of ions (**Table 5S**), although this is lower than that of the oxygen to ion charger transfers.

The result of the second perturbation theory emphasises the fact that electron transfer is prevalent from oxygen and nitrogen atoms of NOTA to the alkali metals in the complexes. A similar result was obtained from our previous work, where we evaluated the interaction between diazacrown and sodium cation.[32] A description of charge transfer that occurs from the NOTA molecule to the cations is represented in **Figure 3**, where arrows indicate the path of charge transfer.
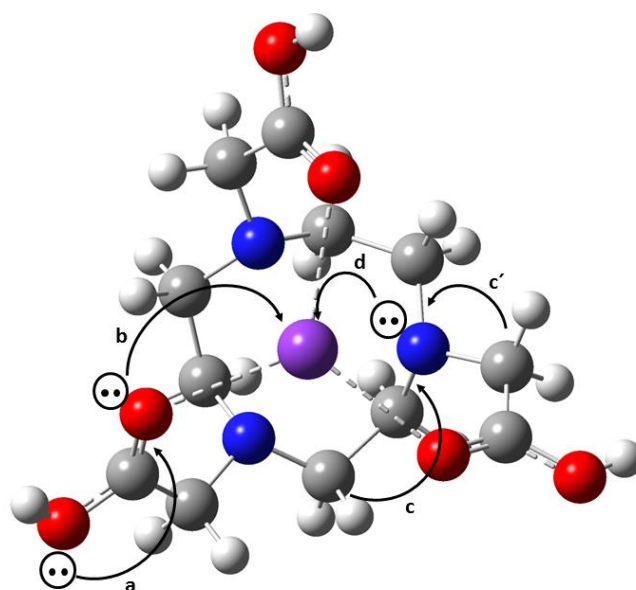
Figure 3: Description of electrons transfers shown in NBO analysis. The curved arrows (**a**, **b**, **c**, **c´** and **d**) depict the direction of charge transfer; **a**: LP (O) → σ* (C=O), **b**: LP (O) → LP* (Ion), **c**: σ (C-H) ring → σ (N-C), **c´**: σ (C-H) arm → σ (N-C), **d**: LP (N) → LP* (Ion).

2.10. Analysis of NMR chemical shifts

The ^{1}H NMR of NOTA, in solutions containing Li$^+$, Na$^+$ and K$^+$ ions, was measured experimentally[30], with the chemical shifts being influenced by the presence of the ions. To compare our theoretical results with the experiment, we performed the ^{1}H NMR calculations in vacuum and water media (**Table 8**). This comparison is particularly informative, as it has been shown that the hydrogen atoms are a source of electron density from NOTA to the ions, and that the charge transfer should be the driving force for chemical shift changes. A detailed understanding of the chemical environment of the hydrogens, especially in relation to the alkali metal ions, can therefore be derived. Experimental and theoretical ^{1}H chemical shifts (δ) are given in **Table 8** for a set of NOTA— alkali metal complexes.

Table 8: Proton NMR chemical shifts (δ) of NOTA— alkali metal complexes in vacuum and water media.

Proton	δ_{Theo} Li$^+$ (ppm)	δ_{Exp} (ppm)	δ_{Theo} Na$^+$ (ppm)	δ_{Exp} (ppm)	δ_{Theo} K$^+$ (ppm)	δ_{Exp} (ppm)
G1	7.18 [6.81] NAC=0.50	Not reported	7.09 [6.84] NAC=0.50	Not reported	6.99 [6.76] NAC=0.50	Not reported
G2	3.83 [3.74] NAC=0.23	3.76 Δ_{vac} = 0.07 Δ_{solv} = -0.02	3.71 [3.65] NAC=0.23	3.48 Δ_{vac} = 0.23 Δ_{solv} = 0.17	3.69 [3.60] NAC=0.22	3.52 Δ_{vac} = 0.17 Δ_{solv} = 0.08
G3	3.23 [3.14] NAC=0.20	3.26 Δ_{vac} = -0.03 Δ_{solv} = -0.12	3.34 [3.19] NAC=0.20	3.03 Δ_{vac} = 0.31 Δ_{solv} = -0.16	3.20 [3.18] NAC=0.20	3.06 Δ_{vac} = -0.14 Δ_{solv} = -0.12
G4	3.00 [2.97] NAC=0.20	Not reported	2.84 [2.88] NAC=0.20	Not reported	2.58 [2.71] NAC=0.19	Not reported
G5	2.68 [2.68] NAC=0.21	Not reported	2.80 [2.78] NAC=0.20	2.98 Δ_{vac} = -0.18 Δ_{solv} = -0.20	2.95 [2.94] NAC=0.20	3.03 Δ_{vac} = -0.08 Δ_{solv} = -0.07
G6	2.55 [2.52] NAC=0.21	Not reported	2.40 [2.40] NAC=0.21	Not reported	2.32 [2.33] NAC=0.20	Not reported

δ_{Exp} are experimental results[30]. Δ_{vac} and Δ_{solv} indicate the difference between the experimental and theoretical chemical shift, in vacuum and solvent, respectively.

In most cases, the theoretical δ values follow a decreasing order down the group, which is due to the ions having a deshielding effect on the protons of the NOTA that are in close proximity. The decrease in the δ values is consistent with the decrease in the electron withdrawing effect of the ions, which causes a decline in NAC values down the group. It should be noted that the theoretical chemical shift values are in good agreement with the experiment (differences are less than 1 ppm), which indicates the suitability of the applied DFT functional and basis set. Furthermore, there is no significant difference between the ^{1}H NMR in the vacuum and the water.

Figure 4 shows the groups of protons (**G1** to **G6**) characterized by different theoretical chemical shifts. It is notable that the theoretical NMR analysis implies that each group has different chemical environments, which could not be detected in the experiment. This motivated a measurement of the theoretical chemical shifts for all proton groups, for which a detailed discussion is provided.
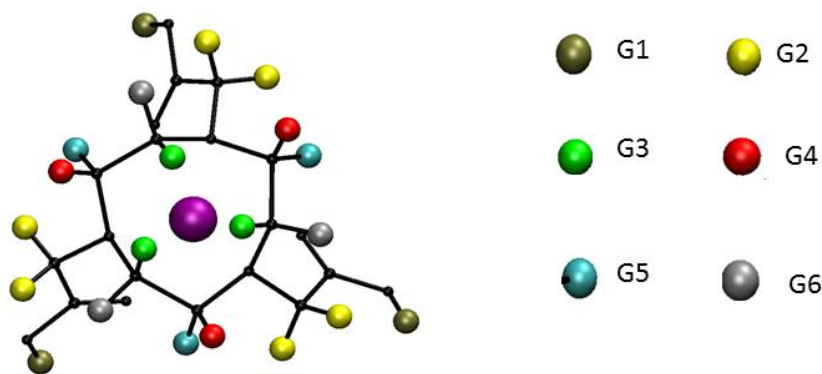
Figure 4: NOTA—alkali ions complex based on the intensity of the different chemical shifts. G indicates the different groups of hydrogen. Hydrogen atoms with the same colour code belong to the same chemical environment. (Indicated by the number of the chemical **Table 8**).

For both Na^+ and K^+ complexes, the highest δ values are found for the carboxyl protons (**G1**), which have the most positive atomic charges, followed by the proton of the methylene group ($-CH_2-$) within the pendant arm (**G2**), this ranking of δ values agreeing with experimental results. The **G3** to **G6** are protons in the ring with the same functional group but different chemical environments, the protons in **G3** having higher δ values than the other protons, which is caused by the **G3** protons facing towards the each other.

It should be noted that the δ ranking for **G3** to **G6** is not only caused by their proximity to the ion, but by their environment in relation to other atoms within the NOTA. This is evident by the fact that the δ ranking for the free NOTA is exactly the same as for complexed NOTA (**Table 6S**).The free NOTA **G3** has the highest δ value amongst **G3** to **G6**, which appears to be due to these protons facing towards each other. Furthermore, **G2, G3** and **G4** become less deshielded upon complexation, while **G1, G5** and **G6** become more deshielded. In contrast, natural atomic charges of all groups (**G1**-**G6**) are more positive upon complexation suggesting two different electronic effects that contribute to the chelation process. First, the inductive effect, through charge transfer from σ(C-H) ring to the σ(N-C), as demonstrated in **Figure 3** (arrow C), could be responsible for the observed trend in natural atomic charges. Secondly, short-range coupling should affect δ values, although this effect is complicated by the chemical environment of the proton with respect to the other NOTA atoms as well as the ions.

2.11. Analysis of the frontier molecular orbitals

Frontier molecular orbitals are the highest occupied molecular orbitals (HOMO) and the lowest unoccupied molecular orbitals (LUMO). The energy difference between the two frontier molecular orbitals ($\Delta E_{LUMO-HOMO}$) is referred to as the $\Delta E_{LUMO-HOMO,}$ and is used to predict the reactivity and stability of transition metal complexes.[70,71,72] A highly polarizable molecule is generally highly chemically reactive possesses low kinetic stability and low energy gap.[73] The energy eigenvalue of the HOMO (E_{HOMO}) is the energy of the highest occupied orbital containing electrons that are donated, while LUMO can be considered to be the lowest unoccupied orbital, with free places to accept.[74]

To evaluate the stability of complexation, the HOMO and LUMO energy eigenvalue (E_{HOMO}, E_{LUMO}) of the NOTA— ion complexes, and individual components in the complexes, are presented in **Table 9**.

Table 9: The E_{HOMO}, E_{LUMO} and $\Delta E_{LUMO-HOMO}$ of the optimized NOTA—ion structures at B3LYP/6-311+G(d,p) level of theory

Complexes/ions	E_{HOMO} (eV)	E_{LUMO} (eV)	$\Delta E_{LUMO-HOMO}$ (eV)
Li^+	-63.92	-6.95	56.97
Na^+	-39.16	-7.10	24.33
K^+	-26.53	-5.94	20.59
Rb^+	-22.88	-5.53	17.34
NOTA	-7.80	-2.86	4.93
NOTA—Li^+	-9.11 [-8.17]	-3.27 [-3.35]	5.84[-4.81]
NOTA—Na^+	-8.92 [-8.14]	-3.20 [-3.39]	5.72 [-4.76]
NOTA—K^+	-8.79 [-8.11]	-3.17 [-3.40]	5.62 [-4.71]
NOTA—Rb^+	-8.84 [-8.14]	-3.28 [-3.50]	5.57 [-4.64]

Bracket indicates values for complexes in conformation '**B**'

The E_{HOMO} energy value of the individual alkali metal becomes less negative down the group. In conformations '**A**' and '**B**' , the E_{HOMO} becomes less negative down the group from Li^+ to K^+, whilst E_{HOMO} for NOTA—Rb^+ is slightly higher than for the K^+ complex, which could be an artefact of using a different basis sets for Rb^+. The E_{HOMO} values for conformation '**A**' are slightly more negative than those for '**B**' due to the greater stability of conformation in the former.

A question may arise regarding the impact on E_{HOMO} of NOTA upon complexation with each ion. The presence of the ion, in the NOTA complexes, has a significant effect on the E_{HOMO}

of the complexes, and increases the ability of NOTA to donate an electron; this effect is decreased down the alkali metal series.

The $\Delta E_{LUMO\text{-}HOMO}$ gap is a commonly used stability index,[75] the higher its value, the more stable the chemical system.[76] For the alkali metal ions before complexation, the order is $Li^+>Na^+>K^+>Rb^+$. The $\Delta E_{LUMO\text{-}HOMO}$ for free metals is significantly higher than the complexes. For both conformations '**A**' and '**B**', the $\Delta E_{LUMO\text{-}HOMO}$ energy gap decreases down the group in the following order: NOTA—Li^+> NOTA—Na^+> NOTA—K^+> NOTA—Rb^+. However, the $\Delta E_{LUMO\text{-}HOMO}$ gap for complexes in conformation '**A**' is slightly greater than that of complexes '**B**'. This signifies that complexes in conformation '**A**', with six atoms in close proximity to the cations, are more stable than conformation '**B**', with only four atoms. The $\Delta E_{LUMO\text{-}HOMO}$ energy gap values imply that the stability for the alkali metal, and that of the NOTA—ion complexes, decreases down the group.

2.11.1. DFT-based properties related to chelator—ion stability

Density Functional Theory can be used to calculate the global reactivity descriptors, such as chemical potential, hardness, softness .[77] Ionization potential describes the capability of an atom or molecule to donate electrons, while electron affinity describes the capability of an atom or molecule to attract electrons. Chemical hardness describes the resistance to modification in electron distribution, and correlates with the stability and reactivity of the chemical system. The inverse of the hardness is expressed as the global softness.[78,79] A hard molecule should have a large $\Delta E_{LUMO\text{-}HOMO}$ energy gap, and a soft molecule should have a small one.[78, 80]

The calculated DFT-based quantities, such as electron affinity (EA), ionization potential (IP), chemical hardness (η) and softness (S) for the complexes are presented in **Table 10**.

Table 10: DFT-based quantities for alkali metals (Li$^+$, Na$^+$, K$^+$ and Rb$^+$) complexes with NOTA, calculated at B3LYP/6-311+G(2d,2p) level of theory.

Complex	EA (eV)	IP (eV)	η (eV)	S (eV)
Li$^+$	-5.62	76.04	40.83	0.01
Na$^+$	-5.42	47.62	26.52	0.02
K$^+$	-4.50	31.69	18.10	0.03
Rb$^+$	-4.30	27.92	16.11	0.03
NOTA	0.60	7.11	3.26	0.15
NOTA—Li$^+$	-2.44 [-2.73]	11.58 [11.04]	7.01 [6.89]	0.071 [0.0726]
NOTA—Na$^+$	-2.40 [-2.80]	11.47 [10.96]	6.94 [6.88]	0.072 [0.0727]
NOTA—K$^+$	-2.41 [-2.84]	11.28 [10.77]	6.84 [6.81]	0.073 [0.0735]
NOTA—Rb$^+$	-2.41 [-2.94]	11.09 [10.61]	6.75 [6.77]	0.074 [0.0738]

Parenthesis indicates values of complex '**B**'

For the free metals, the electron affinity (EA) becomes less negative and the ionization potential (IP) becomes less positive, which leads to a decreasing chemical hardness down the group.

A comparison of free-NOTA with the complexes revealed that the presence of the ions leads to an increase in hardness, and therefore an increase in stability upon complexation. The smaller the ion, the greater the hardness, this observation being consistent with the trend in interaction energies and thermochemical properties (**Tables 2** and **3**). Furthermore, these results indicate that the ability of the complexes to exchange electrons, and their electron polarizability, increases down the group.

The hardness values for conformations '**A**' and '**B**' follows a similar decreasing order, although conformation '**A**', with 6 heteroatoms interacting with ions, has a higher hardness values. It is notable that the decreasing order of hardness is consistent with the decreasing $\Delta E_{LUMO-HOMO}$. The softness value is the inverse of the hardness value, and thus follows an increasing order down the group.

2.12. Implication of results

The outcome of the present study revealed a significant level of intermolecular interaction between alkali metals and NOTA. The electronic structure properties, such as interaction energy, frontier molecular orbitals, ^{1}H NMR chemical shifts, hardness, ionization potential

and electron affinity values, offer an explanation for the stability of NOTA—alkali metal complexes. It should be noted that the structural stability of chelator—ion complexes is one of the factors that influences the radiolabelling efficiency[3]. This implies that the presence of competitive alkali metals in the body may have a significant effect on the radiolabelling yield of NOTA.

The displacement of radio metals, as a result of competition from alkali metals or other competing ions, can be disastrous, as some radio metals, when released from bifunctional chelators (BFC), are stored in some organs in the body. For example, ^{89}Zr and ^{68}Ga are known to accumulate in the bone, where ^{64}Cu accumulates in the liver.[3] Furthermore, it is assumed that the rate of the competition of alkali metals with radio metals, during complexation with NOTA, decreases down the group, as NOTA—Li$^+$ is the most stable complex. Another factor that should be noted is that the concentration of alkali metals in the biological system varies considerably: Li$^+$=3.1×10^{-8} kg/kg, Na$^+$ =2.5×10^{-3} kg/kg, K$^+$=1.5×10^{-3} kg/kg, Rb$^+$ 4.6×10^{-6} kg/kg.[81] Despite Li$^+$ being the most optimal match to NOTA (**Tables 2** and **3**), it might not constitute much competition as it is in low quantities in the body. Na$^+$ and K$^+$ are in much higher quantities and can reasonably bind with NOTA, which can constitute competition with radio metals for complexation with NOTA. Amongst the aforementioned ions, Na$^+$ should be the greatest competitor, as it has the highest concentration and binds more strongly to NOTA than K$^+$. There is a need to establish the level of alkali metal competition with radio metals by comparing the stability of NOTA—radio metal with NOTA—alkali metal complexes. It is therefore our future intention to evaluate the complexation of NOTA chelator with some selected radio metals. This information can be used to propose chelators that bind to alkali metals less strongly than NOTA does, yet maintains radio metal stability.

2.13. Conclusions

Density Functional Theory (DFT), at the B3LYP/6-311+G(2d, 2p) level of theory, has been used to determine quantum chemical quantities that occurred in the complexation process of NOTA with alkali metals (Li$^+$, Na$^+$, K$^+$ and Rb$^+$). We reported on two groups of complexes, namely in conformation '**A**', have six hetero atoms in close proximity to the cations, while complexes in conformation '**B**' have six hetero atoms in close proximity. Complex '**A**' is more stable than complex '**B**', as is evidenced by more negative interaction and relaxation energies, and higher $\Delta E_{LUMO-HOMO}$ values. The obtained theoretical ^{1}H NMR chemical shifts of NOTA,

in vacuum and water media, agreed with experimental observation. The deshielding effect of the ions on the protons of NOTA lead to a decrease in NAC and δ values down the group. Overall, the interaction energies, bond distances, NBO and chemical shift analysis, global reactivity-related properties, chemical hardness and softness revealed a significant level of interaction between NOTA and alkali metal ions, with the stability of NOTA—alkali metal complexes decreasing down the periodic table. Consequently, the presence of alkali metal ions, specifically Na^+, which is the most abundant in the body, can compete with radio metals for complexation with NOTA and affect the radiolabelling yield. Understanding the competitive non-covalent interactions of NOTA with alkali metals will provide important information for our ongoing project of matching the appropriate chelators with specific radio metals.

Acknowledgment

REFERENCES

1.   Sugiura, G., Kühn, H., Sauter, M., Haberkorn, U., and Mier, W. (2014) Radiolabeling strategies for tumor-targeting proteinaceous drugs, *Molecules 19*, 2135-2165.

2.   Massicano, A. V., Alcarde, L. F., Oliveira, R. S., Mengatti, J., and de Araújo, E. B. (2013) Radiolabeling parameters of 177 Lu-DOTA-RITUXIMAB.

3.   Price, E. W., and Orvig, C. (2014) Matching chelators to radiometals for radiopharmaceuticals, *Chemical Society Reviews 43*, 260-290.

4.   McBride, W. J., D'Souza, C. A., Karacay, H., Sharkey, R. M., and Goldenberg, D. M. (2012) New lyophilized kit for rapid radiofluorination of peptides, *Bioconjugate chemistry 23*, 538-547.

5.   Kang, C. S. (2014) *Antibody and peptide conjugates of bifunctional chelators for targeted cancer therapy and imaging*, Illinois Institute of Technology.

6.   Cooper, M. S., Ma, M. T., Sunassee, K., Shaw, K. P., Williams, J. D., Paul, R. L., Donnelly, P. S., and Blower, P. J. (2012) Comparison of 64Cu-Complexing Bifunctional Chelators for Radioimmunoconjugation: Labeling Efficiency, Specific Activity, and in Vitro/in Vivo Stability, *Bioconjugate Chemistry 23*, 1029-1039.

7.   Rasaneh, S., Rajabi, H., Babaei, M. H., Daha, F. J., and Salouti, M. (2009) Radiolabeling of trastuzumab with 177 Lu via DOTA, a new radiopharmaceutical for radioimmunotherapy of breast cancer, *Nuclear medicine and biology 36*, 363-369.

8.   Rasaneh, S., Rajabi, H., Babaei, M. H., and Daha, F. J. (2010) 177 Lu labeling of Herceptin and preclinical validation as a new radiopharmaceutical for radioimmunotherapy of breast cancer, *Nuclear medicine and biology 37*, 949-955.

9.   Dwyer, F. (2012) *Chelating agents and metal chelates*, Elsevier.

10.   Varadwaj, P. R., Varadwaj, A., Peslherbe, G. H., and Marques, H. M. (2011) Conformational Analysis of 18-Azacrown-6 and Its Bonding with Late First Transition Series Divalent Metals: Insight from DFT Combined with NPA and QTAIM Analyses, *The Journal of Physical Chemistry A 115*, 13180-13190.

11.   Förster, C., Schubert, M., Pietzsch, H.-J., and Steinbach, J. (2011) Maleimido-Functionalized NOTA Derivatives as Bifunctional Chelators for Site-Specific Radiolabeling, *Molecules 16*, 5228-5240.

12.   Lang, L., Li, W., Guo, N., Ma, Y., Zhu, L., Kiesewetter, D. O., Shen, B., Niu, G., and Chen, X. (2011) Comparison study of [18F] FAl-NOTA-PRGD2,[18F] FPPRGD2, and [68Ga] Ga-NOTA-PRGD2 for PET imaging of U87MG tumors in mice, *Bioconjugate chemistry 22*, 2415-2422.

13.   Berry, D. J., Ma, Y., Ballinger, J. R., Tavaré, R., Koers, A., Sunassee, K., Zhou, T., Nawaz, S., Mullen, G. E., and Hider, R. C. (2011) Efficient bifunctional gallium-68 chelators for positron emission tomography: tris (hydroxypyridinone) ligands, *Chemical Communications 47*, 7068-7070.

14.   Jeong, J. M., Kim, Y. J., Lee, Y. S., Lee, D. S., Chung, J. K., and Lee, M. C. (2009) Radiolabeling of NOTA and DOTA with positron emitting 68Ga and investigation of in vitro properties, *Nuclear Medicine and Molecular Imaging 43*, 330-336.

15.   Notni, J., Pohle, K., and Wester, H.-J. (2012) Comparative gallium-68 labeling of TRAP-, NOTA-, and DOTA-peptides: practical consequences for the future of gallium-68-PET, *EJNMMI research 2*, 1-5.

16.   Drahoš, B., Kubíček, V., Bonnet, C. S., Hermann, P., Lukeš, I., and Tóth, É. (2011) Dissociation kinetics of Mn 2+ complexes of NOTA and DOTA, *Dalton Transactions 40*, 1945-1951.

17.   Kiviniemi, A., Mäkelä, J., Mäkilä, J., Saanijoki, T., Liljenbäck, H., Poijärvi-Virta, P. i., Lönnberg, H., Laitala-Leinonen, T., Roivainen, A., and Virta, P. (2012) Solid-Supported NOTA and DOTA Chelators Useful for the Synthesis of 3′-Radiometalated Oligonucleotides, *Bioconjugate chemistry 23*, 1981-1988.

18.   Blom, E., Velikyan, I., Monazzam, A., Razifar, P., Nair, M., Razifar, P., Vanderheyden, J. L., Krivoshein, A. V., Backer, M., and Backer, J. (2011) Synthesis and characterization of scVEGF-PEG-[68Ga] NOTA and scVEGF-PEG-[68Ga] DOTA PET tracers, *Journal of Labelled Compounds and Radiopharmaceuticals 54*, 685-692.

19.   Zhang, Y., Hong, H., Engle, J. W., Bean, J., Yang, Y., Leigh, B. R., Barnhart, T. E., and Cai, W. (2011) Positron emission tomography imaging of CD105 expression with a 64Cu-labeled monoclonal antibody: NOTA is superior to DOTA, *PLoS One 6*, e28005.

20.   Baumhover, N. J., Martin, M. E., Parameswarappa, S. G., Kloepping, K. C., O'Dorisio, M. S., Pigge, F. C., and Schultz, M. K. (2011) Improved synthesis and biological evaluation of chelator-modified α-MSH analogs prepared by copper-free click chemistry, *Bioorganic & medicinal chemistry letters 21*, 5757-5761.

21.   Šimeček, J., Hermann, P., Wester, H. J., and Notni, J. (2013) How is 68Ga labeling of macrocyclic chelators influenced by metal ion contaminants in 68Ge/68Ga generator eluates? *ChemMedChem 8*, 95-103.

22.   Ferreira, C. L., Yapp, D. T., Mandel, D., Gill, R. K., Boros, E., Wong, M. Q., Jurek, P., and Kiefer, G. E. (2012) 68Ga small peptide imaging: comparison of NOTA and PCTA, *Bioconjugate chemistry 23*, 2239-2246.

23.   Notni, J., Hermann, P., Havlíčková, J., Kotek, J., Kubíček, V., Plutnar, J., Loktionova, N., Riss, P. J., Rösch, F., and Lukeš, I. (2010) A Triazacyclononane-Based Bifunctional Phosphinate Ligand for the Preparation of Multimeric 68Ga Tracers for Positron Emission Tomography, *Chemistry-A European Journal 16*, 7174-7185.

24.   Ait-Mohand, S., Fournier, P., Dumulon-Perreault, V., Kiefer, G. E., Jurek, P., Ferreira, C. L., Bénard, F. o., and Guérin, B. (2011) Evaluation of 64Cu-labeled bifunctional chelate–bombesin conjugates, *Bioconjugate chemistry 22*, 1729-1735.

25.   Chakravarty, R., Chakraborty, S., Dash, A., and Pillai, M. (2013) Detailed evaluation on the effect of metal ion impurities on complexation of generator eluted 68 Ga with different bifunctional chelators, *Nuclear medicine and biology 40*, 197-205.

26.   Clarke, E. T., and Martell, A. E. (1991) Stabilities of the Fe (III), Ga (III) and In (III) chelates of N, N′, N ″-triazacyclononanetriacetic acid, *Inorganica chimica acta 181*, 273-280.

27.   Clarke, E. T., and Martell, A. E. (1991) Stabilities of trivalent metal ion complexes of the tetraacetate derivatives of 12-, 13-and 14-membered tetraazamacrocycles, *Inorganica Chimica Acta 190*, 37-46.

28.   Velikyan, I., Maecke, H., and Langstrom, B. (2008) Convenient preparation of 68Ga-based PET-radiopharmaceuticals at room temperature, *Bioconjugate chemistry 19*, 569-573.

29.   Chang, A. J., Sohn, R., Lu, Z. H., Arbeit, J. M., and Lapi, S. E. (2013) Detection of rapalog-mediated therapeutic response in renal cancer xenografts using 64Cu-bevacizumab immunoPET, *PloS one 8*, e58949.

30.   Geraldes, C. F., Marques, M. P. M., and Sherry, A. D. (1998) NMR conformational study of diamagnetic complexes of some triazatriacetate macrocycles, *Inorganica chimica acta 273*, 288-298.

31.   Šimeček, J., Schulz, M., Notni, J., Plutnar, J., Kubíček, V. c., Havlíčková, J., and Hermann, P. (2011) Complexation of metal ions with TRAP (1, 4, 7-triazacyclononane phosphinic acid) ligands and 1, 4, 7-triazacyclononane-1, 4, 7-triacetic acid: phosphinate-containing ligands as unique chelators for trivalent gallium, *Inorganic Chemistry 51*, 577-590.

32.   Skelton, A., Fried, J. R., and Agrawal, N. (2015) Quantum Mechanical Calculations of the Interactions Between Diazacrowns and the Sodium Cation: An insight into Na+ Complexation in Diazacrown-Based Synthetic Ion Channels, *RSC Advances*.

33.   Behjatmanesh-Ardakani, R. (2015) NBO–NEDA, NPA, and QTAIM studies on the interactions between aza-, diaza-, and triaza-12-crown-4 (An-12-crown-4, n= 1, 2, 3) and Li+, Na+, and K+ ions, *Computational and Theoretical Chemistry 1051*, 62-71.

34.   Behjatmanesh-Ardakani, R. (2014) DFT-B3LYP and SMD study on the interactions between aza-, diaza-, and triaza-12-crown-4 (A n-12-crown-4, n= 1, 2, 3) with Na+ in the gas phase and acetonitrile solution, *Structural Chemistry 25*, 919-929.

35.   M. J. Frisch, G. W. T., H. B. Schlegel, G. E. Scuseria, , M. A. Robb, J. R. C., G. Scalmani, V. Barone, B. Mennucci, , G. A. Petersson, H. N., M. Caricato, X. Li, H. P. Hratchian, , A. F. Izmaylov, J. B., G. Zheng, J. L. Sonnenberg, M. Hada, , M. Ehara, K. T., R. Fukuda, J. Hasegawa, M. Ishida, T. Nakajima, , Y. Honda, O. K., H. Nakai, T. Vreven, J. A. Montgomery, Jr., , J. E. Peralta, F. O., M. Bearpark, J. J. Heyd, E. Brothers, , K. N. Kudin, V. N. S., R. Kobayashi, J. Normand, , K. Raghavachari, A. R., J. C. Burant, S. S. Iyengar, J. Tomasi, , M. Cossi, N. R., J. M. Millam, M. Klene, J. E. Knox, J. B. Cross, , V. Bakken, C. A., J. Jaramillo, R. Gomperts, R. E. Stratmann, , O. Yazyev, A. J. A., R. Cammi, C. Pomelli, J. W. Ochterski, , R. L. Martin, K. M., V. G. Zakrzewski, G. A. Voth, , P. Salvador, J. J. D., S. Dapprich, A. D. Daniels, , O. Farkas, J. B. F., J. V. Ortiz, J. Cioslowski, , and and D. J. Fox. (2009) Gaussian 09, Revision A.02,, Gaussian Inc., Wallingford CT.

36.   Lee C., Yang W., and R.G, P. (1988) Development of Colle-Salvetti correlation-energy formula into a functional of electron density, *Phsical Review B 37*, 785-789.

37.   Becke, A. D. (1993) Densityfunctional thermochemistry. III. The role of exact exchange, *J. Chem. Phys. 98*, 5648.

38.   Blaudeau, J.-P., McGrath, M. P., Curtiss, L. A., and Radom, L. (1997) Extension of Gaussian-2 (G2) theory to molecules containing third-row atoms K and Ca, *The Journal of chemical physics 107*, 5016-5021.

39.   Curtiss, L. A., McGrath, M. P., Blaudeau, J. P., Davis, N. E., Binning Jr, R. C., and Radom, L. (1995) Extension of Gaussian-2 theory to molecules containing third-row atoms Ga–Kr, *The Journal of chemical physics 103*, 6104-6113.

40.   McGrath, M. P., and Radom, L. (1991) Extension of Gaussian-1 (G1) theory to bromine-containing molecules, *The Journal of chemical physics 94*, 511-516.

41.   Binning, R., and Curtiss, L. (1990) Compact contracted basis sets for third-row atoms: Ga–Kr, *Journal of Computational Chemistry 11*, 1206-1216.

42.   Weigend, F., and Ahlrichs, R. (2005) Balanced basis sets of split valence, triple zeta valence and quadruple zeta valence quality for H to Rn: design and assessment of accuracy, *Physical Chemistry Chemical Physics 7*, 3297-3305.

43.   Cances, E., Mennucci, B., and Tomasi, J. (1997) A new integral equation formalism for the polarizable continuum model: Theoretical background and applications to isotropic and anisotropic dielectrics, *The Journal of chemical physics 107*, 3032-3041.

44.   Mennucci, B., Cances, E., and Tomasi, J. (1997) Evaluation of solvent effects in isotropic and anisotropic dielectrics and in ionic solutions with a unified integral equation method: theoretical bases, computational implementation, and numerical applications, *The Journal of Physical Chemistry B 101*, 10506-10517.

45.   Tomasi, J., Mennucci, B., and Cances, E. (1999) The IEF version of the PCM solvation method: an overview of a new method addressed to study molecular solutes at the QM ab initio level, *Journal of Molecular Structure: THEOCHEM 464*, 211-226.

46.   Coropceanu, V., Malagoli, M., da Silva Filho, D., Gruhn, N., Bill, T., and Brédas, J. (2002) Hole-and electron-vibrational couplings in oligoacene crystals: intramolecular contributions, *Physical review letters 89*, 275503.

47.   Reed, A. E., Curtiss, L. A., and Weinhold, F. (1988) Intermolecular interactions from a natural bond orbital, donor-acceptor viewpoint, *Chemical Reviews 88*, 899-926.

48.   Reed, A. E., Weinstock, R. B., and Weinhold, F. (1985) Natural population analysis, *The Journal of Chemical Physics 83*, 735-746.

49.   Weinhold, F. (2012) Natural bond orbital analysis: a critical overview of relationships to alternative bonding perspectives, *Journal of computational chemistry 33*, 2363-2379.

50.   Liu, J.-n., Chen, Z.-r., and Yuan, S.-f. (2005) Study on the prediction of visible absorption maxima of azobenzene compounds, *Journal of Zhejiang University. Science. B 6*, 584.

51.   Sebastian, S., Sylvestre, S., Jayabharathi, J., Ayyapan, S., Amalanathan, M., Oudayakumar, K., and Herman, I. A. (2015) Study on conformational stability, molecular structure, vibrational spectra, NBO, TD-DFT, HOMO and LUMO analysis of 3,5-dinitrosalicylic acid by DFT techniques, *Spectrochimica Acta Part A: Molecular and Biomolecular Spectroscopy 136, Part B*, 1107-1118.

52.   Fogarasi, G., Zhou, X., Taylor, P. W., and Pulay, P. (1992) The calculation of ab initio molecular geometries: efficient optimization by natural internal coordinates and empirical correction by offset forces, *Journal of the American Chemical Society 114*, 8191-8201.

53.   James, C., Raj, A. A., Reghunathan, R., Jayakumar, V., and Joe, I. H. (2006) Structural conformation and vibrational spectroscopic studies of 2, 6-bis (p-N, N-dimethyl benzylidene) cyclohexanone using density functional theory, *Journal of Raman Spectroscopy 37*, 1381-1392.

54.   Geerlings, P., De Proft, F., and Langenaeker, W. (2003) Conceptual density functional theory, *Chemical reviews 103*, 1793-1874.

55.   Lameira, J., Alves, C., Moliner, V., and Silla, E. (2006) A density functional study of flavonoid compounds with anti-HIV activity, *European journal of medicinal chemistry 41*, 616-623.

56.   Mähler, J., and Persson, I. (2011) A study of the hydration of the alkali metal ions in aqueous solution, *Inorganic chemistry 51*, 425-438.

57.   Bouazizi, S., and Nasr, S. (2007) Local order in aqueous lithium chloride solutions as studied by X-ray scattering and molecular dynamics simulations, *Journal of molecular structure 837*, 206-213.

58.   Du, H., Rasaiah, J. C., and Miller, J. D. (2007) Structural and dynamic properties of concentrated alkali halide solutions: a molecular dynamics simulation study, *The Journal of Physical Chemistry B 111*, 209-217.

59.   Mancinelli, R., Botti, A., Bruni, F., Ricci, M., and Soper, A. (2007) Hydration of sodium, potassium, and chloride ions in solution and the concept of structure maker/breaker, *The Journal of Physical Chemistry B 111*, 13570-13577.

60.   Azam, S. S., Hofer, T. S., Randolf, B. R., and Rode, B. M. (2009) Hydration of sodium (I) and potassium (I) revisited: a comparative QM/MM and QMCF MD simulation study of weakly hydrated ions, *The Journal of Physical Chemistry A 113*, 1827-1834.

61.   Tongraar, A., Liedl, K. R., and Rode, B. M. (1998) Born-Oppenheimer ab initio QM/MM dynamics simulations of Na$^+$ and K$^+$ in water: from structure making to structure breaking effects, *The Journal of Physical Chemistry A 102*, 10340-10347.

62.   Ohtomo, N., and Arakawa, K. (1980) Neutron diffraction study of aqueous ionic solutions. II. Aqueous solutions of sodium chloride and potassium chloride, *Bulletin of the Chemical Society of Japan 53*, 1789-1794.

63.   Ramos, S., Barnes, A., Neilson, G., and Capitan, M. (2000) Anomalous X-ray diffraction studies of hydration effects in concentrated aqueous electrolyte solutions, *Chemical Physics 258*, 171-180.

64.   San-Román, M. L., Hernández-Cobos, J., Saint-Martin, H., and Ortega-Blake, I. (2010) A theoretical study of the hydration of Rb+ by Monte Carlo simulations with refined ab initio-based model potentials, *Theoretical Chemistry Accounts 126*, 197-211.

65.   Hofer, T. S., Randolf, B. R., and Rode, B. M. (2005) Structure-breaking effects of solvated Rb (I) in dilute aqueous solution—An ab initio QM/MM MD approach, *Journal of computational chemistry 26*, 949-956.

66.   Balachandran, V., and Parimala, K. (2012) Tautomeric purine forms of 2-amino-6-chloropurine (N9H10 and N7H10): Structures, vibrational assignments, NBO analysis, hyperpolarizability, HOMO–LUMO study using B3 based density functional calculations, *Spectrochimica Acta Part A: Molecular and Biomolecular Spectroscopy 96*, 340-351.

67.   Szafran, M., Komasa, A., and Bartoszak-Adamska, E. (2007) Crystal and molecular structure of 4-carboxypiperidinium chloride (4-piperidinecarboxylic acid hydrochloride), *Journal of Molecular Structure 827*, 101-107.

68.   Kavitha, E., Sundaraganesan, N., Sebastian, S., and Kurt, M. (2010) Molecular structure, anharmonic vibrational frequencies and NBO analysis of naphthalene acetic acid by density functional theory calculations, *Spectrochimica Acta Part A: Molecular and Biomolecular Spectroscopy 77*, 612-619.

69.   Rajamani, T., and Muthu, S. (2013) Electronic absorption, vibrational spectra, non-linear optical properties, NBO analysis and thermodynamic properties of 9-[(2-hydroxyethoxy) methyl] guanine molecule by density functional method, *Solid State Sciences 16*, 90-101.

70.   Griffith, J., and Orgel, L. (1957) Ligand-field theory, *Quarterly Reviews, Chemical Society 11*, 381-393.

71.   Sinha, L., Prasad, O., Narayan, V., and Shukla, S. R. (2011) Raman, FT-IR spectroscopic analysis and first-order hyperpolarisability of 3-benzoyl-5-chlorouracil by first principles, *Molecular Simulation 37*, 153-163.

72.   Govindarajan, M., Karabacak, M., Periandy, S., and Tanuja, D. (2012) Spectroscopic (FT-IR, FT-Raman, UV and NMR) investigation and NLO, HOMO–LUMO, NBO analysis of organic 2, 4, 5-trichloroaniline, *Spectrochimica Acta Part A: Molecular and Biomolecular Spectroscopy 97*, 231-245.

73.   Obot, I., Gasem, Z., and Umoren, S. (2014) Understanding the Mechanism of 2-mercaptobenzimidazole Adsorption on Fe (110), Cu (111) and Al (111) Surfaces: DFT and Molecular Dynamics Simulations Approaches, *Int. J. Electrochem. Sci 9*, 2367-2378.

74.   Gece, G. (2008) The use of quantum chemical methods in corrosion inhibitor studies, *Corrosion Science 50*, 2981-2992.

75.   Lewis, D., Ioannides, C., and Parke, D. (1994) Interaction of a series of nitriles with the alcohol-inducible isoform of P450: Computer analysis of structure—activity relationships, *Xenobiotica 24*, 401-408.

76.   Zhou, Z., and Parr, R. G. (1990) Activation hardness: new index for describing the orientation of electrophilic aromatic substitution, *Journal of the American Chemical Society 112*, 5720-5724.

77.   Pathak, S., Srivastava, R., Sachan, A., Prasad, O., Sinha, L., Asiri, A., and Karabacak, M. (2015) Experimental (FT-IR, FT-Raman, UV and NMR) and quantum chemical studies on molecular structure, spectroscopic analysis, NLO, NBO and reactivity descriptors of 3, 5-

Difluoroaniline, *Spectrochimica Acta Part A: Molecular and Biomolecular Spectroscopy 135*, 283-295.

78.   Kotena, Z. M., Behjatmanesh-Ardakani, R., Hashim, R., and Achari, V. M. (2013) Hydrogen bonds in galactopyranoside and glucopyranoside: a density functional theory study, *Journal of molecular modeling 19*, 589-599.

79.   Hizaddin, H. F., Anantharaj, R., and Hashim, M. A. (2014) A quantum chemical study on the molecular interaction between pyrrole and ionic liquids, *Journal of Molecular Liquids 194*, 20-29.

80.   Amin, M. A., Hazzazi, O., Kandemirli, F., and Saracoglu, M. (2012) Inhibition Performance and Adsorptive Behavior of Three Amino Acids on Cold-Rolled Steel in 1.0 M HCl-Chemical, Electrochemical, and Morphological Studies, *Corrosion 68*, 688-698.

81.   Sigel, A., Sigel, H., and Sigel, R. K. The Alkali Metal Ions: Their Role for Life. *Spinger International Publising Switzerland* (2016).

CHAPTER THREE

DFT study on the complexation of NOTA as a bifunctional chelator with radiometal ions

F. Y. Adeowo, B. Honarpavar*, A. A. Skelton*,

School of Health Sciences, Discipline of Pharmacy, University of KwaZulu-Natal, Durban 4001, South Africa.

Corresponding authors: Skelton@ukzn.ac.za (A.A Skelton); Honarparvar@ukzn.ac.za (B. Honarparvar), School of Pharmacy and Pharmacology, University of KwaZulu-Natal, Durban 4001, South Africa. Tel.: +27 31 2608520, +27 31 26084.

Abstract

1,4,7 triazacyclononane-1,4,7 triacetic acid (NOTA) is a key bifunctional chelator utilized for the complexation of a large number of metal ions in radiopharmaceutical applications; the ability of these chelators depends on the strength of their binding with the ions. The focus of the present work is to evaluate the complexation of Cu^{2+}, Ga^{3+}, Sc^{3+} and In^{3+} radiometal ions with NOTA using density functional theory (B3LYP functional) and 6-311+G(2d,2p) or DGDZVP basis sets.

Interaction and relaxation energies, Gibbs free energies and entropies show that the Ga^{3+}—NOTA complex is the most stable while the Cu^{2+}—NOTA complex is the least stable. Implicit water solvation affects the complexation of NOTA—ions, causes a decrease in the stability of the system; Ga^{3+}—NOTA complex is the least affected by solvent. NBO analysis performed through the natural population charges and second order perturbation analysis reveals charge transfer between NOTA and radiometal ions. The theoretical ^{1}H NMR chemical shifts of NOTA, in vacuum and water media, are in good agreement with experiment; these values are influenced by the presence of the ions, which have a deshielding effect on the protons of NOTA. Global scalar properties such as HOMO/LUMO energies, $\Delta E_{LUMO\text{-}HOMO}$ gap, chemical hardness and softness values confirms that the NOTA—Cu^{2+} complex, which has a singly occupied molecular orbital, has the lowest $\Delta E_{LUMO\text{-}HOMO}$ value, the least chemical hardness value and the highest chemical softness value. It is however noted that the hardness value and $\Delta E_{LUMO\text{-}HOMO}$ gap values of the complexes varies considerable. This can, however, be attributed to the different positions of the metals on the periodic table (Cu^{2+} and Sc^{3+} are both transition metals while In^{3+} and Ga^{3+} are group III metals with different ionic radii).

A notable conclusion that can be made from the present study is that the different positions of the different ions influenced their interactions with NOTA. Furthermore, the study affirms that amongst other radiometal ions, Ga^{3+} can be used to effectively radiolabel NOTA chelator for radiopharmaceutical usage as it binds tightly to NOTA and more stable with NOTA when compared to other ions under investigation.

Keywords: 1, 4, 7 triazacyclononane-1,4,7 triacetic acid (NOTA); Density functional theory (DFT); Natural bond orbital (NBO).

3.1. Introduction

For more than 30 years, nuclear imaging modalities have transformed the field of analytical medicine, particularly cardiology, neurology, and oncology.[1, 2] Early detection of disease, convenient deployment of therapies and easy access of the efficacy of a particular therapy[3], justifies the reason for the increase in the use of chelators in molecular imaging. Molecular imaging adequately allows visualizing, characterisation and evaluation of not only the molecular, cellular entities of the human body system but also the whole organs in the body, using some distinct imaging probes without interfering with biological functions.[4] Radiometals (e.g., ^{64}Cu, ^{89}Zr, ^{68}Ga, ^{86}Y and ^{99m}Tc) are used with imaging devices to provide labelling of biologically important macromolecules like proteins, peptides and antibodies, which are responsible for diagnosis or treating of various diseases.[5] Furthermore, the existence of biological targeting agents with a different range of half-lives, necessitates the need to produce new radionuclides with half-lives that match their biological properties.[6, 7]. For example, agents that can stay for a long period of time *in-vivo* can be labelled with gallium-68 (^{68}Ga: $t_{1/2}$ =68 min) or technetium-99m (^{99}Tc: $t_{1/2}$ = 6 h), while vectors that demand longer amounts of time to reach their target can be labelled with copper-64 (^{64}Cu: $t_{1/2}$ =12.7 h), yttrium-86 (^{86}Y: $t_{1/2}$ =14.7 h), indium-111 (^{111}In: $t_{1/2}$ =2.8 days), or zirconium-89 (^{89}Zr: $t_{1/2}$ = 3.2 days).[7-9] Before these isotopes can be used for a particular biological application, there is need to seclude the 'free' radiometal ions from aqueous solution, using chelators (ligands) to prevent the transchelation and hydrolysis processes[6]. Chelators are a crucial component of radiopharmaceutical procedures, that is used to form a tight, stable coordination complex by binding the radiometal ion firmly together so that it can be properly connected to a preferred molecular target *in vivo*[6].

66

Chelators that are commonly used to produce radiopharmaceuticals are bifunctional chelators (BFCs). As the name implies, BFCs are chelators that consist of one functional group covalently conjugated to a targeting vector (*e.g.* peptides, antibodies) and a chelating unit, which connects the radioisotope to form a complex. [6, 10, 11]

A plethora of studies have been performed on diverse chelators combined with different radiometal ions, for purpose of comparison or identifying a gold standard chelator for a particular radiometal. M.A. Deri *et al.*,[12] confirms that the use of [89]Zr with 3,4,3-(Li-1,2,-HOPO) is a superior replacement to Desferrioxamine (DFO) because, [89]Zr-HOPO is completely emptied from the body without any sign of demetalation. A research by Gabor Mate *et al.*, asserts that radiolabelling chelators NOPO and NOPA (1,4,7-triazacyclononane-7-acetic-1,4-bismethylenephosphinic acid) with ^{68}Ga exhibits a better labelling efficiency at room temperature and 95°C compared to NO2AP (1, 4, 7, triazacyclononane- 4,7 diacetic -1-[methylene(2-carboxyethl] phosphinic) acid.[13] Darpan and co-workers discovered that the macrocyclic bifunctional chelator that incorporates propylene cross-bridges is capable of forming strong complex with Cu.[14] A recent review on some features and current development in using antibodies to target radionuclides for tumor imaging and therapy was published by Kraeber-Bodere *et al.*[15]

The chelator under investigation in the present study is 1, 4, 7 triazacyclononane-1,4,7 triacetic acid (NOTA). NOTA, a hexadentate chelator is one of the most extensively investigated macrocyclic BFCs, utilized for the complexation of a large number of bi- and trivalent metal ions.[16] NOTA chelator has the geometry of the N_3O_3 coordination sphere and consists of three carboxylic (—COOH) functional arms (**Figure 1**).
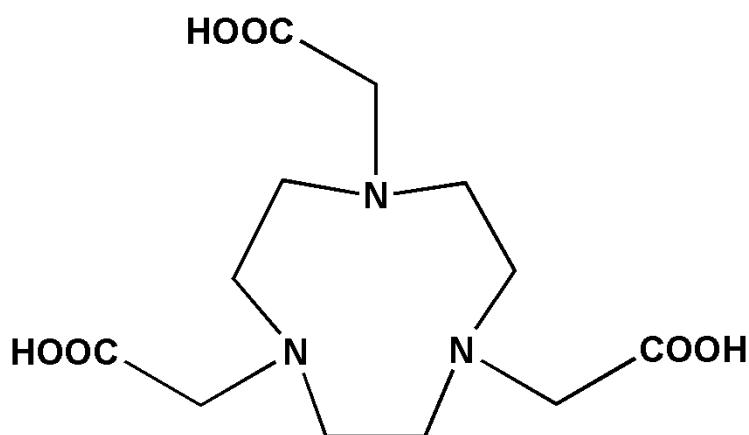
Figure 1. NOTA, 1, 4, 7-triazacyclononane-1,4,7- triacetic acid, coordination number = 6, N_3O_3.

All the aforementioned studies are experimental and investigation into the literature reveals that, there have been little or no theoretical investigations to evaluate the complexation of NOTA with radiometal ions. We have recently reported DFT studies of NOTA complexation with alkali metal ions[17]; it was concluded that there is a significant level of interaction between NOTA and alkali metals.

The present study however, is focused on evaluating the complexation of NOTA with selected radiometal ions (Cu^{2+}, Ga^{3+}, Sc^{3+} and In^{3+}) using Density Functional Theoretical (DFT). It should be noted that Cu^{2+} and Sc^{3+} are both transition metals whereas In^{3+} and Ga^{3+} are group III metals. The main objective of this study is to compare DFT results with experimental binding constants and to understand the molecular and electronic factors, which dictate the binding of NOTA with different radiometal ions; the information gained should then be used to aid in the selection of the radiometal and chelator for radiopharmaceuticals. A further objective is to ascertain whether or not there exists competition between radiometal and alkali metal ions, found in the body, upon complexation with NOTA.

3.2 Computational details

The Gaussian 09 program[18, 19] was used to perform all quantum chemical calculations. The Becke, 3-parameter, Lee-Yang-Parr (B3LYP)[20, 21] hybrid exchange correlation functional was used[22-25]. The 6-311+G(2d,2p)[22] basis set was used for NOTA and the DGDZVP basis set was applied for the radiometal ions for all complexes.

Interaction energies (E_{int}) between NOTA and the different metal ions were calculated using the following equation[26]:

$$E_{int} = E_{MOL1-MOL2} - E_{MOL2} - E_{MOL1} \tag{1}$$

MOL1 and MOL2 are components of the complex. For instance, in the NOTA—Cu^{2+} complex, MOL1 represents a NOTA molecule and MOL2 represents Cu^{2+}.
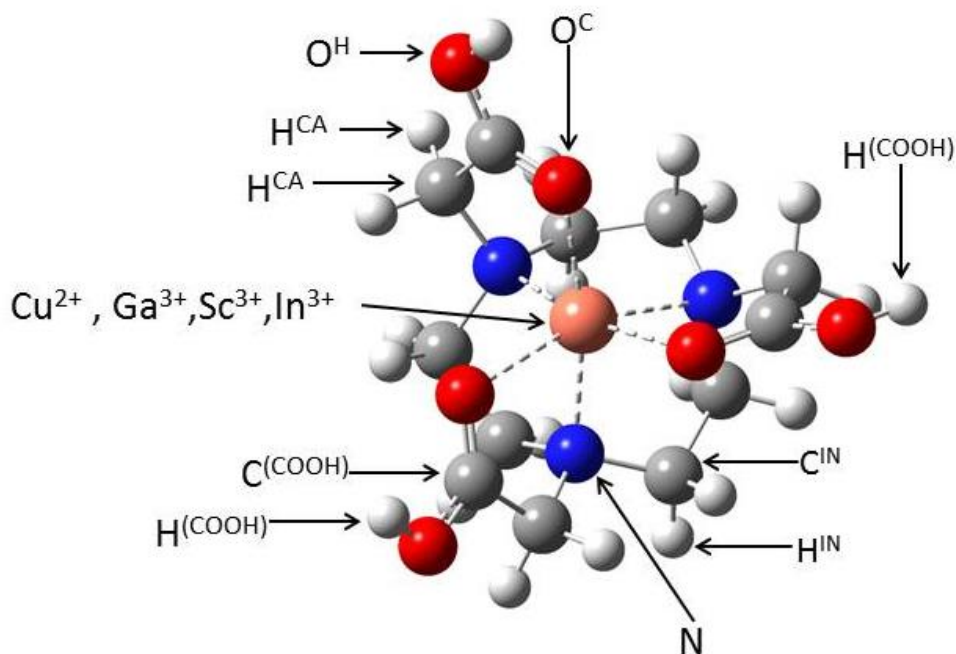
Figure 2 Conformation of the NOTA—radiometal ion complexes. The dotted lines in the diagrams indicate intermolecular distances between radiometal ions and hetero atoms that are in close proximity. H^{IN}, C^{IN}, N are hydrogen, carbon and nitrogen atoms in the ring, respectively. H_C^A are hydrogen atoms attached to the arm. $C^{(COOH)}$, $H^{(COOH)}$ are carbon and hydrogen atoms in the functional group. O^H is hydroxyl oxygen atoms and O^C is carbonyl oxygen atoms.

Relaxation energy measures the degree to which the ion affects the conformation of the NOTA[27-29] and was calculated by subtracting the complexation energy value (unrelaxed) from the interaction energy (relaxed). This process involves the geometry optimization of the cations and NOTA, the cation was separated from the NOTA molecule and two different situations were compared. First, the single point energy of the NOTA in that configuration was performed. Secondly, a further geometry optimization of the NOTA was carried out to allow the NOTA molecule to relax. The difference in energy between these two cases is the relaxation energy.

The solvent effect on the NOTA complexation with radiometal ions was evaluated using, the Polarizable Continuum Model (PCM) using integral equation-formalism polarizable continuum model (IEF-PCM). Thermodynamic properties (free energy, enthalpy, and entropy) were performed. The vibrational, translational and rotational contributions to entropy were calculated using normal mode analysis.[30] The second-order Fock matrix was presented to assess the donor-acceptor interaction in the system.[31, 32] A clearer picture of the electron delocalization between NOTA and the ions in the complexes; that is, the donor and acceptor orbitals, with the highest stabilization energy in term of E^2 from the second order

theory was investigated.[33] The second order perturbation energy E^2 of the occupied NBO (i) of an electron donor, which interacts with unoccupied NBO (j) of electron acceptor, is defined by the expression:

$$E^2 = \frac{qiF(i,j)^2}{\varepsilon_j - \varepsilon_i}$$ (2)

The energy values of the highest occupied molecular orbital (E_{HOMO}) and the lowest unoccupied molecular orbital (E_{LUMO}) of all the complexes were calculated. Several other electronic properties such as ionization potential (IP), electronic affinities (EA), hardness (η) and softness (S) were calculated. The ionisation potential (IP) is defined as the difference in ground state energy between the radical cationic (E_c) and the neutral species (E_n):

$$IP = E_C - E_n$$ (3)

The electron affinity (EA) is defined as the difference in ground state energy between the radical anionic (E_a) and its corresponding neutral species (E_n):

$$EA = E_a - E_n$$ (4)

The term "neutral" is actually the standard charge state, for instance, the charge state for Cu^{2+} is +2, and therefore the cationic and anionic species would have +3 and +1 charges, respectively.

The DFT-based structural features (chemical hardness, η, and softness, S) were obtained using the following equations[34, 35] :

$$\eta = 1/2(IP - EA)$$ (**5**)

$$S = \frac{1}{2\eta}$$ (**6**)

3.3 RESULT AND DISCUSSIONS

For a clearer data interpretation, the classification of atoms in the NOTA—radiometal ion complexes was made based on the position, connectivity of the atoms and different functional groups, which dictates their different chemical environment (**Figure 2**).

3.4 Interaction and relaxation energies

The interaction energies of the NOTA—radiometal ion complexes, basis set superposition error (BSSE) and relaxation energies for complexes are shown in this section to gain insight into the binding of NOTA with the radiometal ions. The interaction energy values provide us with a measure of the specific interactions that are important for the complexation of NOTA with radiometal ions. The interaction energies (E_{int}) of the complexes in vacuum and solvent, BSSE energy (E^{BSSE}) values and relaxation energies (E_{relax}) of the complexes are reported in **Table 1**.

Table 1: Interaction energy values of the complexes in vacuum and with implicit water solvation Basis set superposition error (BSSE) energy values and relaxation energy values of the complexes.

Complex	E_{int} kcal mol^{-1}	E_{relax} kcal mol^{-1}	E^{BSSE} kcal mol^{-1}
NOTA—Cu^{2+}	-410.37 [-201.2]	12.20	11.13
NOTA—Sc^{3+}	-639.18 [-142.51]	24.00	21.25
NOTA—In^{3+}	-655.51 [-365.34]	24.37	14.83
NOTA—Ga^{3+}	-810.59 [-507.35]	36.01	8.19

Brackets indicate interaction energy values of the complexes in solvent
Eint: Interaction energy; EBSSE: Basis sets superposition error

The interaction energy values follow the order NOTA—Ga^{3+}> NOTA—In^{3+}> NOTA—Sc^{3+}> NOTA—Cu^{2+}. The order of the interaction energies can be rationalized when we consider the different features of the ion. Ga^{3+} is in the same group as In^{3+}(group III) but is a smaller ion and, therefore, should have a stronger interaction. This is in agreement with results of our previous work, where it was found that the interaction strength of alkali metal ions increased up the group of the periodic table.[17] The difference in interaction energy between Sc^{3+} and Cu^{2+}, both transition metals, is related to their charge, Sc^{3+} being +3 has a stronger interaction than that of Cu^{2+} with a +2 charge.

The long range and dispersion interactions were taken into account by performing the geometry optimization of the complexes using the ωb97XD functionals and the interaction energies are also reported in **Table 4S**. The differences between interaction energies obtained by B3LYP and the ωB97XD functional may be due to different factors contributing to complexation the since dispersion should have a less significant effect on the reported, large interaction energies in **Table 1**. In other words, it is assumed that the observed range of E_{int} values are far stronger than intermolecular in nature and should be treated as bonding interactions. It is notable that the interaction energies obtained with both B3LYP and

ωb97XD functionals corresponds to the same trend. Thus, the results obtained with B3LYP are qualitatively similar.

3.4.1. Solvent effect

To gain an understanding of how NOTA—radiometal ion complexes behave in bulk water, the IEFPCM solvation model was used to calculate the interaction energies of the complexes in implicit water (**Table 1**). The results reveal that in the presence of water solvent, the interaction energy values of the systems are significantly lower than the interaction energy values in the absence of water. The interaction of NOTA—radiometal ions in water solvent is less favourable and less stable because the presence of water creates competitions and interferes with the stability of the system. It should be noted that in water medium Cu^{2+} has more attractive interaction energy than Sc^{3+}; this is because the solvation has less effect on the Cu^{2+}, which has a lower charge than Sc^{3+}. In both solvent and vacuum, Ga^{3+} has more negative interaction energy than all other complexes.

3.5 Thermodynamic properties

To gain an insight into the favorability of NOTA—ion complexation, the analysis of the enthalpies, Gibbs free energies, entropy and its individual contributions (translational, rotational, and vibrational) of the radiometal ions complexed with NOTA are discussed (Table 2).

Table 2: Enthalpies, Gibb free energies, entropy and its individual contributions, (translational, rotational, and vibrational) of the radiometal ions complexed with NOTA.

Complexes	ΔH kcal mol^{-1}	ΔG kcal mol^{-1}	ΔS cal mol^{-1} K^{-1}	ΔS_{Rot} cal mol^{-1} K^{-1}	ΔS_{Trans} cal mol^{-1} K^{-1}	ΔS_{Vib} cal mol^{-1} K^{-1}
NOTA—Cu^{2+}	-389.16	-376.352	-52.58	-0.52	-37.78	-14.28
NOTA—Sc^{3+}	-618.00	-605.08	-52.94	-0.34	-36.92	-15.68
NOTA—In^{3+}	-634.29	-622.38	-49.55	-0.27	-39.18	-10.11
NOTA—Ga^{3+}	-788.96	-773.87	-60.20	-0.60	-38.00	-21.60

ΔH values are significantly less negative than the interaction energy values (**Table 1**). The **Δ***H* and **Δ***G,* values for the complexes, follows the order; NOTA—Ga^{3+}> NOTA—In^{3+}> NOTA—Sc^{3+}> NOTA—Cu^{2+} matching the trend of the interaction energy values. The ΔS values are all negative as there is a loss in entropy due to two species, ion and NOTA, becoming one complex. The negative ΔS values act against the stability of the complexation of NOTA with radiometal ions considering the equation: $\Delta G = \Delta H - T\Delta S$. This is similar to the result of our previous study on the complexation of NOTA with alkaline metals.[17] The ΔS

values of NOTA—Cu^{2+} and NOTA—In^{2+} are similar but ΔS for NOTA—Ga^{3+} is considerably more negative (**Table 2**). The main factor that dictates the more negative ΔS value is the more negative vibrational contribution to the entropy change (**Table 2S**); this change should be related to the greater interaction strength as stronger vibrational modes will restrict the freedom of the complex to a greater extent.

Table 3. Thermodynamic properties for NOTA—ion complexes in solvent.

Complexes	ΔH (kcal mol^{-1})	ΔG (kcal mol^{-1})	ΔS (cal mol^{-1} K^{-1})	ΔS_{Rot} (cal mol^{-1} K^{-1})	ΔS_{Trans} (cal mol^{-1} K^{-1})	ΔS_{Vib} (cal mol^{-1} K^{-1})
NOTA—Cu^{2+}	-197.34	-186.19	-42.37	-0.43	-37.78	-4.16
NOTA—Sc^{3+}	-139.23	-124.61	-49.02	-0.23	-36.92	-11.87
NOTA—IN^{3+}	-361.94	-348.11	-46.42	-0.19	-39.17	-7.05
NOTA—Ga^{3+}	-492.01	-446.68	-50.20	-0.53	-38.00	-11.68

3.5.1. Solvent effect

The effect of implicit solvation on the enthalpy, Gibbs free energy and entropy was considered. **Table 3** shows that the ΔH and ΔG values of the complexes are significantly less negative than the ΔH and ΔG values of the complexes in the absence of water (**Table 2**); this predictably follows the behaviour of the interaction energies in water medium. The ΔS values are less negative in water medium than in vacuum and this is due to less negative vibrational contributions, which is caused by weaker NOTA—ion interactions.

Table 2S shows a decrease in vibrational entropy for free NOTA (difference of -9.52 cal mol^{-1} K^{-1}) upon solvation which account for the increase in ΔS_{Vib} of the complexes. The reason for the drastic change in vibrational entropy could be attributed to the fact that in vacuum, there is great repulsion between the carboxylic pendant arms, which causes the distance between these arms to be greater than in water medium where the repulsion between arms is reduced (**Figure 1S**). The larger distance between carboxylic arms may lead to an increase in structural flexibility of NOTA, and hence, an increase in entropy compared to the shorter distance that appears in water medium. These findings are similar to our previous study on the complexation of NOTA with alkali metal ions.[17]

3.6 Comparison of experimental and theoretical binding constants

The theoretical and experimental Gibbs free energies (ΔG_{theo} and ΔG_{exp}) of the selected complexes.[6, 7] are related to the experimental binding constants (logK$_{exp}$) using Vant Hoff equation (ΔG = -RTlnK). Experimental ΔG_{exp} and theoretical binding constants (logK$_{theo}$)

were calculated at the standard temperature (298K) and molar gas constant R (8.315 Jk^{-1}mol^{-1}). The experimental and theoretical values of both the Gibbs free energies and binding constants are reported in **Table 4**.

Table 4. Experimental and theoretical Gibbs free energies and binding constant values.

Complexes	ΔG_{theo} (kcal mol^{-1})	ΔG_{exp} (kcal mol^{-1})	logK$_{exp}$	logK$_{theo}$
NOTA—Cu^{2+}	-186.19	-12.78	21.65	314.62
NOTA—Sc^{3+}	-124.61	-9.75	16.57	210.57
NOTA—In^{3+}	-348.11	-15.51	26.28	588.23
NOTA—Ga^{3+}	-446.68	-18.35	31.04	754.78

It should be noted that although the experimental Gibbs free energies are significantly more negative than the theoretical ΔG values and the theoretical binding constant values are significantly higher that the experimental binding constants, both the experimental and theoretical values follow the same trend. This reveals an agreement between the experimental and theoretical results. The difference between the calculated binding constants (logK$_{theo}$) with experiment (logK$_{exp}$) might be due to the fact that at specific temperature, pH and solvent which affect the stability constants were not defined in our calculations.

3.7 Geometries and Interatomic distances

To further validate the theoretically optimized structures of NOTA—radiometal ion complexes with experimentally observed conformations, the geometries of the complexes were compared with experiment.[6, 7] This analysis is also helpful to assess the strength of intermolecular interactions between NOTA and radiometal ions.

The geometry of NOTA—Cu^{2+} was reported as distorted trigonal prism[36, 37], NOTA—Ga^{3+}, NOTA—Sc^{3+} and NOTA—In^{3+} as distorted octahedral.[38] [39-44] **Figures 3** and **4** show the geometries of NOTA—Cu^{2+} and NOTA—Ga^{3+} complexes. **Figure 3** shows distorted trigonal prism geometry for NOTA—Cu^{2+}, experiment (Cu^{a}) and theoretical (Cu^{b}), and **Figure 4** shows the distorted octahedral geometry for the rest of the complexes under study.
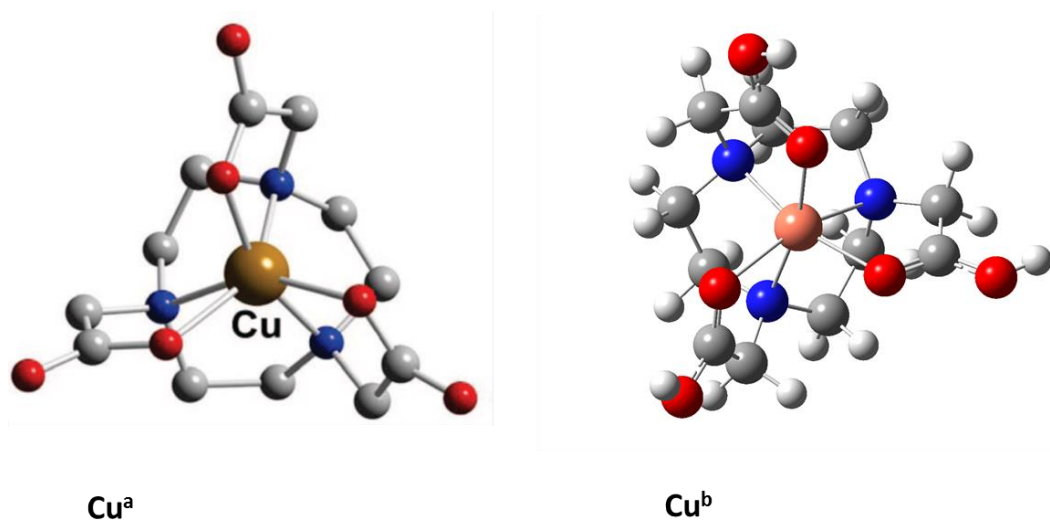
Figure 3. The distorted trigonal prism geometry of NOTA—Cu^{2+} complex. Cu^a indicates geometry from literature.[7] Cu^b indicates geometry from our geometry optimization.
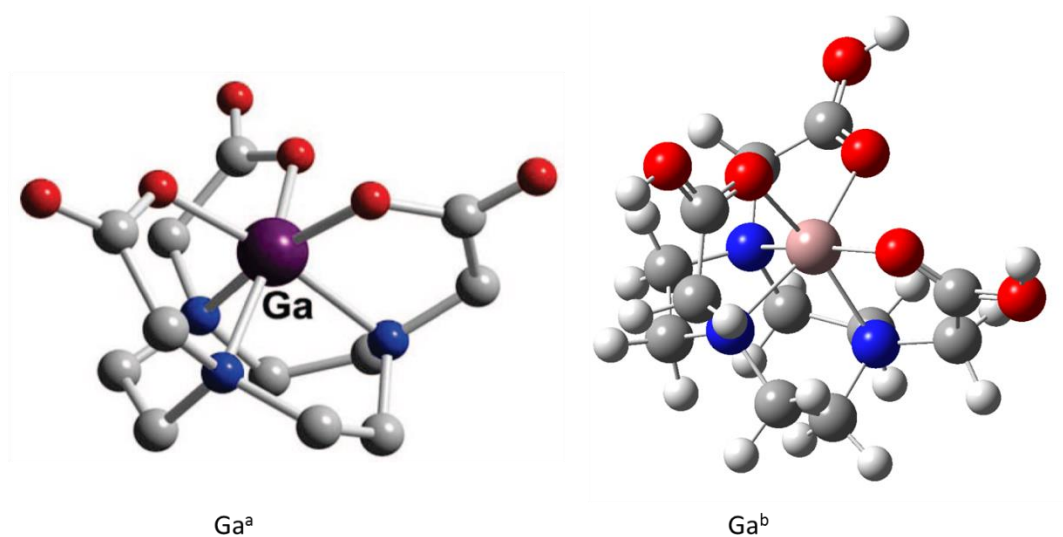
Figure 4. The distorted octahedral geometry of NOTA—Ga^{3+} complex. Ga^a indicates geometry from literature.[7] Ga^b indicates geometry from our geometry optimization.

It can be noticed that our results qualitatively match experimental crystal structure results. The short-range interatomic distances between the radiometal ions and NOTA's heteroatoms, in each optimized complex, were reported in **Table 5**. This analysis was performed to analyse and assess the level of intermolecular interaction between NOTA and radiometal ions. Heteroatom-ion distances lower than 3.0 Å were considered for all complexes. The average interatomic distances were recorded for all the complexes.

Table 5. The interatomic distances between radiometal ions (Cu^{2+}, Ga^{3+}, Sc^{3+} and In^{3+}) and NOTA's heteroatoms in the optimized structure at B3LYP/6-311G+(2d, 2p) and DGDZVP basis sets. O^C and N are presented in **Figure 2**. Heteroatom-ion distances ≤ 3 Å were considered as the short-range interatomic distances for the selected complexes.

Complex	O^C —ion (≤ 3Å)	N—ion (≤ 3Å)
NOTA—Cu^{2+}	2.13 [2.15]	2.16 [2.15]
NOTA—Sc^{3+}	2.09 [2.15]	2.34 [2.36]
NOTA—In^{3+}	2.18 [2.19]	2.33 [2.31]
NOTA—Ga^{3+}	2.01 [2.01]	2.11 [2.10]

Brackets indicate bond distances between heteroatoms and radiometal ions in complexes in water.

NOTA—Ga^{3+} complex with the highest interaction energy (-810.59 kcal mol^{-1}) has the shortest ion-heteroatom distances (**Table 5**). It should be noted that, the close proximity of the heteroatom—ions (O^C and N) of NOTA to the ions, after optimization, and the high negative charge (see "Natural Bond Orbital (NBO) analysis" section, **Table 6**) indicate that both oxygen and nitrogen atoms are important binding elements during the complexation of NOTA with radiometal ions. This observation is similar to our previous study of NOTA complexation with alkali metals[17]. It is notable that the proximity of the heteroatoms to the ions varies considerably; the nitrogen atom of the NOTA—Cu^{2+} complex is closer to the ion than the nitrogen of NOTA—Sc^{3+} even though the NOTA—Cu^{2+} complex is less stable than the NOTA—Sc^{3+}. Furthermore, the oxygen atoms of NOTA are the farthest in distance to the Sc^{3+} ion regardless of the fact that it is more stable than NOTA—Cu^{2+} and NOTA—Sc^{3+} complexes; this can be attributed to the larger size of In^{3+}, which is a row lower in the periodic table than the other ions. It should be noted that the interatomic distances between ions and heteroatoms in solvent are similar to the distances in vacuum for all the complexes.

To evaluate the dispersion effect on the geometric parameters, the interatomic distances using ωB97XD functional are reported in **Table 5S**. It can be observed that the average distances between the hetero-atoms are shorter with ωB97XD than with B3LYP; this could be due to the inclusion of dispersion contributions in ωB97XD within the selected complexes.

3.8. Natural bond orbital (NBO) analysis

The charge transfer within the chelator-ion complexes is of importance because it influences the interaction of radiometal ions with NOTA. Charge transfer can be investigated using Natural bond orbital (NBO) analysis through monitoring the atom charges, change of atom charges upon complexation and second order perturbation theory[45].

Natural atomic charge estimation plays a role in the application of quantum mechanical calculations for molecular systems because atomic charge affects the electronic structure, dipole moment and other properties of the molecule[31]. Charge distribution within the NOTA complexes and from NOTA to the radiometal ions is reported in **Table 6**. The atoms in all the complexes have been categorized into groups (**Figure 2**) and the average natural atomic charges have been reported.

The NBO analysis shows that for all the complexes, there are considerable changes in charges for the cations after complexation with radiometal ions. The complexes, with initial charge of +2 for Cu^{2+} and +3 for Sc^{3+}, In^{3+} and Ga^{3+}, before complexation, become less electron deficient after complexation. The charges of Cu^{2+}, Sc^{3+}, In^{3+} and Ga^{3+}, after complexation, are 1.02, 1.93, 2.05 and 1.89, respectively. The observed charge reduction, particularly for In^{3+} and Ga^{3+}, which are in the same group of the periodic table, could be a key factor in the stronger interaction energies observed in **Table 1**.

Furthermore, for all complexes, N, O^{C}, C^{IN} and C^{A} are more negatively charged in the complexed NOTA than in the free NOTA. Conversely, H^{IN}, H^{CA}, C^{COOH} and H^{COOH} are more positively charged in the complexed NOTA than in the free NOTA. This is an indication that there was electron density transfer from NOTA to the radiometal ions upon complexation (**Table 6**); this will be addressed in more detail using second order perturbation theory in the next section.

Table 6. Natural atomic charges (NAC) of atoms in optimized structure of NOTA complex with radio metals and NOTA before complexation at B3LYP/6-311G+(2d,2p) and DGDZVP basis sets.

Atoms groups	Avg. of all atoms in group NOTA—Cu^{2+}	Avg. of all atoms in group NOTA—Sc^{3+}	Avg. of all atoms in group NOTA—In^{3+}	Avg. of all atoms in group NOTA—Ga^{3+}	Free NOTA
Ions	1.02	1.93	2.05	1.89	Not applicable
N (3)	-0.62	-0.653	-0.645	-0.654	-0.57
O^H (3)	-0.56	-0.56	-0.57	-0.56	-0.71
O^C (3)	-0.62	-0.72	-0.71	-0.70	-0.61
C^{IN} (6)	-0.19	-0.19	-0.20	-0.19	-0.18
H^{IN} (12)	0.22	0.24	0.22	0.24	0.19
C^A (3)	-0.28	-0.27	-0.29	-0.28	-0.26
H^{CA} (6)	0.25	0.27	0.27	0.28	0.22
C^{COOH} (3)	0.85	0.89	0.87	0.88	0.81
H^{COOH} (3)	0.52	0.56	0.54	0.54	0.49

The numbers in parentheses represent the number of atoms within the specific group shown in **Figure 2**.

3.9. Second perturbation stabilization energies

The second-order Fock matrix was presented to evaluate the donor–acceptor interactions in the system.[31, 46]. The larger the stabilization energy(E^2), the greater the charge transfer between electron donors and electron acceptors.[47-49] The second-order perturbation theory analysis for all the complexes shows the charge transfer within NOTA—ion complexes (**Table 7**).

The observed depletion of NAC charges of the ions (**Table 6**) should be attributed to charge transfer from NOTA to the ions. This was observed for all NOTA—ion complexes where the highest stabilization energy values for electron transfer from NOTA to ions are from the lone pair (LP) of the nitrogen atom of NOTA to the LP* of the radiometal ions; this follows the order, NOTA—Ga^{3+}>NOTA—In^{3+}>NOTA—Sc^{3+}>NOTA—Cu^{2+}, which matches that of the interaction energy values (**Table 1**). There are charge transfers from LP orbitals of O^C atoms to LP* of the ions but these are less evident than the transfer from the LP of nitrogen atoms.

It is noticed that the presence of different ions within the complexes can affect the charge transfer within NOTA. The highest E^2 values within NOTA are electron donations from LP orbitals in O^H to the antibonding acceptor σ*(C-O^C). The stabilization energy follows the order: NOTA—Ga^{3+} $\approx$ NOTA—Sc^{3+} $\approx$ NOTA—In^{3+} > NOTA—Cu^{2+}; this is related to the contribution of charge for +3 charge ions compared to the divalent Cu^{2+} ion.

The result of the second perturbation theory emphasises the fact that electron transfer from O^C and N atoms of NOTA to the radiometal ions in the complexes is prevalent. A similar observation was made from the our previous works where we evaluated the interaction between diazacrown and the sodium cation [26] and the interaction between NOTA and alkali metal ions[17].

We can now provide a description of charge transfer (the highest stabilization energy values) that occurs from the NOTA molecule to the cations and this is represented in **Figure 5**, where arrows point the path of charge transfer.

There is electron movement, from O^H to the carbonyl bond followed by the direct transfer of electron from the NOTA oxygen atoms to the metal ions in the complexes and also electron from C^A, followed by a direct transfer from nitrogen atoms to the metal ions in the complexes.

Table 7. The second-order perturbation energies, E^2 (kcal/mol), corresponding to the most important charge transfer interaction (donor →acceptor) within NOTA—radiometal ions complexes obtained by B3LYP/6-311+G(2d,2p) level of theory.

Complex	Donor	Acceptor	E^2(kcal/mol)
From NOTA to ions			
NOTA—Cu^{2+}	LP(N)LP	LP*(Cu^{2+})	11.50
	LP(O)	LP*(Cu^{2+})	10.11
	σ(N-C)	LP*(Cu^{2+})	12.84
NOTA—Sc^{3+}	LP(N)	LP*(Sc^{3+})	31.90
	LP(O)	LP*(Sc^{3+})	11.68
	σ(N-C)	LP*(Sc^{3+})	13.38
NOTA—In^{3+}	LP(N)	LP*(In^{3+})	40.02
	LP(O)	LP*(In^{3+})	13.26
	σ(N-C)	LP*(In^{3+})	16.32
NOTA—Ga^{3+}	LP(N)	LP*(Ga^{3+})	76.65
	LP(O)	LP*(Ga^{3+})	24.23
	σ(N-C)	LP*(Ga^{3+})	8.49
Within NOTA			
NOTA—Cu^{2+}	LP (O)	σ*(C-O)	31.87
NOTA—Sc^{3+}	LP (O)	σ*(C-O)	57.02
NOTA—In^{3+}	LP(O)	σ*(C-O)	56.38
NOTA—Ga^{3+}	LP (O)	σ*(C-O)	57.03
NOTA	LP(O)	σ*(C-O)	43.46
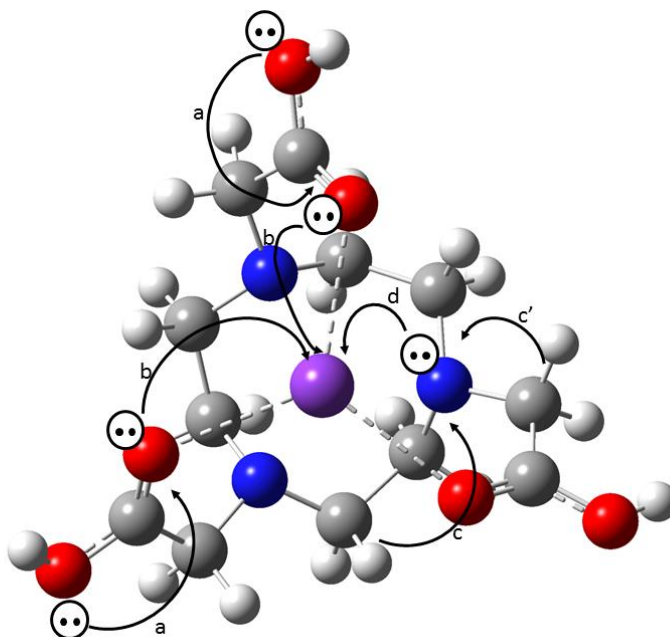
Figure 5. Description of electrons transfers shown in NBO analysis. The curved arrows (**a**, **b**, **c**, **c´** and **d**) depict the direction of charge transfer; **a**: LP (O) → σ* (C=O), **b**: LP (O) → LP* (Ion), **c**: σ (C-H) ring → σ (N-C), **c´**: σ (C-H) arm → σ (N-C), **d**: LP (N) → LP* (Ion).

3.10. Analysis of ^{1}H NMR chemical shifts

To gain a better understanding of the chemical environment of different fragments involved in the NOTA complexed with radiometal ions, the (^{1}H NMR) in vacuum and water media was studied and compared with the experimentally measured proton NMR chemical shifts for the NOTA―Ga^{3+} and NOTA―In^{3+} complexes[50]. Experimental and theoretical ^{1}H chemical shifts (δ) are given in **Table 8** for a set of NOTA― radiometal ion complexes.

Table 8: Proton NMR chemical shifts (δ) of NOTA—Ga^{3+} and NOTA—In^{3+} complexes in vacuum and water media.

Proton	δ_{Theo} Ga^{3+} (ppm)	δ_{Exp} Ga^{3+} (ppm)	δ_{Theo} In^{3+} (ppm)	δ_{Exp} In^{3+} (ppm)
G1	9.54 [9.29] NAC=0.54	Not reported	9.46 [9.09] NAC=0.54	Not reported
G2	4.54 [4.57] NAC=0.28	3.88 Δ_{vac} =- 0.66 Δ_{solv} = -0.69	4.514 [4.511] NAC=0.27	3.70 Δ_{vac} = 0.81 Δ_{solv} = 0.81
G3	4.05 [3.90] NAC=0.26	3.23 Δ_{vac} = -0.82 Δ_{solv} = -0.67	3.99 [3.80] NAC=0.25	3.07 Δ_{vac} = 0.92 Δ_{solv} = -0.73
G4	3.47 [3.67] NAC=0.25	Not reported	3.65 [3.60] NAC=0.25	Not reported
G5	3.62[3.68] NAC=0.24	3.51 Δ_{vac} = -0.11 Δ_{solv} = -0.17	3.64 [3.67] NAC=0.25	3.24 Δ_{vac} = -0.4 Δ_{solv} = -0.43
G6	3.03 [3.20] NAC=0.23	Not reported	2.92 [3.18] NAC=0.22	Not reported

δ_{Exp} are experimental results[50]. Δ_{vac} and Δ_{solv} indicate the difference between the experimental and theoretical chemical shift, in vacuum and solvent, respectively.

To compare our theoretical results with experiment, we performed the ^{1}H NMR calculations in vacuum and water media (**Table 8**). This comparison is particularly informative, as it has been shown that the hydrogen atoms are source of electron density for charge transfer from NOTA to ions, which should be the driving force for chemical shift changes.

In most cases, the theoretical chemical shift values follows a decreasing order (NOTA—Ga^{3+} > NOTA—In^{3+}) down group III of the periodic table. The decreasing effect is due to the ions having a deshielding effect on the protons of the NOTA that are in close proximity. The decrease in the δ values is consistent with the decrease in the electron withdrawing effect of the ions, which cause a decline in the NAC values down the group. It is observed that the theoretical δ values are in reasonable agreement with the experiment (differences are less than 1ppm), which confirms the suitability of the applied DFT functional and basis set. Furthermore, there is no significant difference between the ^{1}H NMR in the vacuum and the water.

The proton in the complexes has been characterized (G1 to G6) based on the different theoretical δ. This classification highlighted the fact that each group operates in different chemical environments, which could be identified in the experiment. This motivated a measurement of the theoretical chemical shifts for all proton groups.

For both Ga^{3+} and In^{3+} complexes, carboxyl protons (G1) are identified as the protons with the highest chemical shift values and correspondingly the most positive atomic charges, followed by the proton of the methylene group ($-CH_2-$) within the pendant arms (G2); this ranking of chemical shift values are in agreement with experimental results. The G3 to G6 are protons in the ring with the same functional group but different chemical environments. It is observed that the protons in G3 have higher chemical shift values than the other protons in the ring because G3 protons are located facing each other. Another factor that dictates the chemical shift, is the chemical environment of protons in relation to other atoms within NOTA. This is demonstrated by the fact that the ranking for the free NOTA is exactly the same as for the complexed NOTA (**Table 3S**). G2, G3 and G6 become less deshielded upon complexation, while G1, G4 and G5 become more deshielded; this is in contrast to the natural atomic charge of all groups (G1 to G6), which are more positive upon complexation, suggesting two different chemical environments that affect chelation. First, the inductive effect, through charge transfer from σ(C-H) ring to the σ(N-C), as illustrated in **Figure 5**, could be responsible for the observed trend in natural atomic charges. Secondly, short-range coupling could probably affect the chemical shift values. It is noted that our observations regarding ^{1}H NMR results for NOTA—radiometal ion complexes agree with those of our recent study where we evaluated the ^{1}H NMR on NOTA—alkali metal ions.[17]
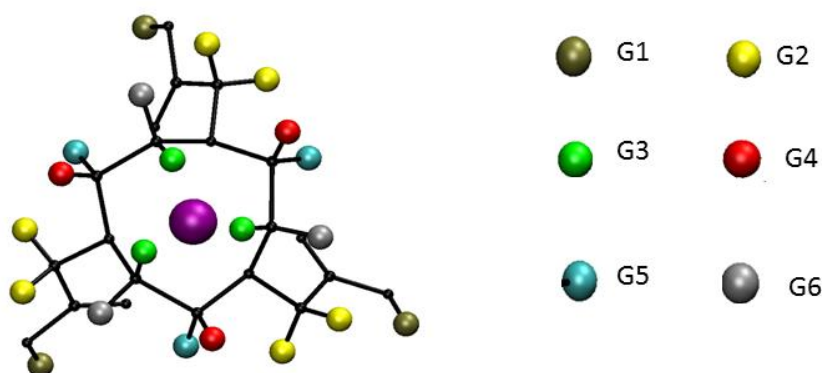

Figure 6 NOTA—radiometal ion complex based on the intensity of the different chemical shifts. G indicates the different groups of hydrogen. Hydrogen atoms with the same colour code belong to the same chemical environment.

3.11 Analysis of the frontier molecular orbital

Frontier molecular orbitals are the highest occupied molecular orbitals (HOMO) and the lowest unoccupied molecular orbitals (LUMO). The energy difference between the two frontier molecular orbitals ($\Delta E_{LUMO-HOMO}$), is referred to as the HOMO-LUMO gap and is used in predicting the reactivity and stability of transition metal complexes.[51][85][86] A highly polarizable molecule generally is highly chemically reactive and possesses low kinetic stability.[52,53] The energy eigenvalue of HOMO (E_{HOMO}) is related to the ionization potential ($IP = E_c - E_n$) as it is the outer orbital containing electrons that are donated while LUMO can be considered to be the innermost orbital with free places to accept electrons and, therefore, its energy is related to electron affinity ($EA = E_a - E_n$).[54]

To evaluate the stability of the complexation, the HOMO and LUMO energy eigenvalue (E_{HOMO}, E_{LUMO}) of the NOTA—radiometal ion complexes, and individual components in the complexes, are presented in **Table 9**.

Table 9: The E_{HOMO}, E_{LUMO} and $\Delta E_{HOMO-LUMO}$ of the optimized NOTA—ion structures at B3LYP/6-311+G(d,p) and DGDZVP level of theory.

Complex/ion	E_{HOMO} (eV)	E_{LUMO} (eV)	$\Delta E_{LUMO-HOMO}$ (eV)
Cu^{2+}	-32.88	-28.25	4.62
Sc^{3+}	-68.58	-30.58	37.99
In^{3+}	-51.89	-31.31	20.57
Ga^{3+}	-57.97	-35.64	22.33
NOTA	-7.80	-2.86	4.93
NOTA—Cu^{2+}	-3.70	-3.62	0.07
NOTA—Sc^{3+}	-10.47	-4.49	5.98
NOTA—In^{3+}	-10.48	-4.21	6.27
NOTA—Ga^{3+}	-9.66	-3.88	5.78

The E_{HOMO} energy value of the individual radiometal ions follows the order; $Sc^{3+} > Ga^{3+} > In^{3+} > Cu^{2+}$. The $\Delta E_{LUMO-HOMO}$ for free metal ions are significantly higher than the complexes. It is noted that the presence of the ion, in the NOTA complexes, causes E_{HOMO} and E_{LUMO} values to be more negative and $\Delta E_{LUMO-HOMO}$ values to become greater; this implies that the ions cause increases in the ability of NOTA to both donate and accept electrons; this effect follows the order, NOTA—$In^{3+} >$ NOTA—$Sc^{3+} >$ NOTA—$Ga^{3+} >$ NOTA—Cu^{2+}.

It noted that the ΔE_{HOMO}, ΔE_{LUMO} and $\Delta E_{LUMO-HOMO}$ values for free Cu^{2+} and complexes are significantly lower than other complexes. This is a result of the odd number of electron or

unpaired electrons occupying the orbital which makes the orbitals SOMO (singly occupied molecular orbitals).

When we compare down the group III of the periodic table (Ga^{3+} vs In^{3+}), more negative ΔE_{HOMO} and a lower $\Delta E_{LUMO-HOMO}$ value was observed for Ga^{3+} with the smaller ionic radius than In^{3+}. In the case of Sc^{3+} and Cu^{2+}, the ion charge plays the greater role; that is, the more charge of Sc^{3+} than Cu^{2+} brings more negative ΔE_{HOMO} and a lower $\Delta E_{LUMO-HOMO}$ value. Judging by the $\Delta E_{LUMO-HOMO}$ energy gap, the stability of NOTA— radiometal ions follows the order; NOTA—In^{3+} > NOTA—Sc^{3+} > NOTA—Ga^{3+} > NOTA—Cu^{2+}.

3.11.1 Conceptual DFT-based properties

Various chemical reactivity descriptors have been proposed for understanding different facets of pharmacological sciences including drug design and possible eco-toxicological attributes of drug molecules[55]. Density Functional Theory can be used to calculate the global reactivity descriptors like chemical potential, electronegativity, hardness, softness and electrophilicity index .[56] Ionization potential describes the capability of an atom or molecule to donate electrons while electron affinity describes the capability of an atom or molecule to attract electrons. Chemical hardness, describes the resistance to modification in electron distribution, and correlates with the stability of the chemical system. The inverse of the hardness is expressed as the global softness and correlated with the reactivity of the chemical system.

The calculated DFT-based quantities such as electron affinity (**EA**), ionization potential (**IP**), chemical hardness ($\boldsymbol{\eta}$) and softness (*S*) for the complexes are presented in **Table 10**.

For the free ions, the more negative EA, greater IE and chemical hardness was observed for Ga^{3+} than In^{3+} with a larger ionic radius. As for divalent Cu^{2+} compared with the trivalent ions (Ga^{3+}, Sc^{3+} and In^{3+}), the less negative EA, smaller IE and chemical hardness was obtained for Cu^{2+}.

The DFT based parameters revealed a chemically soft nature of NOTA compared to the ions and consequently, the complexation of NOTA with the ions should have a considerable effect, which depends on specific ion in question. Indeed, in all cases, there is a significant increase in chemical hardness upon complexation.

It is evident that the IP and hardness values of all trivalent complexes are similar and higher than the divalent NOTA—Cu^{2+} complex. Moreover, NOTA—Ga^{3+} complex has a slightly more negative EA and hardness values than NOTA—In^{3+} complex; this could be attributed to the smaller ionic radius of Ga^{3+} than In^{3+} and is consistent with the result from our previous

study on the interaction of alkali metal ions with NOTA[17]. The changes in EA, IP, softness and hardness provide trends in complex stability that are related to the trends in interaction energies and thermodynamic properties (**Tables 1** and **2**).

Table 10. DFT-based quantities for radiometal ions (Cu^{2+}, Ga^{3+}, Sc^{3+} and In^{3+}) complexes with NOTA, calculated at B3LYP/6-311+G(2d,2p) level of theory.

System	EA (eV)	IP (eV)	η (eV)	S (eV)
Cu^{2+}	-21.06	45.46	33.26	0.015
Sc^{3+}	-25.73	76.22	50.97	0.01
In^{3+}	-27.75	59.38	43.56	0.011
Ga^{3+}	-31.45	68.76	50.11	0.010
NOTA	0.60	7.11	3.26	0.15
NOTA—Cu^{2+}	-8.81	15.73	12.27	0.04
NOTA—Sc^{3+}	-10.74	20.28	15.51	0.032
NOTA—In^{3+}	-9.82	20.13	14.98	0.033
NOTA—Ga^{3+}	-10.17	20.51	15.34	0.033

3.12. Implication of results

The outcome of the present study revealed a significant level of intermolecular interactions between radiometal ions and NOTA. The electronic structure properties, such as interaction energies, frontier molecular orbitals, ^{1}H NMR chemical shifts, chemical hardness, ionization potential and electron affinity values, offer an explanation for the stability of NOTA—radiometal ion complexes. It should be noted that the structural stability of chelator—ion complexes is one of the factors that influences the radiolabelling efficiency[6]. This study shows that the DFT-based electronic structure calculations can be applied to rank the ions towards finding the optimal match between ions and a specific chelator. According to the experimentally reported binding constants and obtained quantum chemical parameters calculated for NOTA—radiometal ion complexes it is observed that, amongst the radiometal ions under investigation, Ga^{3+} is an optimal match for NOTA chelator for radiopharmaceuticals. Following our previous study on the complexation of NOTA with alkali metal ions[17] and comparing the interaction energy values of the NOTA—radiometal ion complexes with that of the interaction energy values of NOTA—alkali metal ions complexes[17] it can be stated that alkali metal might constitute little or no competition with radiometal ions (Cu^{2+}, Ga^{3+}, Sc^{3+}, In^{3+}) and, therefore, cannot be displaced from NOTA chelator during complexation *in vivo*.

3.13. Conclusions

Density Functional Theory (DFT) using B3LYP functional and 6-311G+(2d,2p)/DGDZVP basis sets was been employed to investigate interactions that occur in the complexation process of NOTA with radiometal ions (Cu^{2+}, Ga^{3+}, Sc^{3+} and In^{3+}). Our study reveals that NOTA—Ga^{3+} complex is more stable than the other complexes (NOTA—Cu^{2+}, NOTA—Sc^{3+} and NOTA—In^{3+}) resulting in more negative interaction and relaxation energies, the close proximity of the hetero-atoms after geometry optimization and higher electron charge transfer from NOTA to the ions. The observed order of interaction energies is in good agreement with the experimental ranking in terms of the measured binding constants (section 3.6). Furthermore, the obtained theoretical ^{1}H NMR chemical shifts of NOTA, in vacuum and water media and the structural geometries of the complexes, were in good agreement with experiment. The δ values and, therefore, the deshielding effect of the ions on the protons of NOTA is related to natural atomic charge exchange within the complexes. Overall, the interaction energies both in vacuum and water, relaxation energies, bond distances, NBO and chemical shift analysis, DFT-based reactivity-related properties, including chemical hardness and softness, revealed a significant level of interaction between NOTA and radiometal ions. The findings of our study help ascertain the fact that alkali metal will not be competition with radiometal ions during complexation with NOTA chelator. Furthermore, Ga^{3+} ion is probably the best match for NOTA chelator for radiopharmaceutical purpose.

REFERENCES

1.   Strauss, H. W., Mariani, G., Volterrani, D., and Larson, S. M. (2012) *Nuclear Oncology: Pathophysiology and Clinical Applications*, Springer Science & Business Media.

2.   Heller, G. V., and Hendel, R. C. (2012) *Handbook of Nuclear Cardiology: Cardiac SPECT and Cardiac PET*, Springer Science & Business Media.

3.   Bartholomä, M. D., Louie, A. S., Valliant, J. F., and Zubieta, J. (2010) Technetium and gallium derived radiopharmaceuticals: comparing and contrasting the chemistry of two important radiometals for the molecular imaging era, *Chemical reviews 110*, 2903-2920.

4.   Pimlott, S. L., and Sutherland, A. (2011) Molecular tracers for the PET and SPECT imaging of disease, *Chemical Society Reviews 40*, 149-162.

5.   Pandey, M. K., Engelbrecht, H. P., Byrne, J. F., Packard, A. B., and DeGrado, T. R. (2014) Production of 89 Zr via the 89 Y (p, n) 89 Zr reaction in aqueous solution: effect of solution composition on in-target chemistry, *Nuclear medicine and biology 41*, 309-316.

6.   Price, E. W., and Orvig, C. (2014) Matching chelators to radiometals for radiopharmaceuticals, *Chemical Society Reviews 43*, 260-290.

7.   Wadas, T. J., Wong, E. H., Weisman, G. R., and Anderson, C. J. (2010) Coordinating radiometals of copper, gallium, indium, yttrium, and zirconium for PET and SPECT imaging of disease, *Chemical reviews 110*, 2858-2902.

8.   Wadas, T., Wong, E., Weisman, G., and Anderson, C. (2007) Copper chelation chemistry and its role in copper radiopharmaceuticals, *Current pharmaceutical design 13*, 3-16.

9.   Zeglis, B. M., and Lewis, J. S. (2011) A practical guide to the construction of radiometallated bioconjugates for positron emission tomography, *Dalton Transactions 40*, 6168-6195.

10.   Bartholomä, M. D., Gottumukkala, V., Zhang, S., Baker, A., Dunning, P., Fahey, F. H., Treves, S. T., and Packard, A. B. (2012) Effect of the prosthetic group on the pharmacologic properties of 18F-labeled rhodamine B, a potential myocardial perfusion agent for positron emission tomography (PET), *Journal of medicinal chemistry 55*, 11004-11012.

11.   Pruszyński, M., Bilewicz, A., and Zalutsky, M. R. (2008) Preparation of Rh [16aneS4-diol] 211At and Ir [16aneS4-diol] 211At complexes as potential precursors for astatine radiopharmaceuticals. Part I: Synthesis, *Bioconjugate chemistry 19*, 958-965.

12.   Deri, M. A., Ponnala, S., Zeglis, B. M., Pohl, G., Dannenberg, J., Lewis, J. S., and Francesconi, L. C. (2014) Alternative chelator for 89Zr radiopharmaceuticals: radiolabeling and evaluation of 3, 4, 3-(LI-1, 2-HOPO), *Journal of medicinal chemistry 57*, 4849-4860.

13.   Máté, G., Šimeček, J., Pniok, M., Kertész, I., Notni, J., Wester, H.-J., Galuska, L., and Hermann, P. (2015) The Influence of the Combination of Carboxylate and Phosphinate Pendant Arms in 1, 4, 7-Triazacyclononane-Based Chelators on Their 68Ga Labelling Properties, *Molecules 20*, 13112-13126.

14.   Pandya, D. N., Bhatt, N., An, G. I., Ha, Y. S., Soni, N., Lee, H., Lee, Y. J., Kim, J. Y., Lee, W., and Ahn, H. (2014) Propylene cross-bridged macrocyclic bifunctional chelator: A new design for facile bioconjugation and robust 64cu complex stability, *Journal of medicinal chemistry 57*, 7234-7243.

15.   Kraeber-Bodéré, F., Rousseau, C., Bodet-Milin, C., Mathieu, C., Guérard, F., Frampas, E., Carlier, T., Chouin, N., Haddad, F., and Chatal, J.-F. (2015) Tumor immunotargeting using innovative radionuclides, *International journal of molecular sciences 16*, 3932-3954.

16.   Förster, C., Schubert, M., Pietzsch, H.-J., and Steinbach, J. (2011) Maleimido-Functionalized NOTA Derivatives as Bifunctional Chelators for Site-Specific Radiolabeling, *Molecules 16*, 5228-5240.

17.   Adeowo, F. Y., Honarparvar, B., and Skelton, A. A. (2016) The interaction of NOTA as a bifunctional chelator with competitive alkali metal ions: a DFT study, *RSC Advances 6*, 79485-79496.

18.   Behjatmanesh-Ardakani, R. (2015) NBO–NEDA, NPA, and QTAIM studies on the interactions between aza-, diaza-, and triaza-12-crown-4 (An-12-crown-4, n= 1, 2, 3) and Li+, Na+, and K+ ions, *Computational and Theoretical Chemistry 1051*, 62-71.

19.   M. J. Frisch, G. W. T., H. B. Schlegel, G. E. Scuseria, , M. A. Robb, J. R. C., G. Scalmani, V. Barone, B. Mennucci, , G. A. Petersson, H. N., M. Caricato, X. Li, H. P. Hratchian, , A. F. Izmaylov, J. B., G. Zheng, J. L. Sonnenberg, M. Hada, , M. Ehara, K. T., R. Fukuda, J. Hasegawa, M. Ishida, T. Nakajima, , Y. Honda, O. K., H. Nakai, T. Vreven, J. A. Montgomery, Jr., , J. E. Peralta, F. O., M. Bearpark, J. J. Heyd, E. Brothers, , K. N. Kudin, V. N. S., R. Kobayashi, J. Normand, , K. Raghavachari, A. R., J. C. Burant, S. S. Iyengar, J. Tomasi, , M. Cossi, N. R., J. M. Millam, M. Klene, J. E. Knox, J. B. Cross, , V. Bakken, C. A., J. Jaramillo, R. Gomperts, R. E. Stratmann, , O. Yazyev, A. J. A., R. Cammi, C. Pomelli, J. W. Ochterski, , R. L. Martin, K. M., V. G. Zakrzewski, G. A. Voth, , P. Salvador, J. J. D.,

S. Dapprich, A. D. Daniels, , O. Farkas, J. B. F., J. V. Ortiz, J. Cioslowski, , and and D. J. Fox. (2009) Gaussian 09, Revision A.02,, Gaussian Inc., Wallingford CT.

20. Lee C., Yang W., and R.G, P. (1988) Development of Colle-Salvetti correlation-energy formula into a functional of electron density, *Phsical Review B 37*, 785-789.

21. Becke, A. D. (1993) Densityfunctional thermochemistry. III. The role of exact exchange, *J. Chem. Phys. 98*, 5648.

22. Petersson, a., Bennett, A., Tensfeldt, T. G., Al-Laham, M. A., Shirley, W. A., and Mantzaris, J. (1988) A complete basis set model chemistry. I. The total energies of closed-shell atoms and hydrides of the first-row elements, *The Journal of chemical physics 89*, 2193-2218.

23. Hay, P. J., and Wadt, W. R. (1985) Ab initio effective core potentials for molecular calculations. Potentials for the transition metal atoms Sc to Hg, *The Journal of Chemical Physics 82*, 270-283.

24. Wadt, W. R., and Hay, P. J. (1985) Ab initio effective core potentials for molecular calculations. Potentials for main group elements Na to Bi, *The Journal of Chemical Physics 82*, 284-298.

25. Hay, P. J., and Wadt, W. R. (1985) Ab initio effective core potentials for molecular calculations. Potentials for K to Au including the outermost core orbitals, *The Journal of Chemical Physics 82*, 299-310.

26. Skelton, A., Fried, J. R., and Agrawal, N. (2015) Quantum Mechanical Calculations of the Interactions Between Diazacrowns and the Sodium Cation: An insight into Na+ Complexation in Diazacrown-Based Synthetic Ion Channels, *RSC Advances*.

27. Cances, E., Mennucci, B., and Tomasi, J. (1997) A new integral equation formalism for the polarizable continuum model: Theoretical background and applications to isotropic and anisotropic dielectrics, *The Journal of chemical physics 107*, 3032-3041.

28. Mennucci, B., Cances, E., and Tomasi, J. (1997) Evaluation of solvent effects in isotropic and anisotropic dielectrics and in ionic solutions with a unified integral equation method: theoretical bases, computational implementation, and numerical applications, *The Journal of Physical Chemistry B 101*, 10506-10517.

29. Tomasi, J., Mennucci, B., and Cances, E. (1999) The IEF version of the PCM solvation method: an overview of a new method addressed to study molecular solutes at the QM ab initio level, *Journal of Molecular Structure: THEOCHEM 464*, 211-226.

30.   Coropceanu, V., Malagoli, M., da Silva Filho, D., Gruhn, N., Bill, T., and Brédas, J. (2002) Hole-and electron-vibrational couplings in oligoacene crystals: intramolecular contributions, *Physical review letters 89*, 275503.

31.   Sebastian, S., Sylvestre, S., Jayabharathi, J., Ayyapan, S., Amalanathan, M., Oudayakumar, K., and Herman, I. A. (2015) Study on conformational stability, molecular structure, vibrational spectra, NBO, TD-DFT, HOMO and LUMO analysis of 3,5-dinitrosalicylic acid by DFT techniques, *Spectrochimica Acta Part A: Molecular and Biomolecular Spectroscopy 136, Part B*, 1107-1118.

32.   Fogarasi, G., Zhou, X., Taylor, P. W., and Pulay, P. (1992) The calculation of ab initio molecular geometries: efficient optimization by natural internal coordinates and empirical correction by offset forces, *Journal of the American Chemical Society 114*, 8191-8201.

33.   James, C., Raj, A. A., Reghunathan, R., Jayakumar, V., and Joe, I. H. (2006) Structural conformation and vibrational spectroscopic studies of 2, 6-bis (p-N, N-dimethyl benzylidene) cyclohexanone using density functional theory, *Journal of Raman Spectroscopy 37*, 1381-1392.

34.   Geerlings, P., De Proft, F., and Langenaeker, W. (2003) Conceptual density functional theory, *Chemical reviews 103*, 1793-1874.

35.   Lameira, J., Alves, C., Moliner, V., and Silla, E. (2006) A density functional study of flavonoid compounds with anti-HIV activity, *European journal of medicinal chemistry 41*, 616-623.

36.   Zhang, Y., Hong, H., Engle, J. W., Bean, J., Yang, Y., Leigh, B. R., Barnhart, T. E., and Cai, W. (2011) Positron emission tomography imaging of CD105 expression with a 64 Cu-labeled monoclonal antibody: NOTA is superior to DOTA, *PLoS One 6*, e28005.

37.   Bevilacqua, A., Gelb, R. I., Hebard, W. B., and Zompa, L. J. (1987) Equilibrium and thermodynamic study of the aqueous complexation of 1, 4, 7-triazacyclononane-N, N', N''-triacetic acid with protons, alkaline-earth-metal cations, and copper (II), *Inorganic Chemistry 26*, 2699-2706.

38.   Boros, E., Ferreira, C. L., Cawthray, J. F., Price, E. W., Patrick, B. O., Wester, D. W., Adam, M. J., and Orvig, C. (2010) Acyclic chelate with ideal properties for 68Ga PET imaging agent elaboration, *Journal of the American Chemical Society 132*, 15726-15733.

39.   Velikyan, I., Maecke, H., and Langstrom, B. (2008) Convenient preparation of 68Ga-based PET-radiopharmaceuticals at room temperature, *Bioconjugate chemistry 19*, 569-573.

40. Strand, J., Honarvar, H., Perols, A., Orlova, A., Selvaraju, R. K., Karlström, A. E., and Tolmachev, V. (2013) Influence of macrocyclic chelators on the targeting properties of 68 Ga-labeled synthetic affibody molecules: Comparison with 111 In-labeled counterparts, *PloS one 8*, e70028.

41. Fuchs, A., Greguric, I., and Roe, G. (2010) Evaluation of radioisotope quality aspects for preparation of high specific activity [Ga-68]-NOTA-AnnexinA1, *Nuclear Medicine and Biology 37*, 692.

42. Majkowska-Pilip, A., and Bilewicz, A. (2011) Macrocyclic complexes of scandium radionuclides as precursors for diagnostic and therapeutic radiopharmaceuticals, *Journal of inorganic biochemistry 105*, 313-320.

43. Tolmachev, V., Altai, M., Sandström, M., Perols, A., Karlström, A. E., Boschetti, F., and Orlova, A. (2011) Evaluation of a maleimido derivative of NOTA for site-specific labeling of affibody molecules, *Bioconjugate chemistry 22*, 894-902.

44. Eisenwiener, K.-P., Prata, M., Buschmann, I., Zhang, H.-W., Santos, A., Wenger, S., Reubi, J. C., and Mäcke, H. R. (2002) NODAGATOC, a new chelator-coupled somatostatin analogue labeled with [67/68Ga] and [111In] for SPECT, PET, and targeted therapeutic applications of somatostatin receptor (hsst2) expressing tumors, *Bioconjugate chemistry 13*, 530-541.

45. Balachandran, V., and Parimala, K. (2012) Tautomeric purine forms of 2-amino-6-chloropurine (N9H10 and N7H10): Structures, vibrational assignments, NBO analysis, hyperpolarizability, HOMO–LUMO study using B3 based density functional calculations, *Spectrochimica Acta Part A: Molecular and Biomolecular Spectroscopy 96*, 340-351.

46. Liu, J.-n., Chen, Z.-r., and Yuan, S.-f. (2005) Study on the prediction of visible absorption maxima of azobenzene compounds, *Journal of Zhejiang University. Science. B 6*, 584.

47. Szafran, M., Komasa, A., and Bartoszak-Adamska, E. (2007) Crystal and molecular structure of 4-carboxypiperidinium chloride (4-piperidinecarboxylic acid hydrochloride), *Journal of Molecular Structure 827*, 101-107.

48. Kavitha, E., Sundaraganesan, N., Sebastian, S., and Kurt, M. (2010) Molecular structure, anharmonic vibrational frequencies and NBO analysis of naphthalene acetic acid by density functional theory calculations, *Spectrochimica Acta Part A: Molecular and Biomolecular Spectroscopy 77*, 612-619.

49. Rajamani, T., and Muthu, S. (2013) Electronic absorption, vibrational spectra, non-linear optical properties, NBO analysis and thermodynamic properties of 9-[(2-

hydroxyethoxy) methyl] guanine molecule by density functional method, *Solid State Sciences 16*, 90-101.

50.   Geraldes, C. F., Marques, M. P. M., and Sherry, A. D. (1998) NMR conformational study of diamagnetic complexes of some triazatriacetate macrocycles, *Inorganica chimica acta 273*, 288-298.

51.   Griffith, J., and Orgel, L. (1957) Ligand-field theory, *Quarterly Reviews, Chemical Society 11*, 381-393.

52.   Sinha, L., Prasad, O., Narayan, V., and Shukla, S. R. (2011) Raman, FT-IR spectroscopic analysis and first-order hyperpolarisability of 3-benzoyl-5-chlorouracil by first principles, *Molecular Simulation 37*, 153-163.

53.   Govindarajan, M., Karabacak, M., Periandy, S., and Tanuja, D. (2012) Spectroscopic (FT-IR, FT-Raman, UV and NMR) investigation and NLO, HOMO–LUMO, NBO analysis of organic 2,4,5-trichloroaniline, *Spectrochimica Acta Part A: Molecular and Biomolecular Spectroscopy 97*, 231-245.

54.   Gece, G. (2008) The use of quantum chemical methods in corrosion inhibitor studies, *Corrosion Science 50*, 2981-2992.

55.   Choudhary, N., Bee, S., Gupta, A., and Tandon, P. (2013) Comparative vibrational spectroscopic studies, HOMO–LUMO and NBO analysis of N-(phenyl)-2,2-dichloroacetamide, N-(2-chloro phenyl)-2,2-dichloroacetamide and N-(4-chloro phenyl)-2,2-dichloroacetamide based on density functional theory, *Computational and Theoretical Chemistry 1016*, 8-21.

56.   Pathak, S., Srivastava, R., Sachan, A., Prasad, O., Sinha, L., Asiri, A., and Karabacak, M. (2015) Experimental (FT-IR, FT-Raman, UV and NMR) and quantum chemical studies on molecular structure, spectroscopic analysis, NLO, NBO and reactivity descriptors of 3, 5-Difluoroaniline, *Spectrochimica Acta Part A: Molecular and Biomolecular Spectroscopy 135*, 283-295.

CHAPTER FOUR

CONCLUSIONS

The structure and electronic features of NOTA chelator was examined with the intention of evaluating the binding and radiolabelling efficiency of the NOTA chelator. This was achieved by studying the complexation of NOTA chelator with alkali metal ions (Li^+, Na^+, K^+ and Rb^+) and radiometal ions (Cu^{2+}, Ga^{3+}, Sc^{3+} and In^{3+}) using density functional theory. The B3LYP functional with the 6-311+G(2d, 2p) basis set was used for Li^+, Na^+ and K^+ and Def2-TZVPD basis set for Rb^+; the DGDZVP basis set was used for the radiometal ions.

For the NOTA—alkali metal ions complexation, the result of our investigation reveals that the stability of alkali metal ions decreases down the group the periodic table, while for NOTA—radiometal ion complexes, the results identified NOTA—Ga^{3+} complex is more stable than the rest of the complexes. This result matches with the experimentally reported binding constants for these complexes (Section 3.6). This study reveals that there is charge transfer between NOTA and ions during complexation and both oxygen and nitrogen atoms of NOTA play a crucial role during the complexation process. It was highlighted in the study that the implicit water solvation reduces the stability of the complexes.

A notable conclusion about this present study is that, even though there is a considerable interaction between NOTA chelator and alkali metal ions, alkali metal ions found in the body cannot compete with radiometal ions for binding site or displace radiometal ions during complexation with NOTA chelator. Overall, this study has highlighted the different electronic factors that can contribute to the complexation of ions to a specific chelator. This study serves as a guide to find the optimal match between NOTA chelator and radiometal ions for radiolabelling applications.

APPENDIX A

Supporting Information for Chapter Two

The Interaction of NOTA as a Bifunctional Chelator with Competitive Alkali Metal ions: A DFT Study

F. Y. Adeowo, B. Honarpavar*, A. A. Skelton*,

School of Health Sciences, Discipline of Pharmacy, University of KwaZulu-Natal, Durban 4001, South Africa.

Figure 1S: The structures of free NOTA in A: vacuum and B: water media. The dotted lines show distances between carboxylic pendant arms of NOTA.
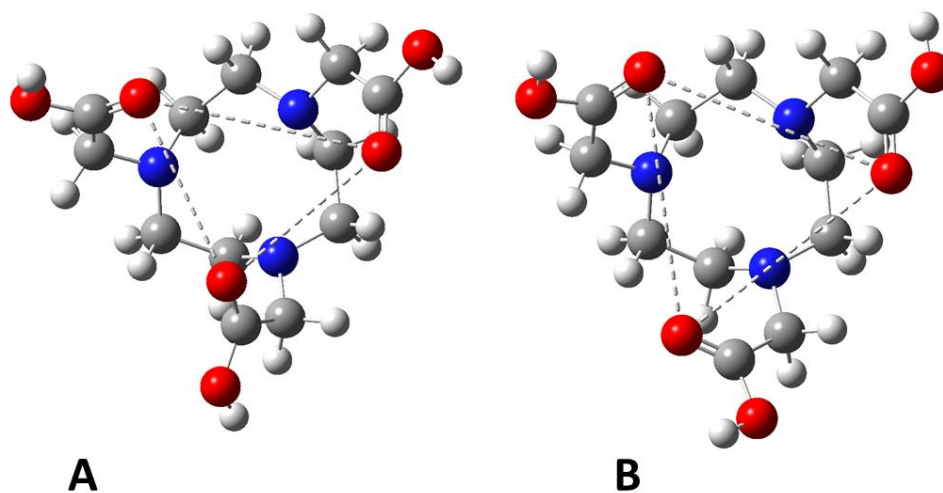
O^H—ion conformation　　　　O^C—ion conformation
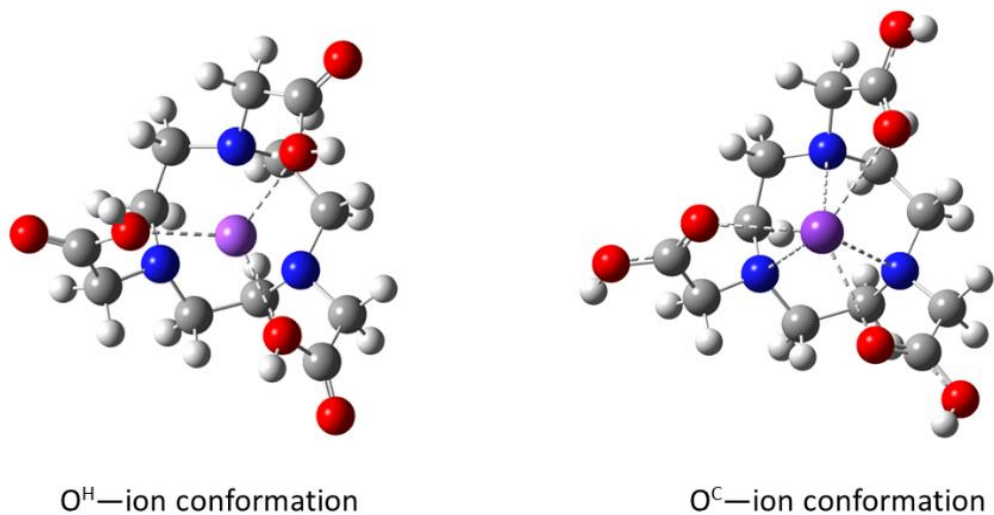
Figure 2S: The structures for O^H—ion and O^C—ion conformations.

B3LYP　　　　ωB97XD
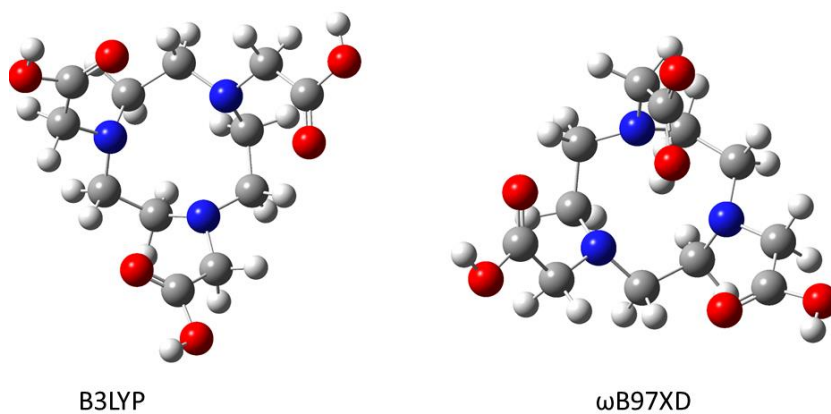
Figure 3S: The geometry optimized structures for free NOTA using B3LYP and ωB97XD functionals.

Table 1S: BSSE values for complexes of Li^+, Na^+, and K^+ ions using different basis set.

Basis sets	BSSE			
	6-31+G(d,p)	6-311G+(d,p)	6-311G+(2d,2p)	6-311G++(3d,3p)
Li^+	1.87	2.11	1.08	0.75
Na^+	2.31	2.05	1.42	1.25
K^+	1.01	0.69	0.55	0.49

Table 2S: BSSE of the different basis set used for complexes of Rb^+ ion.

Basis set	BSSE
6-31G+(d,p)/ LAN2DZ	0.44
6-311G+(d,p)/ LAN2DZ	0.35
6-311G+(2d,2p)/ LAN2DZ	0.34
6-311G++(3d,3p)/ LAN2DZ	0.40
6-311G++(3df,3dp)/ LAN2DZ	0.40
6-311G++(3df,3dp)/ LAN2MB	0.49
6-311G+(2d,2p)/Def2-TZVPD	0.28

Table 3S: Translational entropy contribution of the free ions and NOTA—ion complexes before

calculation

Ion/complex	Translational entropy
Li^+	31.80
Na^+	35.34
K^+	36.91
Rb+	39.23
NOTA—Li^+	43.09
NOTA—Na^+	43.24
NOTA—K^+	43.38
NOTA—Rb^+	43.76

Table 4S: Absolute values of the total entropy and vibrational contribution to entropy

Compounds	Total entropy (cal mol^{-1} K^{-1})		Vibrational entropy (cal mol^{-1} K^{-1})	
	Vacuum	Solvent	Vacuum	Solvent
NOTA	161.67	152.07	84.21	74.69
NOTA—Li^+	149.15	149.33	72.16	72.35
NOTA—Na^+	155.10	158.49	77.61	81.00
NOTA—K^+	159.29	162.55	81.35	84.58
NOTA—Rb^+	163.37	164.61	84.58	86.026

Table 5S: A Charge transfer from lone pairs of nitrogen atoms of NOTA to the ions

Complexes	Donor	Acceptor	E^2(kcal/mol)
NOTA—Li$^+$	LP(N)	LP*(Li$^+$)	8.14 [11.43]
NOTA—Na$^+$	LP(N)	LP*(Na$^+$)	9.89 [5.48]
NOTA—K$^+$	LP(N)	LP*(K$^+$)	11.19 [3.32]
NOTA—Rb$^+$	LP(N)	LP*(Rb$^+$)	1.81 [2.34]

Table 6S: Proton NMR chemical shifts (δ) and natural atomic charges (NAC) of NOTA in vacuum and water media

Proton	δ_{vacuum} (ppm)	$\delta_{solvent}$ (ppm)	NAC
G1	6.22	6.60	0.49
G2	4.93	4.88	0.20
G3	4.14	4.62	0.18
G4	3.45	3.47	0.16
G5	2.32	1.83	0.20
G6	1.31	0.21	0.18

Table 7S: The interaction energy values of NOTA—alkali metal complexes using B3LYP and ωB97XD functional, with 6-311+G(2d,2p) basis sets.

Complexes	B3LYP E_{int} (kcal/mol)	ωB97XD E_{int} (kcal/mol)
NOTA—Li$^+$	-118.04	-107.69
NOTA—Na$^+$	-89.78	-77.40
NOTA—K$^+$	-64.01	-53.78
NOTA—Rb$^+$	-54.25	-46.59

Table 8S: The interatomic distances between alkali metals and heteroatoms of NOTA at the ωB97XD/6-311+G(2d,2p) level of theory for Li^+, Na^+ and K^+. The ωB97XD/Def2-TZVPD level of theory was used for NOTA—Rb^+ complex.

Complex	Average O-ion distance (≤ 3 Å)	Average N-ion distance (≤ 3 Å)
NOTA—Li^+	2.07	2.20
NOTA—Na^+	2.37	2.55
NOTA—K^+	2.72	2.92
NOTA—Rb^+	2.89	3.13

APPENDIX B

Supporting Information for Chapter Three

DFT study on the complexation of NOTA as a bifunctional chelator with radiometal ions

F. Y. Adeowo, B. Honarpavar*, A. A. Skelton*,

School of Health Sciences, Discipline of Pharmacy, University of KwaZulu-Natal, Durban 4001, South Africa.
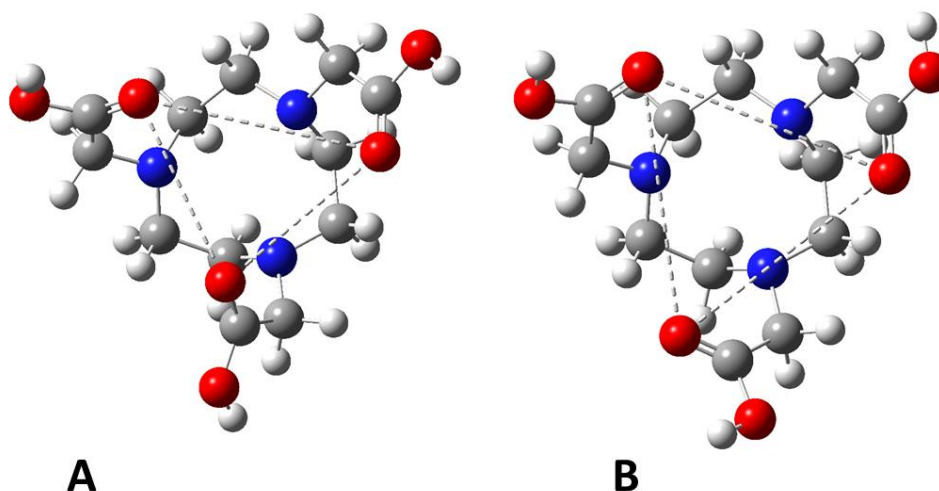
Figure 1S: The structures of free NOTA in A: vacuum and B: water media. The dotted lines show distances between carboxylic pendant arms of NOTA.

Table 1S: Translational entropy contribution of the free ions and NOTA_ion complexes before calculation

Ion/complex	Translational entropy
Cu^{2+}	38.34
Ga^{3+}	38.61
Sc^{3+}	37.34
In^{3+}	40.13
NOTA——Cu^{2+}	43.92
NOTA——Ga^{3+}	43.64
NOTA——Sc^{3+}	43.44
NOTA——In^{3+}	43.98

Table 2S: Absolute values of the total entropy and vibrational contribution to entropy

Compounds	Total entropy $(cal\ mol^{-1}\ K^{-1})$		Vibrational entropy $(cal\ mol^{-1}\ K^{-1})$	
	Vacuum	Solvent	Vacuum	Solvent
NOTA	161.67	152.07	84.21	74.69
NOTA——Cu^{3+}	148.81	149.42	69.93	70.53
NOTA——Ga^{3+}	140.08	140.47	62.61	63.01
NOTA——Sc^{3+}	146.07	I40.38	68.53	62.82
NOTA——In^{3+}	152.25	145.78	74.10	67.64

Table 3S: Proton NMR chemical shifts (δ) and natural atomic charges (NAC) of NOTA in vacuum and water media

Proton	δ_{vacuum} (ppm)	$\delta_{solvent}$ (ppm)	NAC
G1	6.22	6.60	0.49
G2	4.93	4.88	0.20
G3	4.14	4.62	0.18
G4	3.45	3.47	0.16
G5	2.32	1.83	0.20
G6	1.31	0.21	0.18

Table 4S: The interaction energy values of NOTA—radiometal ion complexes using B3LYP and ωB97XD functionals, with 6-311+G (2d,2p) and DGDZVP basis sets.

Complexes	B3LYP E_{int} (kcal/mol)	ωB97XD E_{int} (kcal/mol)
NOTA—Cu^{2+}	-410.37	-391.55
NOTA—Sc^{3+}	-639.18	-618.25
NOTA—In^{3+}	-655.51	-643.36
NOTA—Ga^{3+}	-810.59	-790.96

Table 5S. The interatomic distances between radiometal ions and heteroatoms of NOTA at the ωB97XD/6-311+G (2d,2p) level of theory.

Complex	Average O-ion distance (≤ 3 Å)	Average N-ion distance (≤ 3 Å)
NOTA—Cu^{2+}	2.11	2.13
NOTA—Sc^{3+}	2.08	2.32
NOTA—In^{3+}	2.16	2.31
NOTA—Ga^{3+}	1.99	2.08